FLUIDIZATION AND SEDIMENTATION BEHAVIORS OF NANOPARTICLES

By

Kanku Lubale

In the fulfillment of the Masters of Science in Chemical Engineering, College of Agriculture, Engineering and Science, University of KwaZulu Natal

Date of Submission of the revised thesis: 05 October 2020

Name of Supervisor: Professor Amir H. Mohammadi

Name of Co/Supervisor: Mr. Elly M. Obwaka

As the candidate's Supervisor I agree/do not agree to the submission of this thesis. Form EX1-5

COLLEGE OF AGRICULTURE, ENGINEERING, AND SCIENCE

DECLARATION 1 - PLAGIARISM

I, …**Kanku Lubale**…., declare that

1. The research reported in this thesis, except where otherwise indicated, is my original research.

2. This thesis has not been submitted for any degree or examination at any other university.

3. This thesis does not contain other persons' data, pictures, graphs, or other information unless specifically acknowledged as being sourced from other persons.

4. This thesis does not contain other persons' writing unless specifically acknowledged as being sourced from other researchers. Where other written sources have been quoted, then:

a. Their words have been re-written but the general information attributed to them has been referenced

b. Where their exact words have been used, then their writing has been placed in italics and inside quotation marks and referenced.

5. This thesis does not contain text, graphics, or tables copied and pasted from the Internet unless specifically acknowledged, and the source being detailed in the thesis and the References sections.

Signed

……

Date: **05 October 2020**

Acknowledgments

Many thanks go to Professor Amir H. Mohammadi for financing the entire project from his grant. We will not forget the guidance and academics advice that came from the Supervisor Professor Amir H. Mohammadi and the Co-Supervisor Mr. Elly M. Obwaka from the University of KwaZulu-Natal in the Discipline of Chemical Engineering, during the monthly meeting that never missed from the beginning and the end of the project.

During the experimental, we have spent most of our time in the laboratory of the Discipline of Chemical Engineering, University of KwaZulu Natal, we are addressing our thanks to the technicians in the Discipline of Chemical Engineering. We are acknowledging the assistance from the technicians at the Microscopy Microanalysis Unit (MMU) at Westville campus, University of KwaZulu Natal. To my family, Emily Bebene and my three children, Jordan Kabeja, Acacia Ngalula, and Onyx Idema, many thanks for supporting and encouraging me in the completion of the thesis, I have spent most of my time away from you but you have been patient.

Abstract.

A nanoparticle or ultrafine particle is usually defined as a particle of matter that is between 1 to 100 nanometers in diameter. Nanoparticles were used by artisans since prehistoric times, albeit without knowledge of their nature. Analyzing the outcome from the experiments of the study, the following questions were considered: 1. What will be the behavior of fluidization of 13 nm aluminum oxide and 10-20 nm silicon dioxide nanoparticles that fall under Geldart group C? 2. What is the existing relationship between physical characteristics of 13 nm aluminum oxide and 10-20 nm silicon dioxide nanoparticles with the fluidization enhanced by vibration and acoustic sound? and 3. What is the effectiveness of fluidization enhanced by vibration and acoustic sound on nanoparticles materials under study used in the experiment depending on their physical properties? It was crucial to consider the above-mentioned questions to undertake the study on the fluidization and sedimentation to investigate the behavior of nanoparticles.

From the findings, the experimental measurement of the pressures in different regions of the fluidized bed, in the plenum chamber, on the bed of the solid material, and above the bed of solid material was performed by using pressure transducers and the inverted U-tube manometers to investigate the behavior in the fluidization of samples of size 277 μm, 428 μm, 161 μm, and 338 μm. The applicability of the published correlations such as the Ergun equation was fitted to the experimental pressure drop measured using both measuring methods; the sphericities of the samples were measured using the fitted Ergun equation. The fluidization parameters such as minimum fluidization velocity, voidage, and height were measured from the experimental data and compared with the calculated minimum fluidization parameters obtained from the published correlations. Two methods were used during the experiment; acoustic sound fluidization and vibro-fluidization. During the enhanced fluidization by external forces of aluminum oxide and silicon dioxide nanoparticles, the primary size of nanoparticles formed agglomerate, and their fluidization was of agglomerate particulate fluidization. The use of the Richardson and Zaki equation and Stokes' Law in the experimental data was to estimate the size of the agglomerate formed during fluidization associated with mechanical vibration and acoustic sound. It was found that the size of agglomerate formed during fluidization associated with mechanical vibration was 48 μm when aluminum oxide nanoparticles were under vibro-fluidization.

The sedimentation behavior of nanoparticles was investigated from the batch settling test. It was noticeable by visual observation, aluminum oxide nanoparticles settled after 2 hours in a batch settling test while the silicon dioxide nanoparticles demonstrated different behavior in settling. It was observed that after 72 hours of batch settling test of silicon dioxide nanoparticles, a clear region was observable in the cylindrical tube. The use of Stokes' Law demonstrated that the size of the settled silicon dioxide nanoparticles could be estimated from sedimentation theory.

Contents

List of Tables

List of figures

Nomenclature

Symbol	Expression	Units
A	The cross-sectional area of the column of the fluidized bed	m^2
d_a	The diameter of nanoparticles agglomerates	µm
d_p	The diameter of the solid particles	µm
DLS	Dynamic Light Scattering	
g	Acceleration due to gravity	$\frac{m}{s^2}$
H	Height of the bed solid particles in the column of the fluidized bed	m
H_{mf}	Height of the bed of solid particles at minimum fluidization condition	m
H_o	The initial height of the bed of solid particles in the column of the fluidized column	m
m_p	Mass of the solid particles	kg
n	The Richardson and Zaki index	
Re_{mf}	Reynold number at minimum fluidization condition	
SEM	Scanning Electron Microscopy Analysis	
TEM	Transmission Electron Microscopy Analysis	
u_s	The superficial velocity of dry air	$\frac{m}{s}$
u_t	Terminal velocity of dry air	$\frac{m}{s}$
V_B	The volume of the bed of solid particles	m^3
V_p	The volume of the solid particles	m^3

Greek symbol	**Expression**	**Unit**
ε	Voidage	
ε_{mf}	Voidage at minimum fluidization condition	
ε_o	Initial voidage	
$\emptyset_s$	Sphericity of the solid particles	
ρ	Density of nanoparticles	$\frac{kg}{m^3}$
ρ_{bulk}	Bulk density of the solid particles	$\frac{kg}{m^3}$
ρ_g	The density of dry air	$\frac{kg}{m^3}$
ρ_p	The density of the solid particles	$\frac{kg}{m^3}$
μ	The viscosity of dry air	$Pa.s$

1. INTRODUCTION

1.1. Background

The handling of nanoparticles in the process industry is identifiable in many areas such as in cosmetics, painting, electronics, medicine; nanoparticles are used as catalysts due to their large surface area per volume of particles. Nanoparticles are those particles that exist on a nanometre scale. Their physical properties such as size and density can be determined in a fluidized bed system because nanoparticles can easily be transported, mixed when their hydrodynamics are well understood. Fluidization of nanoparticles become very attractive to daily life for many reasons when utilizing them in many sectors in the industry. In drug delivery, it has been found that nanotechnology is proven beneficial in the treatment of cancer, AIDS, and many other diseases (Rizvi and Saleh, 2018). Processing nanoparticles in the fluidizing system is not as easy as it seems, much research has undergone fluidization of fine/ultrafine particles and has found difficulties fluidizing particles falling in Geldart category of group C (Wang *et al.,* 2007a). Geldart (1986) has classified the fluidization of particles according to different groups; and he has pointed out, that the fluidization of particles differs as their size changes. It has been reported that the fluidization of nanoparticles seems unrealistic in a conventional fluidization process due to the cohesive forces existing between particles. In most cases, they can be fluidized when an external force is applying to the fluidized system, and their fluidization is in the form of agglomerates and is called agglomerate fluidization. Before proceeding to the fluidization of nanoparticles it is very important to understand the theory governing the fine/ultrafine particles. The practice of the traditional fluidization technique has revelled the possibility of fluidizing particles of Geldart Groups A and B.

1.2. Problem statement

Fluidizing nanoparticles in a conventional fluidized bed is a complex matter that needs to be addressed by applying a modified methodology for the use of these nanoparticles in many sectors for applications. This complexity of fluidizing this group C material is due to the presence of the inter-particles forces existing between particles as described in the upcoming chapter. To study the behavior of nanoparticles in the fluidization, it is of interest to be able to expose these materials under fluidization. The use of assisted method: fluidization assisted by acoustic sound and vibration to fluidized nanoparticles come into practice before obtaining any fluidization parameters of nanoparticles. Many researchers have undertaken methodologies to fluidize nanoparticles, however, the use of fluidization assisted by the vibration and acoustic sound for

fluidization of 13 nm aluminum oxide and 10-20 nm silicon dioxide nanoparticles have been used in the study of the fluidization.

The study on the behavior of the samples was to familiarize the autor with an application of the published correlations in the investigation of the fluidization behavior of 13 nm aluminum oxide and 10-20 nm silicon oxide nanoparticles

The results of the thesis were presented in a postgraduate seminar at the University of KwaZulu-Natal, Discipline of Chemical Engineering for an oral presentation[1]; in a conference at South African Institution of Chemical Engineers (SAIChE) Research Day 2019; to a Postgraduate Innovation Symposium 2019 (PRIS) conference; and will be presented to South African Chemical Engineering Congress 2020 (SACEC) conference.

1.3. Justification

- Nanoparticles are found very difficult to be fluidized because the inter-particle forces are dominating
- Nanoparticles can be fluidized in a fluidized bed assisted by external forces such as vibration, the addition of foreign particles, and acoustic sound
- The size of agglomerate formed during fluidization of nanoparticles is estimated using correlation and analytical measurement
- The fluidization of nanoparticles was anticipated by fluidizing samples of solid particles

1.4. Objectives

The study is aimed at investigating the fluidization and sedimentation behaviors of aluminum oxide and silicon dioxide nanoparticles in a fluidized bed column in association with external forces. The objectives were the following:

- To study the fluidization of aluminum oxide and silicon dioxide nanoparticles in an enhanced fluidized bed column
- To investigate the hydrodynamic of nanoparticles by examining the minimum fluidization parameters of nanoparticles
- To investigate the behavior of 13 nm aluminum oxide and 10-20 nm silicon dioxide nanoparticles in fluidization enhanced by vibration and acoustic waves

[1] Postgraduate Seminar - UKZN Chemical Engineering CEE

- To investigate the settling velocity of 13 nm aluminum oxide and 10-20 nm silicon dioxide nanoparticles in sedimentation
- To investigate the effect of drag force and the gravitational force on solid particles (nanoparticles)
- To investigate the rate at which particles (nanoparticles) settle out in sedimentation

1.5. Research Project questions

The research seeks to answer the following questions:

- What will be the behavior of fluidization of 13 nm aluminum oxide and 10-20 nm silicon dioxide nanoparticles that fall under Geldart group C?
- What is the existing relationship between physical characteristics of 13 nm aluminum oxide and 10-20 nm silicon dioxide nanoparticles with the fluidization enhanced by vibration and acoustic sound?
- What is the effectiveness of fluidization enhanced by vibration and acoustic sound on nanoparticles materials under study used in the experiment depending on their physical properties?

2. LITERATURE REVIEW

2.1. Classification of particles according to the Geldart group

Figure 2.1 below is the chart for the classification of solid materials. Geldart has classified solid particles according to their size and density difference.

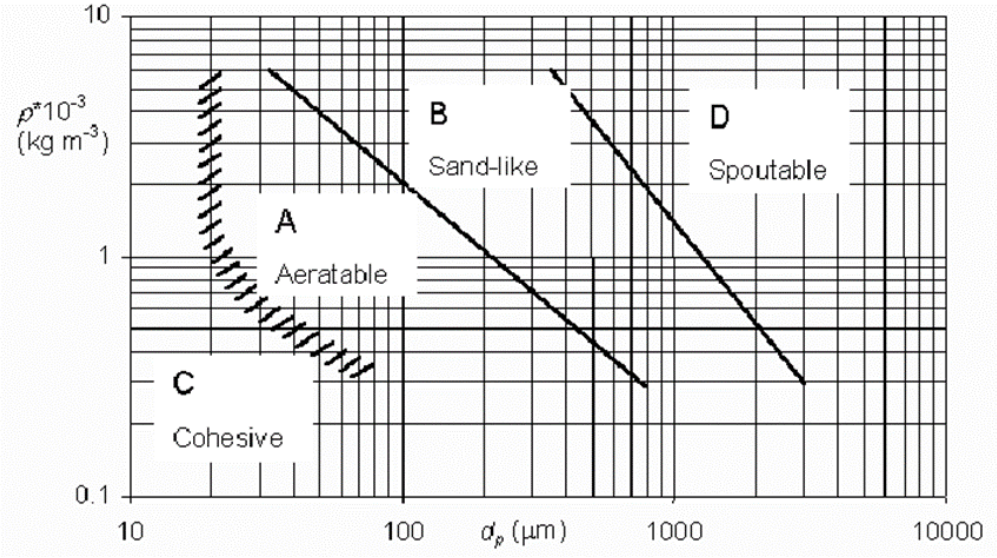

Figure 2. 1**: Geldart chart for classification of solid materials (Cocco *et al.*, 2014)**

Processing fluidization of solid particles without any knowledge makes the process difficult; it is important to know what class of solid particles belong, this will give a physical understanding of their behavior when applying fluidization. The work of Geldart (Wang *et al.*, 2007b) has proven the necessity of classifying particles when studying them in fluidization. He has classified solid particles according to their size and density difference.

Many researchers have taken their work on fluidizing particles of different sizes, and their results have demonstrated how different the fluidization behavior of solids particles are. Their results are just the confirmation of what was found by Geldart in working with particles of different sizes. He has categorized particles in four groups according to their fluidization behavior and these groups are comprising of:

2.1.1. Geldart group A

The handling of particles needs to be done when a better understanding of their particle classification is known. Geldart has spent most of his time working on particles and he has classified them according to their size. The first group of particles that he has worked on were the

particles that he has classified as group A. These particles are of 30-40µm to 150-200µm: sand under the influence of fluidization shows characteristics of smooth fluidization. The literature has published results marking the behavior of this group of particles in a conventional fluidization condition, and it has been observed that the fluidization of group A is liquid-like bubble less fluidization. Geldart has demonstrated the fluidization of particles of this group A is possible in a conventional fluidized bed and he has called solid particles of this group as aeratable particles. Thus the fluidization of particles depended strongly on their sizes.

2.1.2. Geldart group B

This category of the group of solid particles is identified with particles in size of 150-200µm to 700-900µm. Solid particles in this group are called bubble-like particles because of their condition behavior at minimum fluidization. It has been recorded from the published papers (Wang *et al*., 2007a), just when the fluidization commences there is a bubble forming at minimum fluidization condition. In this category of particles, the fluidization is possible in a conventional fluidized bed except that at minimum fluidization for particles Group B there is an appearance of bubbles.

2.1.3. Geldart group C

What makes this group different from others is the properties of particles. They are small size in diameter, the physical properties cause inter-particles forces to influence particles. This group of particles is also called cohesive particles because of the presence of inter-particles forces between them. They are the size of less than 30µm, these solid particles cannot easily be fluidized in a conventional fluidizing bed. Geldart has shown the reason of this phenomenon when He fluidized this group of particles and the reason found was the existence of inter-particles forces having a strong effect on other external forces in a fluidized bed such as draft forces, gravitational forces, and buoyancy forces (Raganati *et al*., 2018). The existence of these inter-particles forces makes the fluidization unrealistic for particles of Group C and even wastes for nanoparticles. When dealing with fluidization of nanoparticles, consideration needs to be taken on their sizes, as nanoparticles getting smaller, and their influences of inter-particles forces on the fluidization of fine or /ultrafine particles predominate the drags forces, gravitational forces, and buoyancy forces**.** As many workers have demonstrated that when trying to fluidize particles of Group C, especially nanoparticles, there is formation of channels or a bed being lift as a plug. Researchers have worked on the fluidization of nanoparticles and they have concluded that the fluidization of

nanoparticles may be possible only when a very large superficial gas velocity is applied to the fluidized bed**.**

2.1.4. Geldart Group D

Geldart (1973**)** has classified this group as the largest particles with particles ranging from 700-900 µm to several millimeters. The fluidization of this group of particles is pronounced by bubble rising velocity. The bubble grows into vertical channels through which particles are swept upwards causing unstable operation**,** they are called spoutable particles.

2.2. Inter-particle forces existing between solid particles of Group C

The classification of Geldart group C particles is strongly dependent on inter-particles forces existing between particles, due to the existence of these forces, the solid particles of such characters are classified in group C from the Geldat's Chart. The fluidization of Group C particles become more difficult compared to Group A, B, and D. The inter-particle forces in solid particles of group A, B and D are insignificant compared to group C. As particles get smaller their inter-particle forces become more predominant. Geldart has defined those forces as the van der Waal force, electrostatics force, and capillary force between solid particles. When working on the solid particles, it is important to define those forces and their effect on particles when they are subjected to the process of fluidization. The solid particles of group C are classified as a powder or fine/ultrafine particles with a size range of less than 30µm. Nanoparticles are within this group. These forces dominate other forces when nanomaterials are fluidized in a conventional fluidized bed, because of this phenomenal existence of inter-particle forces between particles, the fluidization of nanoparticles become impractical because of the bed being lift up or occurrence of channeling or slagging when a gas fluid is injected to the fluidized bed. Some researchers (Zhu *et al*., 2005) have attempted to fluidize nanoparticles in a conventional fluidized bed, they have found that fluidization could happen in form of agglomeration when a very large superficial velocity is applied that is more in magnitude to the minimum fluidization velocity of individual particles.

2.2.1. Van der Waals forces

At a molecular and atomic level, van der Waals force is the force that exists between two electronically charged particles, influencing the attraction situation occurring between particles. This interaction happens in two molecules, atom, surface, or intermolecular forces. In the case of a surface with an opposite charge when two particles are significantly close, there is an appearance of attraction. Literature has shown the van der Waal force is the most significant in all inter-particle forces and it dominates over the gravitational force (Raganati *et al*., 2018)**.** Literature has proposed mathematical correlation to calculate this force, in this literature review, we are still defining, and more details like correlation will be provided in future work to have a clear understanding of the inter-particle forces between nanoparticles. Small size nanoparticles do have the presence of van der Waal forces in between two particles as defined above, these forces are responsible for the cohesiveness of these fine/ultrafine particles. And when nanoparticles are exposed to fluidization they tend to form agglomerates (Tamadondar *et al*., 2016).

2.2.2. Electrostatic forces

Electrostatic forces in nanoparticles arise when two ultrafine particles slide, collide with each other when they are mixed. There is a transfer of electrons occurring into their surface layers when materials a brought into contact. This characteristic of nanoparticles being electrically charged under electrostatic force is called contact electrification. It has been shown from the literature, a mathematical model of this form of force obeyed coulomb's theory.

Many researchers have found that the electrostatic forces in nanoparticles are negligible compared to the van der Waal forces.

2.2.3. Capillary forces

Literature shows that in the presence of humidity capillary forces have an important contribution to the attraction between nanoparticles with a hydrophilic surface (TahmasebpoorThese authors contributed equally to this work *et al*., 2013)**.** When the vapor pressure of the surrounding gas is close to the saturation pressure, capillary forces can be much larger than gravitational force and also van der Waals force as well. Generally, they increase with increasing humidity of the gas and decreasing material porosity**.** Many workers have considered nanoparticles of the nature of hydrophobic where the capillary forces are negligible compared to van der Waals forces.

2.3. Method for sizing solid particles

The industrial processing of the solid particles depends on its physical proprieties such as its size, shape, and density. In this regard, sizing the solid particles is crucial for the prediction of calculated parameters to the experimental. The existence of different methods to size the solid particles have found their way from quantitative to qualitative, simple to complex, and costly to less, all these methods are having the target to determine the more precise size of solid particles of a material. For a powder solid particle, the size can be obtained through a particle size distribution method taken to measure the size. The method includes different methodologies cited in the literature, among known methods, there exists sieve analysis, laser diffraction analysis, dynamic light scattering known as (DLS), and many others. In all of these techniques, the objectiveness is to measure qualitatively the solid particle in terms of its size.

2.3.1. Sieve analysis

Figure 2.2 below is an apparatus for the size analysis of solid materials. A typical image of sieve analysis of solid particles used to size solid particles.

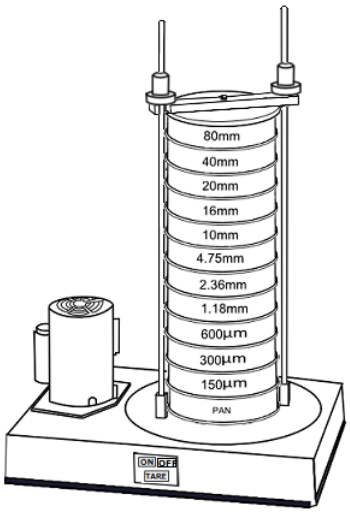

Figure 2. 2**: a set up for sieve analysis of solid particles (Eberhard *et al*., 2012)**

.

The solid particles having a size distributed from larger to a smaller size, the mean diameter of solid particles can be obtained through the sieving method, the sauter mean diameter representing the average size of the solid particles distributed. Plates of different mesh sizes are used in allowing the solid particles to cross through the mesh, the method is less accurate in a way it produces the size of the solid particles distributed as the size of solid particles retained in plates.

Qualitatively, the improvement of precision can be done by increasing the size of the mesh of the plates in a small range of sizes, and the time for the sieving. Many researchers have demonstrated that the determination of the size of the solid particles through sieve analysis is more precise in selecting a narrow range of the size of the mesh (Konert and Vandenberghe, 1997).

2.3.2. Transmission Electron Microscopy analysis (TEM)

This technique served to study the structure of materials on the micro-scale. The true size, shape, and characteristics of a single nanoparticle can be studied in a transmission electron microscope. The analysis allowed nanoparticles to be visualized at a microscopic level and further projected to visualize the distribution of primary nanoparticles.

2.3.3. Scanning Electron Microscopy analysis (SEM)

The structure of agglomerates of nanoparticles can be viewed without disruption of the morphology of the size of the agglomerates, this analysis differs from the Transmission Electron Microscopy in a way, the latest does not require sonication for the measure of the size of the nanoparticles.

2.3.4. Laser diffraction analysis

Figure 2.3 below is describing a schematic of a laser diffraction analysis. An image of a laser diffraction analysis used in size distribution.

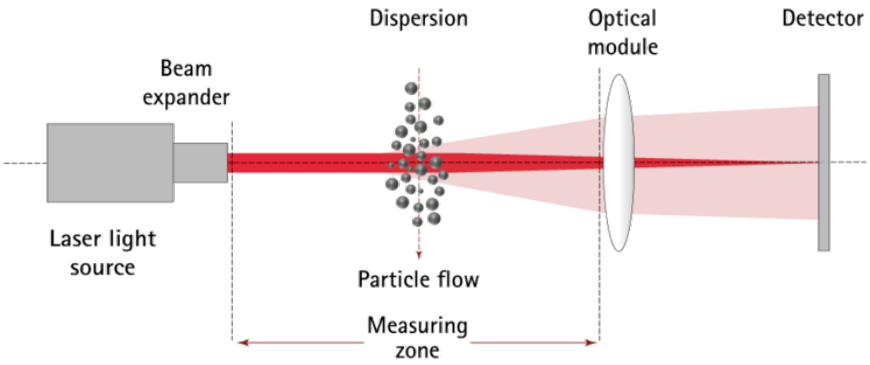

Figure 2. 3**: a schematic of a laser diffraction analysis (Blott and Pye, 2006)**

The laser diffraction method to measure the size of solid particles distributed is defined as a technology that utilizes diffraction patterns of a laser beam passed through any object ranging from nanometers to millimeters in size to quickly measure the geometrical dimensions of a particle (Taubner *et al*., 2009).

2.3.5. Dynamic light scattering analysis

Figure 2.4 is showing a dynamic light scattering analysis serves to determine the size of particles in suspension.

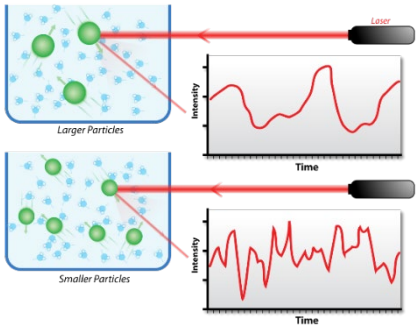

Figure 2. 4**: a dynamic light scattering analysis (Hoo *et al*., 2008)**

This technique serves to determine the size distribution profile of small particles in suspension (Khlebtsov and Khlebtsov, 2011).

2.3.6. Method of measuring the density of solid particles

The density of solid particles remained a physical property that defined the particles. Because this property always necessitates its use in many areas for the prediction of parameters, it is evident to understand and calculate the density of solid particles when particles are under-study. The desire to increase the quality for determining the density of solid particle draws its finding through laboratory tests or the use of advanced equipment.

2.4. Characteristics of Geldart Group C particles

Solid particles of Group C are those with a size below 30µm; literature has published work on the fluidization of Group C and demonstrated that materials of this Group do not fluidize easily in a conventional fluidized bed, as described in section 2.2 but they can be fluidized if the fluidization

is associated with external forces, such as acoustic sound, mechanical vibration, magnetic, and electric fields, centrifugal fluidized bed, and the use of micro-jets as a secondary flow in the bed. Publishers have demonstrated, by associating forces to the fluidization of solid particles of Group C, the inter-forces in solid particles disrupt and cause spaces in between nanoparticles, and enhance the fluidization to occur. Due to the phenomenal behavior of nanoparticles, their fluidization is defined in the form of agglomerates.

2.4.1. Agglomerate fluidization

The study on the agglomerate fluidization of nanoparticles is recorded by many workers in the literature, and is defined by the fluidization of nanoparticles being grouped in particles called agglomerate fluidization. And it has been shown that there exist two forms of agglomerate; natural agglomerate when nanoparticles are packed for storage or transportation before fluidization; and the secondary agglomerate when nanoparticles are subjected to the fluidization processed. As demonstrated in the literature, the nanoparticles belonging to Group C are governed by the predominance of the inter-particles forces that make the fluidization of this type of solid particles difficult. These fine particles are characterized by the presence of channeling, slagging of the bed being lift as a plug when a gas velocity is injected into a fluidized bed (Zhu *et al.*, 2005)**.** Due to the high magnitude of inter-particles forces of nanoparticles, it has been observed the fluidization may occur in form of agglomerate behaving like particles of group A, B, or C, and the superficial gas velocity required for the fluidization is highly compared to the normal minimum fluidization of individual nanoparticles in a conventional fluidized bed. It has been recorded that this fluidization of nanoparticles can be classified as agglomerate particulate fluidization when smooth fluidization is observed and agglomerate bubbling fluidization when there is a presence of bubbles**.**

2.4.1.1. Agglomerate particulate fluidization

The cohesiveness of particles of Group C, especially nanoparticles is dominated by the inter-particles forces. Due to these forces, nanoparticles are in the form of agglomerate rather than single nanoparticle when they are transported or stored. Many works of the literature have proven the fluidization of nanoparticles to behave as smooth fluidization with high bed expansion when their characteristic of the fluidization is defined in the form of agglomerate. It has been mentioned in the literature, agglomerate particles can be considered as single particles and categorized as Group A, B, or C according to their agglomerate sizes. Their fluidization is depended on density

differences and the size of agglomerate. It has found that particles having sizes less than 20 nm when fluidized is characterized as bubbleless or liquid-like fluidization and this type of fluidization is called agglomerate particulate fluidization. And this case, as stated above, when nanoparticles have been fluidized in the form of agglomerate particulate fluidization, there is an observation of smooth fluidization. Literature has shown that this type of fluidization obeys the Richardson- Zaki equation.

2.4.1.2. Agglomerate bubbling fluidization

The fluidization of nanoparticles as agglomerate bubbling fluidization is characterized by poor bed expansion, high minimum fluidization velocity, and occurrence of bubbles. The non-homogeneous of the agglomerate nanoparticles in the bed defined the size of the agglomerate being distributed within the bed. It has been found that the size of the agglomerate is high in magnitudes with a very large density difference.

2.5. Determination of the size of agglomerates

Solid particles that belong to group C are very important due to the increase in the surface-to-volume ratio, this property of solid particles of group C increases the heat and mass transfer in a fluidization process of particulate materials. It is evident, the prediction of the size of the agglomerate will characterize the fluidization of nanoparticles. As mentioned early, the agglomerate fluidization of nanoparticles is defined by the size of the agglomerate and their density different to classify them as agglomerate particulates fluidization or agglomerate bubbling fluidization. The fluidization parameters such, minimum fluidization velocity, bed expansion, the pressure drop across the fluidized bed column are correlated from the model and compared with the experimental value. We are emphasizing in agglomerate particulate fluidization as this has been experimentally shown and their size of agglomerates has been correlated using the Richardson-Zaki equation.

Morooka *et al.* (1988) worked on the energy balance model for agglomerate formation and disintegration and stated that the energy for the agglomerate formation is the same as the energy required to break the agglomerate in two parts. They have assumed that the size of the agglomerate could be obtained by evaluating the energy generated by laminar shear plus the kinetic energy of agglomerate that is balanced with the energy required to break the agglomerate. (i.e., energy due to the inter-particle forces).

It was noted from the literature that the value of n, which is the Richardson and Zaki exponent, an empirical parameter is a value of 5 as reported by many researchers in the small Reynold number regime, while n decrease as Reynold number increase.

2.6. Agglomerate fluidization assisted by external forces

The fluidization of ultrafine particles in a conventional fluidized bed as reported, occur with difficulty because of the presence of the inter-particles forces in between ultrafine particles. The behavior of a bed of nanoparticles in a conventional fluidized bed is characterized by the presence of channeling, or a bed being lift as a plug when fluid gas is injected (Zhu *et al.*, 2005)**.** The fluidization of nanoparticles as reported by workers in the field can be possible when a very high superficial gas velocity is applied to the fluidized bed. Literature has shown works from researchers in fluidizing nanoparticles assisted by external forces, their results have proven the performance of a fluidized bed fill of nanoparticles subjected to external forces and have improved fluidization parameters such as minimum fluidization velocity, bed expansion, superficial gas velocity, pressure drop, and agglomerate size. These assisted methods of fluidizing nanoparticles by using external forces included acoustic sound, mechanical vibration, magnetics and electric fields, centrifugal fluidized bed, the addition of foreign particles, and the use of micro-jets as a secondary flow in the bed. As we have emphasized in this literature review to present tree type of fluidization of nanoparticles assisted by external forces; a mechanical vibration, acoustic sound, and addition of foreign particles.

2.6.1. Agglomerate fluidization assisted by mechanical vibration

As we have mentioned, the fluidization of nanoparticles so-called agglomerate fluidization due to the formation of agglomerate under the influence of a gas superficial velocity is very important because nanomaterials can be easily handled, processed, mixed, transported, and stored when the fluidization is well understood. The formation of channeling, slagging, and a bed being lift as a plug on a conventional fluidized bed is a consequence of the existence of inter-particles forces existing in fine/ultrafine particles. To overcome such forces, researchers have developed many techniques, and their methods have proven satisfactory results in improving fluidization parameters such as minimum fluidization velocity, pressure drop, bed expansion, and agglomerate size. The application of a mechanical vibration as a source of an external force to a fluidized bed disrupts the formation of channels, bubbles, or avoids the bed being lift as a plug. Researchers have worked on the fluidization of nanoparticles using mechanical vibration and they have found

that applying vibration to a fluidized bed of nanomaterials decreases the minimum fluidization velocity, and increased the beds expansion and pressure drop (Zhang and Zhao, 2010). It has been demonstrated that the variation of the parameters of a mechanical vibration as intensity and frequency improves the behavior of the parameters of the fluidization of nanoparticles as a result of a fluidized bed is fully expanded, a lowering in minimum fluidization velocity, a lowering in superficial gas velocity and a reduction in the size of agglomerate. This technique will be tested in the experiment using fine/ultrafine particles of silicon dioxide and aluminum oxide nanoparticles.

2.6.2. Agglomerate fluidization assisted by acoustic sound

Figure 2.5 below is the configuration of a column associated with a loudspeaker, sound amplifier, and signal generator; the camcorder on the diagram serves as an apparatus for in-situ measurement when referring to the figure.

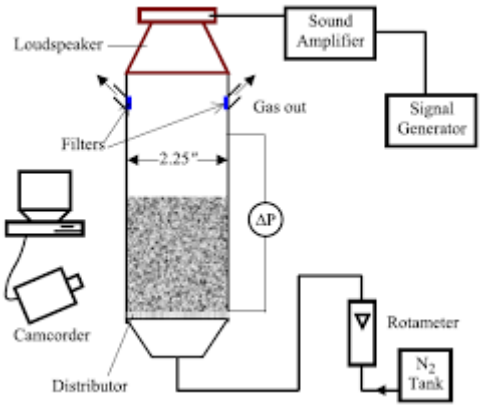

Figure 2. 5**: setup of an acoustic sound fluidization** (Zhu, *et al*., 2005)

The phenomenology of the interaction of fine/ultrafine particles as a consequence of the predominance of the inter-particles forces, make the fluidization of nanoparticles difficult; in implementing an assisted method as acoustic sound does improve the behavior of the fluidization of nanoparticles as reported by many workers (Zhu *et al*., 2004). An acoustic sound is characterized by a loudspeaker, signal generator, and amplifier. These tools can be placed on the bottom or top of a conventional fluidized bed.

When acoustic sound is connected with gas and being injected in the fluidized bed, it has been reported that the phenomenon of channeling, slagging, cracking can disappear under the influence of acoustic sound being coupled with air. Russo *et al* have found that at the natural frequency of the bed of micron size adhesive particles, high-intensity sound waves cause a reduction in both minimum fluidization and minimum bubbling velocities**.** The application of acoustic sound is one

of the methods to enhance the fluidization of nanoparticles and gives good quality of fluidization when a proper sound frequency is applied to the fluidized bed. The disruption of inter-particles forces networks of nanoparticles when an acoustic sound is coupled with air, promoting changes on parameters of fluidization of nanoparticles. It was noted that at a sound frequency of about 50 HZ, the channeling occurred during fluidization of fine/ultrafine materials and was changed to a smooth fluidization mode. Under the influence of acoustic sound, the inter-particles forces do not have a great impact on nanoparticles, therefore, the fluidized bed of agglomerate particles appears to shift their sizes when fluidized under the influence of an acoustic sound.

2.6.3. Agglomerate fluidization by the addition of foreign particles

Another technique used by researchers to enhance the fluidization of agglomerate nanoparticles is the mixing with particles of Group A to nanoparticles. This technique does not require energy like fluidization assisted by external forces does (Ali *et al*., 2018). The nature of nanoparticles is the predominance in the inter-particles forces, and they are formed as agglomerate particles when they are stored or transported. When fluidized these agglomerate particles, they tend to form channeling, slagging, or lifting a bed as a plug. It has shown from the literature that the agglomerates sizes can be a value greater than 100μm. The addition of foreign particles in a fluidized bed of nanoparticles has the effect of eliminating the inter-particles forces and reducing the size of agglomerate of nanoparticles and promoting the fluidization of nanoparticles in a conventional fluidizing system.

3. Experimental approach

The classification of solid particles into a Geldart group strongly depends on the difference in the density of the solid particle with the fluidized medium and the size of solid particles. It is crucial to have a better knowledge of the density and the size of a solid particle. In this project, besides the solid material under-investigation which are: silicon dioxide and aluminum oxide nanoparticles, four types of samples of different sizes and densities have been selected in the purpose of studying their fluidization through the experimental data and the application of published correlations such as Ergun equation, and Kunii and Levenspiel equation. The determination of the size of solid particles will be directed to the classification of solid particles of a sample into the Geldart group, to predict their fluidization behaviors, and this will be verified experimentally from measurement and by empirical correlations.

The methodological approach described in this chapter, conducted to the explanation and derivation of the knowledge of performing experimental measurements that lead to concrete conclusions. The objective of this chapter is to bring attention to the clarity on methods taken during an experiment, from the start to the end of any measurement.

In the first instance, the ongoing of the project starts with the calculation of the size of solid particles and the density of samples. These two physical properties of the solid particles are necessary before fluidization step. A clear explanation of the calculation of these physical properties is described in the next subsection of the chapter.

The methodology for classifying the sample collected is to put solid particles under-investigation through a process such as size distribution analysis as in this case. In this regard, the method used for the determination of the size of the samples will be appropriate for the size of samples.

The nanoparticles, in their turn, will be subjected to other means or methodologies for obtaining the size even though their primary size is known. Silicon dioxide is in the primary size range of 12 to 20 nanometers as the size of nanoparticles and aluminum oxide is on the primary size of 13 nanometers. 500 grams of silicon dioxide and 300 grams of aluminum oxide nanoparticles were purchased from the Sigma Aldrich supplier to investigate the behavior of these materials under acoustic fluidization and vibro-fluidization.

On the other hand, the description of the methodology to calculate parameters related to the fluidization process is demonstrated after the collection of the experimental data from the fluidization process.

3.1. Experimental procedure for the determination of the size of solid particles

It is well known that one of the methodologies for obtaining the size of solid particles is called the size distribution method. In this Project, the method of sieving was directed only to the samples collected in the main Laboratory in the Discipline of Chemical Engineering at University of KwaZulu-Natal. By visual observation of the collected samples, the size of the sieves was selected according to the set of sieves plate for sieve analysis and composed of 300-250-180-125-90-75-45-38 µm and the pan. The second set of sieve plate for sieve analysis was composed of sieves of sizes of 600-425-300-212-150-106-75µm and the pan. Four types of samples, the sieves in small sizes were directed to samples with a small size of solid particles by visual observation as powder, and the second set were subjected to the samples having a larger size of solid particles by just visual observation. One sample was of the nature of powder, this sample was sieved using the first set of sieves and tree other samples were of the nature of sand, larger in sizes than the other sample, and they were subjected to the second set of sieve plates of 600-425-300-212-150-106-75µm and the pan.

3.1.1. Size distribution using sieve analysis

Figure 3.1 below is a sieve system used in sizing solid particles. The apparatus was situated in the main laboratory in the Discipline of Chemical Engineering, Howard College, University of KwaZulu-Natal.

Figure 3. 1**: a set of sieve plates on vibrating sieve equipment**

3.1.1.1. Procedure to determine the size of the sample

For the larger samples, tree different masses 10, 20, and 90 grams of samples were weighed and dropped into the top sieve. The sieve plates were weighed without having any sample on it, and their masses were recorded for further processing. For each mass, four different runs were conducted for sieve analysis. After, the sieve plates were under vibration on sieving equipment for a sieving time of 10 minutes for 10 and 20 grams and 15 minutes for 90 grams. After each run of the sieving process, the amount of sample retained in each sized sieve plate was weighed and recorded. To increase the rate of accuracy to calculate the mass retained in each sieve for the size distribution analysis for the sample collected, 12 runs were conducted, four runs for each mass of 10, 20, and 90 grams respectively. The size of particles was obtained for each masses selected, 10, 20, and 90 grams. For each run in each mass, the mass retained in the sieves was calculated by subtracting the mass of sieve with sample after the sieving process, to the mass of sieve without a sample on it. This mass in each sized sieve was converted into a mass fraction by dividing the mass of the sample in a sieve to the total mass used for the sieving process. The mass fraction was divided by the size of the sieve for the calculation of the sauter mean diameter. The size of solid particles was obtained for 10, 20 and 90 grams as sauter mean diameter, thereafter an average of the size of solid particles in the mass of 10,20 and 90 grams was obtained as average sauter mean diameter for the sample collected. The samples were named as sample 1, sample 2, sample 3, and sample 4.

3.1.1.2. Method to determine the primary size of nanoparticles

The nanomaterials for the investigation of the fluidization parameters in the project for the fluidization and sedimentation behavior of nanoparticles named as 13 nm aluminum oxide in size and 10-20 nm silicon dioxide in size needed determination in the size to be confirmed and study their morphology that could explain their behavior in fluidization and sedimentation. The technique performed for the sizing of nanoparticles included a transmission electron microscopy analysis. The equipment for the analysis was situated at the Microscopy and Microanalysis Unit at the University of Kwazulu Natal Westville campus.

3.1.1.2. (a). Transmission Electron Microscopy (TEM) analysis

TEM images of 13 nm aluminum oxide and 10-20 nm silicon dioxide taken from a transmission electron microscope were studied for visualizing the structures of nanoparticles; thereafter a size

distribution analysis on the images were used to evaluate different sizes. A 13 nm aluminum oxide and 10-20 silicon dioxide nanoparticles were prepared by applying sonication to allowed the nanoparticles to disintegrate in the single nanoparticle in a case of the formation of primary agglomerate due to storage.

3.2. Method to evaluate the densities of samples

The density of the solid particles for each sample collected in the main Laboratory in the Discipline of Chemical Engineering was calculated in the laboratory using the method of weighing solid particles in a pycnometer that was measured on a scale. The method involves of evaluating each sample of a solid particle by collecting a randomly certain amount of solid particles of sample thereafter weigh for density calculation. To reduce the rate of a high percentage of error that could occur during measurement, different run for measurement was considered. It has been observed that when calculating densities of solid particles of samples, the weight of each sample was behaving differently when calculating the densities.

First of all, the volume of the pycnometer had been corrected by not considering the volume in the script on the pycnometer for accuracy purposes. The pycnometer was filled with distilled water collected at a prescribed time and care was taken to calculate the density of the distilled water collected.

3.2.1. Calculation of the density of distilled water

Different cylindrical tubes were taken from the analytical laboratory in the Discipline of Chemical Engineering to measure the density of the distilled water collected at a particular time. The first cylindrical tube was weighed empty and the mass and the volume of the tube were recorded. Care was taken to the prescribed working temperature of the cylindrical tube to ensure that the temperature of distilled water is according to the working temperature of the cylindrical tube. After, the cylindrical tube was filled with distilled water at the working temperature of the tube and weighed. The mass of distilled water that was filled in the cylindrical tube was calculated by subtracting the mass of cylindrical tube fill with distilled water to the mass of the empty cylindrical tube, the mass was recorded in gram unit. As, the cylindrical tubes were measuring tubes, in this case, consideration was taken to evaluate the density in 25 ml at different working temperatures, 20 degrees Celsius and 27 degrees Celsius respectively. The mass of the distilled water recorded after subtraction was divided by the total volume of the cylindrical tube. The value obtained was the density of distilled water at the working temperature of the cylindrical tube. The

density was determined from the two types of cylindrical tubes of 20 degrees Celsius and 27 degrees Celsius. For the verification of the rate of accuracy and the reproducibility of the results obtained, different runs using different types of cylindrical tubes were used. This density was used in the evaluation of the volume which was the corrected volume of the pycnometer.

3.2.2. Correction for the volume of the pycnometer

The chosen pycnometer was in script of the volume of 250 ml, which could not be accurate if filled with distilled water to the indication at top of the pycnometer, this was proven when the total volume of the pycnometer was corrected for verification. The pycnometer was weighed empty and the mass was taken, after that, the pycnometer was filled with distilled water right to the top at the indicated sign of the device, the mass of the pycnometer was filled with distilled water and weighed. The distilled water that contained or filled the pycnometer when empty, was easily determined after subtracting the recorded mass of pycnometer fill with distilled water to the mass of the empty pycnometer. Given that the pycnometer is indicated at the top, the volume of distilled water filled it up until to the indication at the top of the device showed the exact volume of the empty pycnometer. However, the mass of distilled water was divided by the density of the distilled water collected at a particular time to calculate the volume of distilled water which in these circumstances became the true volume of the pycnometer.

For the reason that different runs were performed at different times, the reproducibility of the results was taken into consideration.

3.2.3. The density of the solid particle of the samples

To evaluate the density of the four samples collected in the main laboratory in the Discipline of Chemical Engineering, some methodologies were considered quite similar to the determination of the density of distilled water filled in a measured cylindrical tube described in the previous section. This time, the difference was the evaluation of the density of solid particles of samples when poured into the pycnometer at random masses. We will consider a pathway for evaluating the density for one sample that represented a method taken for the remaining samples.

With the volume of the pycnometer corrected as prescribed in section 3.2.2. different amount of solid particles of the sample was poured into the pycnometer and weighed, the mass of the pycnometer with the solid particle of sample on it was recorded for further calculation. Because the total volume of the pycnometer was corrected as demonstrated in the previous section, distilled

water was filled into the pycnometer with solid particles of the sample to the top indication of the pycnometer, in return was weighed and the mass was recorded. The mass of distilled water added in a pycnometer that was containing a weighed amount of solid particles of the sample was known by the subtraction of the total mass of pycnometer, amount solid particles, and distilled water to the pycnometer with the amount a solid particle of a sample. The mass of distilled water added into the pycnometer with solid particles of the sample was converted into the volume unit as a volume of distilled water added to the pycnometer with several solid particles of a sample. This volume of distilled water was calculated by dividing the mass of distilled water added into the pycnometer with the number of solid particles of sample to the density calculated in section 3.2.1.

For the reason that pycnometer was corrected to a true volume as the total volume of the device, the volume of solid poured in the pycnometer was find by the subtraction of the true volume of the pycnometer to the volume of distilled water added. This way, the weighed mass of solid particles of the sample was divided by the volume of solid particles of samples for the evaluation of the density of the sample. It was in this manner that the densities of all samples collected in the main laboratory in the Discipline of Chemical Engineering were determined.

3.2.4. Classification of samples according to Geldart Groups

Two physical proprieties of solid particles of sample collected have helped to categorize the solid particle of samples into Geldart Group; the size of solid particles of samples collected and their respective densities. The collected samples were named as sample 1 represented sand with a particular size, sample 2 represented sand with a particular size, sample 3 represented powder with a particular size, and sample 4 represented white powder with a particular seize. As we have demonstrated in the previous sections, each sample was subject to the size distribution analysis for the determination of the size of the samples, and a laboratory methodology was undertaken to calculate the density of each sample. Care was taken for reproducibility of the results when the sample was under investigation. Thereafter, many runs were considered to obtain a single result.

3.3. Process description for the recalibration of rotameters and calibration of the fluidized Beds

Figure 3.2 below is the arrangement of rotameters used in measuring the flow of dry air during the fluidization of solid particles and nanoparticles. The devices were situated in the main laboratory, Discipline of Chemical Engineering, Howard College, University of KwaZulu-Natal.

Figure 3. 2**: a set of rotameters on the line to the fluidized beds**

Our process equipment possessed a set of rotameters on the line to the fluidized bed columns, these flow meter devices were necessary to quantify the flow from the compressed air into the fluidized bed's columns. Precision should be taking into consideration because air velocity to the fluidized bed column was an important parameter to pay intention to on the line to the rotameters, compressed air had to pass through a certain pressure that was able to be read on a pressure gauge device installed on the line.

To ensure that the present operating condition was satisfactory to the previous condition on the equipment, the emphasis was directed to recalibrate first before the start of the collection of any experimental data set from any fluidized-bed subjected on the line from rotameters.

On the panel of the set of the rotameters, three calibration equations were in a script from the calibration of rotameters at operation conditions performed in the previous experiment. Three different rotameters were calibrated that corresponded to three different calibration equations. Rotameter 1, rotameter 2, and rotameter 3 as prescribed on the panel were mentioned the calibration equations of $5.4r + 10.83$; $37r + 94.6$ and $98r + 285.3$ respectively. The symbol r on the calibration equation stands for the reading from any rotameter on the line to the fluidized bed columns.

The importance of recalibrating the rotameters on the line to the fluidized bed was to verify the present operating condition to the previous. This condition could differ from the previous in term of the longevity on the standby of the equipment before use in the present project; the disturbances due to phenomenon such as the vibrations on the surrounding of the equipment, the consideration of attaining the precision and accuracy in the recalibration of the equipment before producing the calibration equations, the consideration of human error during calibration and proper standard devices chosen during the calibration process.

All these aspects were redirected to, first of all, investigate the deviation that could occur during the recalibration of rotameters in producing calibration equations by comparing these equations to the previous calibration equations. As the flowing medium to the fluidized bed columns was

the compressed dry air, the only available standard rotameter to measure flowing dry air that was found in the Discipline of Chemical Engineering was a small rotameter of the maximum capacity of 100 liters per minute that was necessary to measure the flow of air. This device was considered as a standard calibration device to recalibrate each rotameter on the line to the fluidized bed columns.

3.3.1. Description of the recalibration of the rotameter 1

The source of the compressed dry air to the fluidized bed through the rotameters was at high pressure flowing through a pressure regulator which served to control the operating pressure of the rotameters. A pressure gauge to the rotameters was reading the pressure on the line. The recommended pressure inscribed on the board of the set of rotameters was 140 kPa. The three rotameters were calibrated previously at 140 kPa. The outlet from rotameters was split into three stream; the first stream directed to three different fluidized beds that could be used at different time, the second stream supplied dry air to a big diameter fluidized bed if in use, and the last stream going to the Vibro-fluidized bed. For the recalibration purpose, the process was maintained at the same operating condition as previously. Before recalibration, the pipeline from the rotameter to the fluidized bed column was disconnected and connected to a streamline of a standard rotameter of the total capacity of 100 liters per minute. Compressed dry air was allowed to flow through a pressure regulator that was read by the pressure gauge at 140 kPa. The operating condition of the present recalibration to the previous calibration was maintained in the same condition. The operating temperature and pressure were 25 degrees Celsius and 140 kPa respectively. The valve at top of the rotameter 1 was opened for the dry air to flow through it to the streamline, to the standard rotameter used to read the volumetric flow rate in liters per minute. The valve from rotameter 1 was opened, for each reading from rotameter 1 corresponding for reading on the standard rotameter. For precision and accuracy, the range of the reading from rotameter 1 was taken at a certain interval with an increment of 0.5 reading. The objective was to produce many possible readings from the rotameter 1 and standard rotameter in other to produce a relation of the reading from the rotameter 1 with the standard rotameter used for recalibration. Three different runs in the recalibration of rotameter 1 were necessary for reducing uncertainty during the recalibration process and increase the accuracy and precision of the recalibration process. Thereafter, the relation of the rotameter reading to the volumetric flowrate from a standard rotameter was producing a linear relation, a linear regression was performed on the relation of rotameter 1 reading with the volumetric flow rate of a standard rotameter used for recalibration.

3.3.2. Description of the recalibration of rotameter 2

The recalibration of rotameter 2 did not differ from the process of recalibrating rotameter 1, as the operating condition for the recalibration process was kept the same, the only change observed was that all the valves of the remaining rotameters on the line were kept closed except the valve of rotameter 2 that was subjected to the recalibration process. In the same manner, compressed dry air flowed through the pressure regulator at 140 kPa at room temperature, this was to maintain the same operating condition of the calibration of rotameters that was done in the previous experiment. In this case, the capacity of rotameter 2 was large compared to the capacity of rotameter 1, thus the recalibration of this rotameter could not be handled in the standard rotameter of the capacity of 100 liters per minute, but was performed under modification in splitting dry air flowing into different parts. The relation of the reading of the rotameter 2 of compressed air to the standard rotameter was produced after performing three different runs of recalibration for the accuracy and precision.

3.3.3. Description of the recalibration of rotameter 3

Figure 3.3 below is showing a pressure gauge on the line to the fluidized bed column. The apparatus was situated in the main laboratory, Discipline of Chemical Engineering, Howard College, University of KwaZulu-Natal.

Figure 3. 3**: a pressure gauge measuring pressure on the line and a regulator**

In the same manner, the recalibration of rotameter 3 was performed using the same procedure as for the recalibration of rotameter 1 and rotameter 2. Care was taken to keep the operating condition the same for all process of recalibration. For example, for any change or deviation on the pressure reading on the pressure gauge on the line through rotameter, the regulator was controlled by opening or closing the valve to maintain the operating pressure at 140 kPa.

This recalibration was done in the present condition such that the producing calibration equation may be compared to the equation of the previous calibration. The operating condition can be changed; especially the operating pressure of the rotameters can be adjusted to any pressure according to the desired operating condition of the rotameters. In recalibrating the rotameters to the line to the fluidized bed, the emphasis was to ensure the rate of accuracy and precision would have produced more confident in the application of calibration equations to the experimental data as the dry air velocity was a flowing medium and a primary parameter to be taking into consideration. Three runs were performed where each run of the reading of the rotameter with the reading of the standard rotameter was a plot to investigate the relation of the calibration curve.

A linear regression analysis was done on each run to produce a calibration linear equation which was used to calculate the volumetric flowrate at any reading of the rotameter. The selection of a more precise run of calibration process was chosen, after calculating a standard deviation value for each run and selected a run with a lower standard deviation. The process of linear regression applied to the calibration of all rotameters under investigation of the calibration curves.

3.3.4. Description of the calibration of the conventional fluidized bed column

Before any solid material was being exposed to the fluidization in the experiment, the fluidized bed column was subjected to the calibration to check the influence of the airflow rate flowing through the fluidized bed and the functionality of the fluidized bed. This was experimentally studied by producing the profile of the pressure at different rotameter reading in the plenum chamber of the fluidized bed, and the pressure profile above the air distributor plate of the fluidized bed, by using three pressure transducers of model S-20, P# 14071134 manufactured in Germany by WIKA supplier. One pressure transducer was connected to a pressure tap at bottom of the fluidized bed column for pressure measurement in the plenum chamber where pressure was read. This pressure transducer possessed a sensor device that sent a signal to a digital display of the model SN5500_5700_105(1749).

Figure 3.4 below is demonstrating the setup of the controller in the control room, from the left to the right, a digital display, two controllers, and a power supplier. The devices were situated in the

main laboratory, Discipline of Chemical Engineering, Howard College, University of KwaZulu-Natal.

Figure 3. 4**: a digital display on the left, at center two-controller and on the right a power supplier**

Figure 3.5 below is demonstrating the installation of electronic devices on a fluidized bed column. The devices were situated in the main laboratory, Discipline of Chemical Engineering, Howard College, University of KwaZulu-Natal.

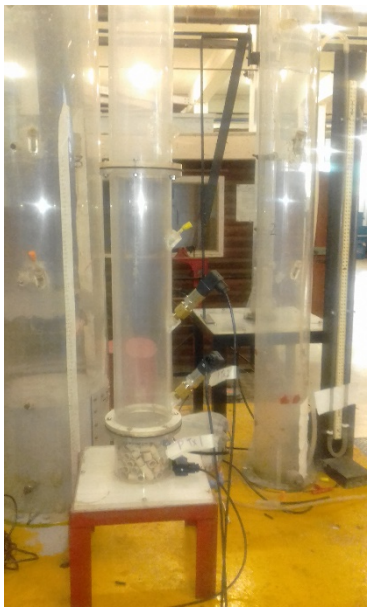

Figure 3. 5**: three pressure transducers connected to 0.12 m fluidized bed**

The pressure sampled in the plenum chamber that contained cylindrical ceramic materials of 1.5 cm in height and diameter, was displayed by the digital display device located in the control room. The second pressure transducer was located on the fluidized bed column, above the air distributor plate, and was transmitting the signal to a controller 1 of model BCS2R00-06 which was connected to a connection cable of model CMD-001. The connection cable was connected to the LapTop via a USB cable to read the pressure from BCx2 console software. The third pressure

transducer was sampling pressure reading at a pressure tap located few centimeters above the second pressure transducer, which was reading the pressure on the fluidized bed column at a third location, and the signal from the sensor was sent to a controller 2 of the model BCS2R00-06 for the pressure reading. The pressure profile on the plenum chamber was produced after measuring the dry airflow rate from the rotameters on the line to the fluidized bed. A plot of rotameter reading with the pressure display on the digital display was producing the pressure profile on the plenum chamber. The pressure increased as the rotameter reading was increased showing a linear relation.

For the same rotameter reading in the airflow rate, the same pressure profile was detected on the second and third locations of the measurement of pressure on the column that gives a profile in the fluidized bed. The pressure at second location increased the same way as a third location as the rotameter reading was increased.

3.3.5. Description of the calibration of the vibro-fluidized bed

Figure 3.6 below is a fluidized bed column connected to a vibration system and controller. The apparatus was situated in the main laboratory, Discipline of Chemical Engineering, Howard College, University of KwaZulu-Natal.

Figure 3. 6**: a vibro-fluidized bed connected to a panel controller**

The vibro-fluidized bed was a cylindrical column in plastic with 0.160 meters as an outside diameter and height of 0.49 meters. The fluidized bed is superposed on a vibration plate that is mounted with two mechanical devices on the left and right of the plate to create vibration. The mechanical devices are connected to an electronic panel where frequency and other parameters for vibration are controlled.

The vibro-fluidized bed is supported with four strings in irons in each corner of a square plate posed on top of the vibro-fluidized bed from the top and attached at the bottom at vibration plate to allow the column sustaining the vibration. The vibro-fluidized bed is connected from one of

the streams that are splitting into a stream that goes to the conventional fluidized beds, to the big column fluidized bed, and to the third stream that is connected to a vibro-fluidized bed. As prescribed in the previous section of the calibration of the conventional fluidized bed, it was important to calibrate the vibro-fluidized bed column to verify its functionality when under fluidization of solid particles. The vibro-fluidized bed composed of two parts, the first part is the plenum chamber where the air coming from the rotameter lines is distributed into the vibro-fluidized bed; and the second part that is the bed of solid particles. To verify the linearity of the pressure profile in the two parts of the vibro-fluidized bed, pressure measurement was taken while the vibro-fluidized bed was subjected to the air flowing through the vibro-fluidized bed. The reading from the rotameter 1 was recorded, and by opening the valve of the rotameter 1, the dry air flowing through the vibro-fluidized bed column was controlled and the pressure was evaluated from the plenum chamber and on the bed of solid particles. The working condition of the vibro-fluidized bed was maintained at the same condition as in the calibration of a conventional fluidized bed. The temperature and pressure of rotameter were 25 ^{o}C and 140 kPa, respectively. Two measuring devices were used to measure the pressure in the plenum chamber and the second part of the vibro-fluidized bed. In the first instance, the inverted U-tube manometers were used to measure pressure in the two-part of the vibro-fluidized bed column and the pressures transducers were used at the same condition for measuring pressure as with the inverted U-tube manometer. The vibro-fluidized bed column was calibrated in this manner, to verify the linearity of the profile in the two-part of the vibro-fluidized bed, by measuring pressures in different regions of the vibro-fluidized bed using an inverted U-tube manometer and pressures transducers.

3.3.6. Description of the calibration for the small diameter fluidized bed

A small diameter fluidized bed of 50 mm was calibrated for the fluidization associated with acoustic sound. Three pressures transducers of model S-20, P#10471134 were connected at different locations of the fluidized bed. The first measured the pressure in the plenum chamber of the fluidized bed, the second was measuring the pressure at top of the perforated plate and the third was connected on the column at a location a few centimeters above the second. All pressure transducers measured pressure in sequence as calibration was occurring. The profile in the plenum chamber shown linearity with the airflow in the fluidized bed column. In the bed of solid particles, both pressure transducers placed at different measuring tap measured the same pressure at different locations. In the bed of solid particles, the pressure at any point in the fluidized bed column proved the uniformity of air flowing through the bed solid particles when calibrated.

3.3.7. Sensitivity analysis of digital display and controllers

The electronic conversion of the pressure from the plenum chamber was displayed by a digital display. The sensitivity of the digital display was checked by setting the device in the range such that the smallest pressure reading might be displayed by the pressure transducer connected to a pressure tap in the plenum chamber. This check was verified by controlling the flow of the air to the fluidized bed using one of the smallest rotameter on the line of the fluidized bed with the controllers. The pressure that was reading in the plenum chamber by opening the valve of the rotameter 1, produced a pressure profile from the reading of the pressure by the digital display device, using the same reading of rotameter 1. When the valve is open and allows the air to flow into the air distributor chamber, a pressure profile was obtained from the reading of the pressure from controller 1 and controller 2.

3.4. Process description for pressure measurement on the fluidized bed column

The reading of the pressure on the fluidized bed column was assisted by the use of inverted U-tube manometers and pressure transducers. The conventional fluidized bed consisted of a cylindrical tube of 0.12 m in outside diameter and 0.49 m in height. The plenum chamber of the fluidized bed column was measuring 9 cm. The plenum chamber was packed with cylindrical materials in ceramic of 1.5 cm in height and diameter. The pressure necessary to fluidized any materials in the column was controlled from the packing materials in the plenum chamber. It was for important to measure the pressure in the plenum chamber to investigate a pressure profile in that section of the fluidized bed, as the first location for pressure measurement was in the plenum chamber. The other section of the fluidized bed was the region of the bed of solid particles. In this second section, the location for pressure measurement was at a distance of 3.5 cm above the air distributor plate, and the third location for pressure reading was at a distance of 20.5 cm above the air distributor plate. The measuring devices used in the experiment were necessary to recalibrate the rotameters and calibrate the fluidized beds. In the collection of experimental data, the prescribed measuring equipment was used for pressure measurement form the fluidized beds. Besides the use of pressure transducers as electronic devices for pressure measurement on the fluidized beds, the inverted U-tube manometers were in use also for measuring the pressure at different locations of the fluidized beds.

3.4.1. Inverted U-tube manometers

Figure 3.7 below is showing a set of inverted U-tube manometers. The assembly was mounted in the Discipline of Chemical Engineering, Howard College, University of KwaZulu-Natal.

Figure 3. 7**: A panel of a set of four inverted U-tube manometers as a pressure-measuring device**

It has been proposed to use the inverted U-tube manometers as devices for pressure measurement in the process of fluidization of samples. The inverted U-tube manometers were attached on a standing board where one leg of an inverted U-tube manometer was connected to the fluidized bed in the region, where the pressure measurement was under investigation and the other leg was connected to another region of pressure measurement.

The tubes were in a glass of length of 110 cm. The standing board constructed in the wood was contained four inverted U-tube manometers used in the process of fluidization. The piping connection that connected the legs of the inverted U-tube manometers to the regions chosen for pressure measurement on the fluidized bed was filled with tap water such that some quantity of water will occupy the tube for the reading of the pressure. Once the fluidized bed in operation, the air as the fluidizing medium that is flowing in the section of the fluidized bed where pressure measurement is desired, then the water occupying the glass tubes of the inverted U-tube manometer will be shifted from its initial position to a new position indicating the measure of the head. This head was converted to pressure by multiplication of the effect of acceleration by gravity on the water in the tubes to the air as a flowing medium in the tubes producing a measured pressure at the chosen region.

3.4.2. Pressure transducers

The measuring devices other than the inverted U-tube manometers, three pressures transducers of model S-20, P# 14071134 was in the use of the pressure measurement for the fluidization process. Each pressure transducer was possessing a sensor that was able to read from at fluidized bed and sending the signal to the controllers. Three different locations of the pressure measurement on the

column were located. The first location for the pressure measurement was placed in the plenum chamber where one pressure transducer was reading the pressure, the sensor from the pressure transducer has transmitted the signal to the control room where the pressure was display electronically from a digital display of model SN5500_5700_105(1749). The plenum chamber was 9 cm in height. The chamber was packed with a cylindrical material of 1.5 cm in height and diameter. A connection pipe measuring 7.5 cm was connected to a pressure transducer from the plenum chamber where pressure was measured. In the fluidized bed, the pressure was measured from a location 3.5 cm above the air distributor plate; a connection pipe measuring 51.5 cm from the fluidized bed to the pressure transducer was reading pressure at the location. This pressure transducer connected to a sensor was sending a signal to the control room where the pressure was display electronically from a controller named controller 1 of model BCS2R00-06; a connection cable of model CMD-001 from controller 1 linked to a USB cable that was connected to the LapTop was reading the pressure using a BCx2 console software installed on the Laptop. At a distance of 20.5 cm above the air distributor plate, the third pressure transducer was connected at a sampling tap on the fluidized bed column to measure the pressure; this pressure transducer was connected to a controller 2 of the model BCS2R00-06 located in the control room. The reading of the pressure from this controller was read from the controller itself.

3.5. Fluidization of solid particles using a conventional fluidized bed

Four different samples were tested in the conventional fluidized bed to investigate the behavior of the fluidization of the samples, the test was performed on a column of 0.12 m of outside diameter and 0.49 m in height. Different samples were exposed in the fluidized bed column at different height as initial height. The air velocity was controlled from the rotameters for the flowrate of superficial velocity to the fluidized bed column. The air flowing into the plenum chamber was measured by the inverted U-tube manometers or a pressure transducers model S-20, this pressure transducer was sending a signal to a digital display that was linked to a control room. The samples in the fluidized bed column were influenced by the increase of the flow of superficial velocity from the rotameter that was in use. Thereafter, while the bed of solid particles was subjected to the influence of the superficial velocity by increasing the rotameter reading, the change in height of the bed, the reading of the pressure above the air distributor plate from pressure transducer model S-20, connected to a controller 1 and the reading of the pressure above the bed of the solid particles in the bedchamber, transmitted by a pressure transducer model S-20 to connected to a controller 2 were recorded simultaneously. In the same manner, when an inverted U-tube manometer was used for pressure measurement during fluidization, one leg of the inverted U-tube manometer was connected in the plenum chamber and the second leg was

placed in the region above the air distributor plate. For each rotameter reading, a change in height of the bed of the solid, the pressure in the plenum chamber, the pressure above the air distributor plate, and the pressure above the bed of the solid in the bedchamber were recorded.

3.5.1. Determination of fluidization parameters

The all-purpose of fluidization of solid particles was to relate the meaning of parameters to the objectiveness of the investigation. In our case, minimum fluidization velocity, voidage, and height from fluidization of samples will distinguish them irrespective of their Geldart'group, their fluidization will be observed differently by investigating the minimum fluidization velocity, voidage, and height.

3.5.1.1. Graphical representation for the minimum fluidization parameters

Each sample was subjected to the fluidization process where a weighed quantity of samples is under fluidization reaching an initial height before studying their fluidization. Depending on the type of pressure measuring devices, the measuring devices will be placed on the fluidized bed column before solid material is in the fluidized bed. For every reading of the rotameter depending on the size of material in the fluidized bed, any change in height will be recorded including the pressure in different location of a different part of the fluidized bed; the sampling of the pressure measurement will be located in the plenum chamber, above the air distributor plate and above the bed of solid materials. Depending on the rotameter chosen on the line, reading on the rotameter will produce a reading on the measuring pressures devices. The experiment data was composed of a range of rotameter reading, vary in the height of the bed and pressure from these three locations; plenum chamber, above the air distributor plate, and above the bed of solid particles. The air velocity with the vary of the height of the bed has produced a relation on the fluidization of the sample, in the same manner, the rotameter is open in an increment of 0.5 in the reading, the height of the bed of solid particles, the pressure in the plenum chamber, the pressure on the bed of solid particles and above the bed are controlled by the measuring pressure devices. The region of concern was the region above the perforated plate where the pressure profile on the bed of solid materials had to be produced during the fluidization process. A plotting of measured pressures with the air velocity produced a profile of the fluidization of the samples. Graphically, the minimum fluidization velocity will be read from the plotting of pressure drop on the bed of solid material with the superficial velocity. The minimum fluidization voidage will be computed from

the volume of the bed at minimum fluidization condition. The height of the bed at minimum fluidization will be measured from the fluidized bed at minimum fluidization condition.

3.5.1.2. Empirical representation of the minimum fluidization parameters

Correlations such as that described by Kunii and Levenspiel (Kunii and Levenspiel, 2013) for the minimum fluidization velocity and voidage were applicable. The minimum fluidization velocity described in the referenced book is for the case of very small particles, in this correlation, the three parameters from the solid particles are necessary; the measured density of the solid particle of the sample, the diameter of a solid particle of the sample and the correcting factor for the effective diameter called sphericity of the solid particles. These parameters are measured and incorporated in the correlation described by Kunii and Levenspiel. For the reason that fluidization, the pressure drop remained unchanged during fluidization, the minimum fluidization voidage will be calculated from the drag pressure drop. The height at minimum fluidization is measured directly from the fluidized bed.

3.5.2. The use of Ergun correlation to the experimental data

In the experiment, the state of the bed of the solid particle move from fixed to a motion state, the theory of Ergun applied to the fluidization curve of all our samples. These correlations will be restricted in the region of a fixed bed. The plotting of the pressure and the superficial velocity in the region of the bed of the solid particles was plotted with the calculated pressure from the Ergun correlation. As our operational pressure will not be as higher as we could think of and that we will be dealing with air as flowing medium in the fluidized bed, the last term in the Ergun correlation was neglected when plotting the calculated pressure from Ergun.

3.6. Process description for fluidization of solid particles using vibro-fluidized bed

The vibro-fluidized bed is comprised of a cylindrical column 0.16 m in outside diameter and 0.49 m in height. The configuration of the column is described in section 3.3.5. the fluidization of the sample as a test to the vibro-fluidization for the nanoparticles materials was performed by applying vibration to the fluidized bed column with frequency in the fluidization of 0 and 250 rpm. Solid particles were subjected under fluidization at an initial height of 10 cm as a height of the solid bed. To run the test in the vibro-fluidized bed, two samples were selected; sample 3 and

sample 4. Firstly, the fluidization of samples was investigated with no vibration on the fluidized bed column, thereafter vibration was applied to the fluidized bed. In the run with no vibration, the air from the rotameter was supplied to the fluidized bed and the bed expansion was recorded. The pressure measurement in the plenum chamber and above the air distributor plate was recorded by means of inverted U-tube manometers and pressure transducers of model S-20. In the vibration condition, the fluidized bed column was under vibration before air is being supplied to the fluidized bed. The air from the rotameter was increased until all bed of solid particles was fluidized keeping the vibration parameters constant. A hysteresis was done on the fluidization of solid particles in the vibro-fluidized bed in decreasing the flowing air from the rotameter from the maximum reading to the minimum.

3.6.1. Determination of fluidization parameters

Fluidization parameters such minimum fluidization velocity, minimum voidage, bed expansion, voidage after minimum fluidization condition depends on the variable parameter, this parameter is the air velocity from rotameters. The existing relation between this parameter and the measuring pressure in the plenum chamber and above the air distributor plate produces profiles that are useful in finding the minimum fluidization velocity, minimum fluidization voidage, and bed expansion at minimum fluidization condition. The graphical representation of the minimum parameters will be observed at minimum fluidization condition after measurement of variables such as superficial velocity and pressure drop on the bed of the solid particles during fluidization. The comparison of these minimum fluidization parameters from graphical representation during fluidization will be done with results from the empirical correlation from the literature.

3.6.2. The measure of the sphericity from the experiment using the vibro-fluidized bed

The sphericity of the solid particle can be measured from the experiment during fluidization after correlating the Ergun equation to the measuring pressure. The measure is obtained by fitting the Ergun equation to the experiment as sphericity is a parameter in the equation correcting the diameter of the solid particles. The pressure drop on the bed of solid particles obey the Ergun equation as the bed still fixed, because the measurement is obtained by the aid of the precise devices such as pressure transducers. This parameter will be correctly estimated by adjusting it to the experiment pressure drop. In this manner, after vibro-fluidization with no vibration and with the vibration of sample 3 and sample 4, the sphericity will be investigated to observe the effect of

vibration on the sphericity of samples 3 and 4. A linear regression on the bed of solid particles while it still fixed before the fluidization of the bed occurs will be performed, the slop from the straight line from the regression is the coefficient of the superficial velocity of the Ergun equation where the sphericity is the only unknown parameter. Noting that the important measuring parameters in the calculation of sphericity from the experiment are the superficial air velocity and the pressure drop on the bed of the solid particles during fluidization.

3.7. Process description for the fluidization of nanoparticle using acoustic sound fluidized bed

Figure 3.8 below is showing the configuration of a fluidized bed column linked to an acoustic sound. The apparatus was situated in the main laboratory, Discipline of Chemical Engineering, Howard College, University of KwaZulu-Natal.

Figure 3. 8**: a configuration of fluidization enhanced by acoustic sound**

A 0.12 m diameter fluidized bed was chosen to associate with the acoustic sound for the fluidization of nanoparticles. The fluidized bed was 0.49 m in height. A line from the set of rotameters was connected to the fluidized bed associated with acoustic sound where the airflow was controlled through the rotameter.

A speaker was placed at top of the fluidized bed to produce waves from the sound coming from a 2 MHz function generator of model ALP-1614B, the working range of the frequency of the sound to the fluidized bed was from 0 to 200 Hz. The sound from the 2 MHz functional generators was sent to a speaker placed at top of the fluidized bed before the circulation of the flowing air through the fluidized bed.

Figure 3.9 below is a 2 MHz function generator of model ALP-1614B, a digital display, and controllers. The devices were situated in the main laboratory, Discipline of Chemical Engineering, Howard College, University of KwaZulu-Natal.

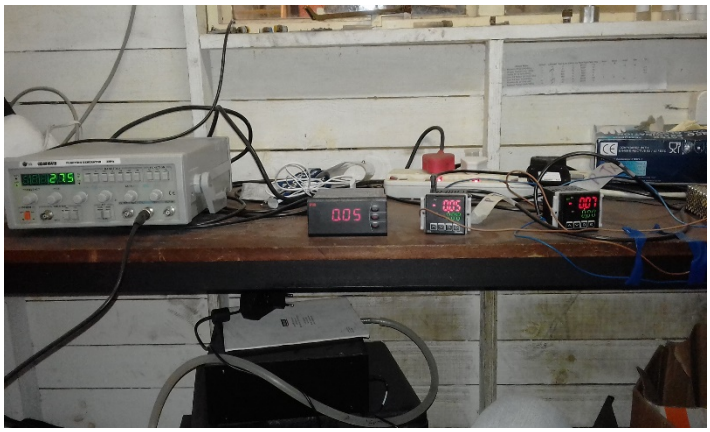

Figure 3. 9**: a 2 MHz function generator of model ALP-1614B, a digital display connected to one pressure transducer reading pressure from the plenum chamber, a controller connected to a pressure transducer reading pressure on the bed of nanoparticles, and the third controller connected a pressure transducer reading pressure above of the bed of nanoparticles**

The processes for measuring devices were three pressure transducers of model S-20, they were connected at different measuring pressure tap on the fluidized bed. The first in the plenum, the second above the perforated plate, and the third few centimeters above the second. All pressures measuring devices were connected to controllers where pressure was recorded during fluidization. After, the air was allowed to flow through the fluidized bed column by controlling the flow from a rotameter 1.

Figure 3.10 below are images from TEM analysis. pictures were taken at the microscopy and micro-analysis unit, Westville Campus, University of KwaZulu Natal.

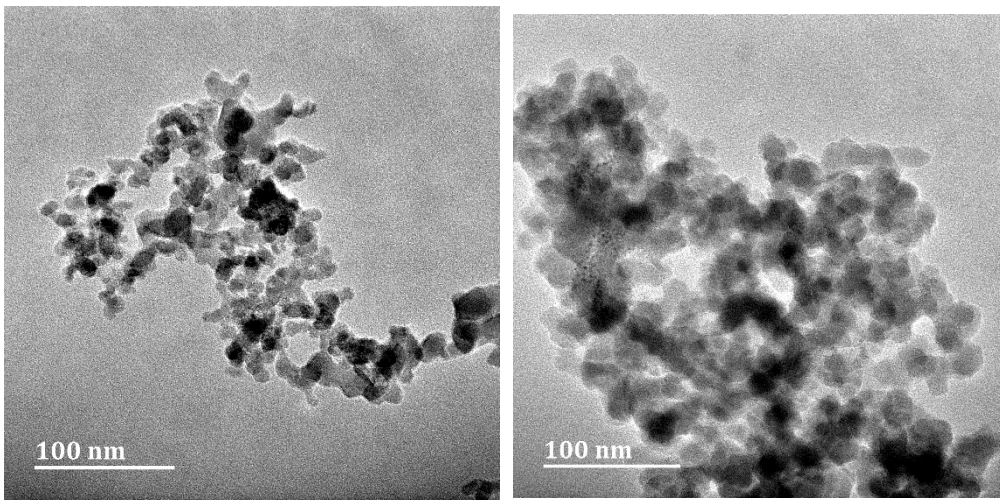

Figure 3. 10**: TEM image of 13 nm Al_2O_3 on the left and TEM image of 10-20 nm SiO_2, picture captured at microscopy and micro-analysis unit at the University of KwaZulu-Natal-Westville campus**

3.7.1. Determination of the fluidization parameters

The minimum fluidization velocity, voidage, and height should be determined after reproducing a graphical plotting of the superficial velocity and pressure measured on the bed of nanoparticles. The minimum fluidization velocity can be easily interpreted when the pressure on the bed of nanoparticles remained unchanged during acoustic sound fluidization. From the model of the mass of the bed of nanoparticles when it is at rest with its mass when it under acoustic fluidization, it has been demonstrated that the voidage was related to the ratio of the initial height of the bed to its change in height. As the acoustic fluidization of nanoparticles was falling under agglomerate particulate fluidization, the Richardson and Zaki correlation became applicable. The equation was linearized after substitution of the relation of initial voidage with the ratio of initial height to the height of the bed of nanoparticles. This relation was obtained from a simple model of the mass of the bed of nanoparticles at rest and fluidization state. From a linear regression curve, an initial voidage of nanoparticles was calculated, this in return, allowed the calculation of the voidage as the bed of nanoparticles expanded.

3.7.2. Determination of the size of agglomerates nanoparticles from Stokes' Law

A mathematical representation of the size of the agglomerated nanoparticles can be obtained after calculation of the diameter of the agglomerated from Stokes' Law. The application of the equation is an approximate evaluation of the average size of agglomerates after fluidization and not the exact size of the nanoparticles. The method not taken in the experiment was the in situ measurement of the size of the agglomerates nanoparticles, this technique could produce an exact size of the agglomerates.

3.8. Process description of fluidization of nanoparticles using vibro-fluidized bed

A vibro-fluidized bed is used to investigate the fluidization of nanoparticles enhanced by vibration, it was equipped with a control panel where the frequency of the vibration is controlled. Nanoparticles materials were poured into the vibro-fluidized bed; the fluidization of nanoparticles was occurring in a 0.5 meters in height and 0.16 meters in diameter, thereafter a frequency of 250 rpm was applied to the fluidized bed to initiate the vibration of the fluidized bed. One pressure transducer of model S-20 was connected to the measuring tap in the plenum chamber and another pressure transducer of the same model was connected on the measuring tap located on the bed of nanoparticles. All these pressures measurement devices were sending a signal to controllers

located in the control room hut 2 where pressures were displayed. One was reading the pressure from the plenum chamber displayed from a digital display device and the other was reading the pressure from the bed of the nanoparticles displayed from a controller connected to a LapTop. Before the fluidization, a vibration was applied to the fluidized bed, thereafter, a fluidizing medium was allowed to flow through one of the rotameter. The reading from the rotameter was recorded including the bed expansion of nanoparticles and the pressures on the plenum chamber and the bed of the nanoparticles.

3.9. Sedimentation of nanoparticles

The sedimentation behavior of nanoparticles was investigated from the batch settling test. This test was performed using measuring cylindrical tubes containing tap water. Nanoparticles were weighed and immersed in a measuring cylindrical tube containing tap water. The behavior of nanoparticles in tap water was observed after 1 hour of immersing nanoparticles in tap water and after 3 days. The observation was done by taking photographs of a measuring cylindrical tube containing nanoparticles at each time of observation. The images were taken to distinguish and observed the trend of the behavior of nanoparticles in tap water at different times. After the observation of nanoparticles in tap water, settled nanoparticles were filtered using a filter paper, and allowed nanoparticles to dry for weigh.

4. RESULTS AND DISCUSSION

4.1. Sieving Analysis

Some of the samples of solid particles were collected from the Discipline of Chemical Engineering for the investigation of the fluidization behavior, the samples were named as sample 1, 2, 3 and 4. By visualizing the samples, we were able to distinguish them from their sizes of solid particles. Thus a particle size distribution analysis was necessary to determine their sizes. And the measurement of their particular density was necessary to group the samples according to their classification as referenced by the Geldart group chart.

The methodology of the size distribution analysis of the samples is explained in more detail in section 3.1 of chapter 3.

4.1.1. Sample 1

The determination of the size of this sample was performed using the technique of size distribution by using the sieve analysis. A mass of 10, 20, and 90 grams was chosen as the amount of sample to be used in size distribution analysis. The total mass of the sample after the sieve analysis process was found by the summation of the mass retained in each sieve plate. Thereafter as the mass fraction of sands and powders were calculated by dividing the mass retained in each plate by the total mass that represented the total mass of the sample under investigation of the size of the sample.

Table 4.1 below shows the sieve analysis for sample 1 evaluated from the first run of 10 grams, data obtained from the sieve plates system. The apparatus is described in figure 3.1.

Table 4. 1: Sieve analysis for the first run of 10 grams for sample 1 to evaluate the size of solid particles

Size of sieve(µm)	Mass of empty sieve	Mass of sieve + sample(g)	Mass of sample(g)	d_i(µm)	Mass fraction f_i	f_i/d_i
600	322.8	324.2	1.4	424.3	$1.41*10^{-1}$	$0.33*10^{-3}$
425	309.1	310.4	1.3	505	$1.31*10^{-1}$	$0.26*10^{-3}$
300	288.7	290.6	1.9	357.1	$1.92*10^{-1}$	$0.54*10^{-3}$
212	284.8	288.1	3.3	252.2	$3.33*10^{-1}$	$1.32*10^{-3}$

150	266.8	268.6	1.8	178.3	$1.82*10^{-1}$	$1.02*10^{-3}$
106	272.4	272.6	0.2	126.1	$0.2*10^{-1}$	$0.16*10^{-3}$
75	257	257	0	89.2	0	0
pan	245.5	245.5	0	53.03	0	0

For the sieve plate of size 600, 425, 300, 212, 150, 106, 75 µm and the pan, the mass retained of sample 1 was found as 1.4;1.3; 1.9; 3.3; 1.8; 0.2; 0; and 0 gram respectively when referring to table 4.1. For the accuracy of the experimental data, four different runs were completed. On the second run, the masses retained on the sieve plate were: 1.8; 1.4; 1.9; 3.2; 1.7; 0.2; 0; and 0 gram corresponding to the sieve plate of 600, 425, 300, 212, 150, 106, 75 µm and the pan. In the third run with the same set of the sieve plates, the masses retained were observed as 1.5; 1.5; 1.9; 3.1; 1.8; 0.3; 0; and 0 gram corresponding to the setup of the size of the sieve plate described above. The fourth run retained the mass on each sieve plate of: 1.5; 1.3; 1.9; 3.2; 1.8; 0.3; 0; and 0 gram. The fraction of the sample in each sieve plate represented the mass fraction used in the calculation of the sauter mean diameter. The first run, a sauter mean diameter of 275.3 µm was calculated after sieve analysis, in the second run, a sauter mean diameter of 282.2 µm, in the third run, the sauter mean diameter was 276 µm and the fourth run the sauter mean diameter was 273.3 µm. Noting that for sieve analysis mentioned in the four different runs, 10 grams of sample 1 was taken as mass for the sieve analysis.

Table 4.2 below shows the sieve analysis for sample 1 evaluated from the first run of 20 grams, data obtained from the sieve plates system. The apparatus is described in figure 3.1.

Table 4. 2: Sieve analysis for the first run of 20 grams for sample 1 to evaluate the size of solid particles

Size of sieve(µm)	Mass of empty sieve(g)	Mass of sieve + sample(g)	Mass of sample(g)	d_i(µm)	Mass fraction f_i	f_i/d_i
600	322.8	325.4	2.6	424.3	$1.29*10^{-1}$	$0.3*10^{-3}$
425	309	311.4	2.4	505	$1.19*10^{-1}$	$0.24*10^{-3}$
300	288.5	292.1	3.6	357.1	$1.79*10^{-1}$	$0.5*10^{-3}$
212	284.6	291.3	6.7	252.2	$3.33*10^{-1}$	$1.32*10^{-3}$
150	266.6	270.5	3.9	178.3	$1.94*10^{-1}$	$1.09*10^{-3}$
106	272.2	273	0.8	126.1	0.4	$0.32*10^{-3}$
75	256.9	257	0.1	89.2	$4.98*10^{-3}$	0.56×10^{-4}
pan	245.4	245.4	0	53	0	0

After four runs for the size distribution analysis with 10 grams of a sample as a typical amount of sample used in the determination of the size of sample 1, the quantity was increased to 20 grams following the same procedure as for the size distribution analysis for 10 grams of sample. For the first run with the same set up as described in the sieving analysis of the 10 grams of sample, the retained masses in sieve plate were: 2.6; 2.4; 3.6; 6.7; 3.9; 0.8; 0.1; and 0 gram, this retained masses can be referring to the table 4.2. The procedure corresponded to the same set up of the size of the sieve plate described in the sieve analysis for 10 grams of sample 1, for the second run: 3.3; 2.8; 3.6; 6.4; 3.5; 0.5; 0; and 0 gram correspondings to the same set up of the size of the sieve plate described in the sieve analysis for 10 grams, for the third run: 1.8; 2.9; 3.4; 6.5; 3.1; 0.6; 0; and 0 gram correspondings to the same set up of the sieve plate described in the sieve analysis for 10 grams, for the fourth run: 2.5; 2.5; 3.6; 6.6; 3.9; 0.7; 0.1; and 0.1 grams corresponding to the same set up described in the sieve analysis for 10 grams of sample. All these masses were used to calculate the mass fraction of the sample in each run for the determination of the sauter mean diameter. For these different four runs, the sauters mean diameter was found to be: 261.5; 277.7; 271.4; and 257.9 μm. A difference in the masses of sample 1 retained in each sieve plate was observed in the analysis for 10 grams and 20 grams. Because the emphasis was to calculate with accuracy the size of the sample, the mass of the sample to be subjected under sieve analysis was increased from 20 grams to 90 grams. The only change observed was the masses of the sample left out on each sieve plate after sieving analysis which differs from the masses left out in the sieve plate when sieving 10 grams or 20 grams. In this analysis of 90 grams, the first run covered the following masses of sample left out in each plate: 17.2; 12; 25.6; 26.1; 7.7; 1.2; 0.2; and 0 grams, this masses can be referring to table 4.3. In the second run: 17.7; 12.7; 18.2; 28.7; 11.1; 1.7; 0.2; and 0 gram. For the third run:15.9; 12.1; 15.9; 31.7; 12.1; 2.1; 0.2; and 0 gram. For the fourth run:13.9; 11; 16.3; 29.7; 16.3; 2.6; 0.2; and 0 gram. The sauter mean diameter in run 1, run 2, run 3, and run 4 were calculated to a value of 305.7; 291.7; 282.6, and 270.9 μm respectively. The expectation was to calculate the size of the sample for the mass of 10, 20, and 90 grams and having the same sauter mean diameter. Irrespective of the sieve analysis of different masses of a sample, the sauter mean diameter appeared to be at different value for all the runs of the masses of 10, 20, and 90 grams. For the calculation of the size of the solid particles of sample 1, the average on the sauter mean diameter was considered and the size of a solid particle of sample 1 was determined to be equal to 277.2 μm.

Table 4.3 below shows the sieve analysis for sample 1 evaluated from the first run of 90 grams, data obtained from the sieve plates system. The apparatus is described in figure 3.1.

Table 4. 3: Sieve analysis for the first run of 90 grams for sample 1 to evaluate the size of solid particles

Size of sieve(µm)	Mass of empty sieve(g)	Mass of sieve + sample(g)	Mass of sample(g)	d_i(µm)	Mass fraction f_i	f_i/d_i
600	322.8	340	17.2	424.3	$1.91*10^{-1}$	$0.45*10^{-3}$
425	309	321	12	505	$1.33*10^{-1}$	$0.26*10^{-3}$
300	288.5	314.1	25.6	357.1	$2.84*10^{-1}$	$0.8*10^{-2}$
212	284.6	310.7	26.1	252.2	$2.9*10^{-1}$	$1.15*10^{-3}$
150	266.6	274.3	7.7	178.3	$0.86*10^{-1}$	$0.48*10^{-3}$
106	272.2	273.4	1.2	126.1	$0.13*10^{-1}$	$0.11*10^{-3}$
75	256.9	257.1	0.2	89.2	$2.2*10^{-3}$	0.25×10^{-4}
pan	245.4	245.4	0	53	0	0

4.1.2. Sample 2

Because the procedure for the determination of the size of solid particles for the samples did not differ, we have used the same methodology described in chapter 3 section 3.1.1.1. For sample 2, the choice for the setting up of the sieve plates depended on the first observation of the size of solid particles, in this regards, the same set up of the sieve plate mentioned in the analysis of sample 1 remained the same as used in the sieve analysis of sample 2. 600; 425; 300; 212; 150; 106; 75 µm and the pan were sieves superposed for the sieve analysis process. To keep the same trend and accuracy on the collection of the experimental data, four runs were used in the determination of the size of sample 2. Each run covered the masses retained in each sieve plate. 10 grams of sample 2 was chosen for the sieve analysis, in the first run, the masses of sample retained were: 4.7 grams in the sieve plate of 600 µm, 3.5 grams in the sieve plate of 425 µm, 1.5 grams in the sieve plate of 300 µm, 0.1 grams in the sieve plate of 212 µm, 0 gram in the sieve plate of 150 µm, 0 gram in the sieve plate of 106 µm, 0 gram in the sieve plate of 75 µm and 0 gram in the pan. This can be seen easily by reading table 4.4**.** In the second run, the masses retained in each sieve plates corresponded to 4.2 grams in the sieve plate of 600 µm, 3.5 grams in the sieve plate of 425 µm, 2.1 grams in the sieve plate of 300 µm, 0.1 grams in the sieve plate of 212 µm, 0 gram in the sieve plate of 150 µm, 0.1 grams in the sieve plate of 106 µm, 0 gram in the sieve plate of 75 µm and 0 gram as the mass retained in the pan.

Table 4.4 below shows the sieve analysis for sample 2 evaluated from the first run of 10 grams, data obtained from the sieve plates system. The apparatus is described in figure 3.1.

Table 4. 4: Sieve analysis for the first run of 10grams for sample 2 to evaluate the size of solid particles

Size of sieve(µm)	Mass of empty sieve(g)	Mass of sieve + sample (g)	Mass of sample(g)	d_i(µm)	Mass fraction f_i	f_i/d_i
600	322.8	327.5	4.7	424.3	$4.8*10^{-1}$	$1.13*10^{-3}$
425	309.1	312.6	3.5	505	$3.57*10^{-1}$	$0.71*10^{-3}$
300	288.6	290.1	1.5	357.1	$1.53*10^{-1}$	$0.43*10^{-3}$
212	284.6	284.7	0.1	252.2	$0.1*10^{-1}$	0.04×10^{-3}
150	266.6	266.6	0	178.3	0	0
106	272.2	272.2	0	126.1	0	0
75	256.9	256.9	0	89.2	0	0
pan	245.5	245.5	0	53	0	0

In the third run, in the same way after the sieve analysis process, different masses of the sample were retained in each sieve plate and these masses corresponded to 4.7, 3.7, 1.4, 0.1, 0, 0, 0, and 0 gram corresponding to the mass retained in the sieve plate of 600, 425, 300, 212, 150, 106, 75 µm and the pan.

In the fourth run, the masses retained in the sieve plate were: 4.5µm as mass retained in the sieve plate of 600 µm, 3.6 grams as mass retained in the sieve plate of 425 µm, 1.7 grams as mass retained in the sieve plate of 300 µm, 0 gram as mass retained in the sieve plate of 212 µm, 0 gram as mass retained in the sieve plate of 150 µm, 0 gram as mass retained in the sieve plate of 106 µm, 0 gram as mass retained in the sieve plate of 75 µm and 0 gram as mass retained in the receiver.

In each run, the size of a solid particle of sample 2 was calculated as the sauter mean diameter, and for all four runs, the sauter mean diameter was calculated individually and represented to the values of 433.5; 418.4; 435.7; 435.6 µm respectively.

The mass of sample 2 was increased to 20 grams for the sieve analysis, and four runs were conducted to determine the sauter mean diameter of the sample.

Table 4.5 below shows the sieve analysis for sample 2 evaluated from the first run of 20 grams, data obtained from the sieve plates system. The apparatus is described in figure 3.1.

Table 4. 5: Sieve analysis for the first run of 20 grams for sample 2 to evaluate the size of solid particles

Size of sieve(µm)	Mass of empty sieve(g)	Mass of sieve + Sample(g)	Mass of sample(g)	d_i(µm)	Mass fraction f_i	f_i/d_i
600	322.8	331.7	8.9	424.3	$4.45*10^{-1}$	$1.05*10^{-3}$
425	309.1	317.4	8.3	505	$4.15*10^{-1}$	$0.82*10^{-3}$
300	288.5	291.2	2.7	357.1	$1.35*10^{-1}$	$0.38*10^{-3}$
212	284.6	284.7	0.1	252.2	$0.05*10^{-1}$	0.02×10^{-3}
150	266.6	266.6	0	178.3	0	0
106	272.4	272.4	0	126.1	0	0
75	257.1	257.1	0	89.2	0	0
pan	245.4	254.4	0	53	0	0

The procedure did not differ from the above to keep the accuracy and precision of the collection of the experimental data. The first run, the sieve plate retained masses of 8.9 grams in sieve plate of 600 µm, 8.3 grams in the sieve plate of 425 µm, 2.7 grams in the sieve plate of 300 µm, 0.1 grams in the sieve plate of 212 µm, 0 gram in the sieve plate of 150 µm, 0 gram in the sieve plate of 106 µm, 0 gram in the sieve plate of 75 µm, and 0 gram in the pan.

The second run, the sieve plate retained masses of 9.2 grams in the sieve plate of 600 µm, 7.7 grams in the sieve plate of 425 µm, 3 grams in the sieve plate of 300 µm, 0.2 grams in the sieve plate of 212 µm, 0 gram in the sieve plate of 150 µm, 0 gram in the sieve plate of 106 µm, 0 gram in the sieve plate of 75 µm, and 0 gram in the pan.

The third run covered the masses retained in the sieve as 8.3 grams as mass retained in the sieve plate of 600 µm, 8.1 grams as mass retained in the sieve plate of 425 µm, 3.3 grams as retained in the sieve plate of 300 µm, 0.3 grams as mass retained in the sieve plate of 212 µm, 0 gram as mass retained in 150 µm, 0 gram as mass retained in 106 µm, 0 gram as mass retained in 75 µm, and 0 gram as retained in the receiver.

The fourth run, the mass of sample retained in the sieve plate were:7.8 grams in sieve plate of 600 µm, 7.5 grams in the sieve plate of 425 µm, 3.9 grams in the sieve plate of 300 µm, 0.6 grams in the sieve plate of 212 µm, 0.1 grams in the sieve plate of 150 µm, 0 gram in the sieve of a plate of 106 µm, 0 gram in the sieve plate of 75 µm and 0 gram in the receiver.

The sauter mean diameters of the solid particle calculated when the mass of sample 2 was increased to 20 grams were equal to 440.8 µm as sauter mean diameter for the first run, 435.7 µm as sauter mean diameter for run 2, 434.5 µm as sauter mean diameter for run 3 and 422.5 µm as sauter mean diameter for run 4.

Table 4.6 below shows the sieve analysis for sample 2 evaluated from the first run of 90 grams, data obtained from the sieve plates system. The apparatus is described in figure 3.1.

Table 4. 6: Sieve analysis for the first run of 90 grams for sample 2 to evaluate the size of solid particles

Size of sieve(µm)	Mass of empty sieve(g)	Mass of sieve + sample(g)	Mass of sample(g)	d_i(µm)	Mass fraction f_i	f_i/d_i
600	322.8	365.1	42.3	424.3	$4.7*10^{-1}$	$1.11*10^{-3}$
425	309.1	337.5	28.4	505	$3.16*10^{-1}$	$0.62*10^{-3}$
300	288.6	306.5	17.9	357.1	$1.99*10^{-1}$	$0.56*10^{-3}$
212	284.7	285.9	1.2	252.2	$0.13*10^{-1}$	5.3×10^{-5}
150	266.7	266.7	0	178.3	0	0
106	272.4	272.5	0.1	126.1	$0.01*10^{-1}$	8.8×10^{-6}
75	256.8	256.9	0.1	89.2	$0.01*10^{-1}$	1.2×10^{-5}
pan	245.4	245.4	0	53	0	0

The mass was increased to 90 grams for measurement of the size of the solid particle of a sample. The above table 4.6 is showing, all four runs having the masses of sample retained in the sieve plate as run 1: 42.3, 28.4, 17.9, 1.2, 0, 0.1, 0.1, and 0 gram correspondings to the mass retained in the sieve plate of 600, 425, 300, 212, 150, 106, 75 µm and the pan, for run 2: 48, 24.3, 15.6, 1.8, 0.2, 0.1, 0.1, and 0 gram correspondings to the mass retained in the sieve plate of 600, 425, 300, 212, 150, 106, 75 µm and the pan, for run 3: 50.7, 25.1, 12.2, 1.4, 0.3, 0.3, 0.1, and 0 gram correspondings to the mass retained in the sieve plate of 600, 425, 300, 212, 150, 106, 75 µm and the pan. For run 4: 56.2, 18.5, 12.4, 2 ,0.4, 0.3, 0.1, and 0 gram corresponding the mass retained in the sieve plate of 600, 425, 300, 212, 150, 106, 75 µm and the pan.

The sauter mean diameter for all four runs after the sieving process of 90 grams of sample was found to the values of 423, 418.8, 420.8, and 413.3 µm. All runs regardless of the masses of a sample taken for sieving analysis produced the value of sauter mean diameter quite closer. By just observing the closeness of the sauter diameters of solid particle for sample 2, the solid particles for the sample 2 were homogeneously distributed. And the average sauter mean diameter for the sample 2 were found to be equal to 427.7µm.

4.1.3. Sample 3

This type of sample differs from other samples in the way that the sample by just observation was of solid particles smaller in size compared to other samples. So an adjustment on the size of sieve plates for the sieving analysis of this sample was done. The methodology remained the same as how to determine the size of the solid particles using size distribution analysis as described in the previous section. The sieve plates were superposed from 300 µm to the receiver. The proper set up comprised of the sieve plates of 300, 250, 180, 125, 90, 75, 45, 38 µm and the pan. In the same way, four different runs were conducted to calculate the sauter mean diameter of the solid particles which was representing the size of the solid particle for sample 3. On the experimental for the sieving analysis for sample 3; 10 grams, 20 grams, and 90 grams were chosen as masses to be used in the sieving equipment. In the first run of 10 grams of sample 3, solid material of this type of sample was subjected under the sieving process. The masses retained on each sieve plates were:2 grams as mass retained in a sieve plate 300 µm, 0.9 grams as mass retained in sieve plate of 250 µm, 2.3 grams as mass retained in sieve plate of 180 µm, 2.8 grams as mass retained in sieve plate of 125 µm, 1.3 grams as mass retained in sieve plate of 90 µm, 0.1 grams as mass retained in sieve plate of 75 µm, 0.4 grams as mass retained in sieve plate of 45 µm, 0.1 grams as mass retained in sieve plate of 38 µm and 0 gram as mass retained in the pan. For the repeatability in the sieve analysis, a second run was performed and the masses retained in the sieving plate corresponded to 0.3 grams as mass retained in sieve plate of 300 µm, 2.3 grams as mass retained in sieve plate of 250 µm, 0.9 grams as mass retained in sieve plate of 180 µm, 4.4 grams as mass retained in sieve plate of 125 µm, 1.8 grams as mass retained in sieve plate of 90 µm, 0.1 grams as mass retained in sieve plate of 75 µm, 0.2 grams as mass retained in sieve plate of 45 µm, 0 gram as mass retained in sieve plate of 38 µm and 0 gram as retained in the pan. The third run was run and the masses retained in the sieving plate were:0.4, 0.3, 0.6, 7.5, 0.6, 0.1, 0.4, 0.1, and 0 gram. The fourth run coved solid particle retained on the sieve plates of 300, 250, 180, 125, 90, 75, 45, 38 µm and the pan. The masses retained were: 1.5, 1, 1.9, 4.5, 0.9, 0, 0.3, 0 and 0 gram. In the analysis of this sieving process, the sauter mean diameter for each run were found to be: 152.3, 153.8, 153.8, 159.5 µm.

The mass of sample 3 was increased to 20 grams and in the first run, the masses retained in the sieving plates were: 1.2, 0.3, 0.6, 14.3, 3.1, 0, 0.3, 0, and 0 gram corresponding to the sieving plate of 300, 250, 180, 125, 90, 75, 45, 38 µm and the pan.

Table 4.7 below shows the sieve analysis for sample 3 evaluated from the first run of 10 grams, data obtained from the sieve plates system. The apparatus is described in figure 3.1.

Table 4. 7: Sieve analysis for the first run of 10 grams for sample 3 to evaluate the size of solid particles

Size of sieve(µm)	Mass of empty sieve (g)	Mass of sieve + sample(g)	Mass of sample(g)	d_i(µm)	Mass fraction f_i	f_i/d_i
300	280.3	282.3	2	212.1	$2.02*10^{-1}$	$0.95*10^{-3}$
250	286.6	287.5	0.9	273.9	$0.91*10^{-1}$	$0.33*10^{-3}$
180	275	277.3	2.3	212.1	$2.32*10^{-1}$	$1.1*10^{-2}$
125	275.7	278.5	2.8	150	$2.83*10^{-1}$	$1.89*10^{-3}$
90	272.4	273.7	1.3	106.1	$1.31*10^{-1}$	$1.24*10^{-3}$
75	256.8	256.9	0.1	82.2	$0.1*10^{-1}$	$0.12*10^{-3}$
45	266.9	267.3	0.4	58.1	$0.4*10^{-1}$	$0.7*10^{-3}$
38	257.9	258	0.1	41.4	$0.1*10^{-1}$	$2.4*10^{-4}$
pan	517.2	517.2	0	26.9	0	0

Table 4.8 below shows the sieve analysis for sample 3 evaluated from the first run of 20 grams, data obtained from sieve plates system. The apparatus is described in figure 3.1.

Table 4. 8: Sieve analysis for the first run of 20 grams for sample 3 to evaluate the size of solid particles

Size of sieve(µm)	Mass of empty sieve(g)	Mass of sieve + sample(g)	Mass of sample(g)	d_i(µm)	Mass fraction f_i	f_i/d_i
300	288.5	289.7	1.2	212.1	$0.61*10^{-1}$	$0.29*10^{-3}$
250	286.6	286.9	0.3	273.9	$0.15*10^{-1}$	0.55×10^{-4}
180	275.1	275.7	0.6	212.1	$0.3*10^{-1}$	$0.14*10^{-3}$
125	275.8	290.1	14.3	150	$7.22*10^{-1}$	$4.81*10^{-3}$
90	272.4	275.5	3.1	106.1	$1.57*10^{-1}$	$1.48*10^{-3}$
75	257.4	257.4	0	82.2	0	0
45	266.9	267.2	0.3	58.1	$0.15*10^{-1}$	$0.26*10^{-3}$
38	257.9	257.9	0	41.4	0	0
pan	517.2	517.2	0	26.9	0	0

The second run, the masses retained on the sieve plates were: 1.8, 4, 3.5, 8.5, 1.1, 0.1, 0.8, 0.1, and 0 gram corresponding to the mass retained in the sieve plate of 300, 250, 180, 125, 90,75,45, 38 µm and the pan. The masses remained in the sieve plate for the third run were: 2, 1.5, 5.1, 9.4,

1.4, 0.1, 0.6, 0 and 0 gram corresponding to the mass retained in the sieve plate of 300, 250, 180, 125, 90, 75, 45, 38 µm and the pan. For the fourth run, the masses retained in the sieve plate were: 1.7, 0.4, 2.3, 10.5, 2.6, 0.2, 1.6, 0.3, and 0.3 correspond to the mass of sample 3 retained in the sieve plates of 300, 250, 180, 125, 90, 75, 45, 38 µm and the pan, the sauter mean diameter for each run were find to be: 142.1, 160.4, 159, 121.9 µm. The mass was increased to 90 grams where four runs in the sieving analysis were performed. In the first run, the masses retained on the sieve plate of 300, 250, 180, 125, 90, 75, 45, 75, 45, 38 µm and the pan where; 25 grams as mass retained in the sieve plate of 300 µm, 8.6 grams as mass retained in sieve plate of 250 µm, 25.8 grams as mass retained in the sieve plate of 180 µm, 26 grams as mass retained in sieve plate of 125 µm, 3.6 grams as mass retained in sieve plate of 90 µm, 0.2 grams as mass retained in sieve plate of 75 µm, 1,0 grams as mass retained in sieve plate of 45 µm, 0 gram as mass retained in sieve plate of 38 µm and 0 gram as mass retained on the pan.

Table 4.9 below shows the sieve analysis for sample 3 evaluated from the first run of 90 grams, data obtained from the sieve plates system. The apparatus is described in figure 3.1.

Table 4. 9: Sieve analysis for the first run of 90 grams for sample 3 to evaluate the size of solid particles

Size of sieve(µm)	Mass of empty sieve(g)	Mass of sieve + sample(g)	Mass of sample(g)	d_i(µm)	Mass fraction f_i	f_i/d_i
300	288.5	313.5	25	212.1	$2.77*10^{-1}$	$1.31*10^{-3}$
250	286.6	295.2	8.6	273.9	$0.95*10^{-1}$	$0.35*10^{-1}$
180	275	300.8	25.8	212.1	$2.86*10^{-1}$	$1.35*10^{-3}$
125	275.7	301.7	26	150	$2.88*10^{-1}$	$1.92*10^{-3}$
90	272.5	276.1	3.6	106.1	$0.4*10^{-1}$	$0.38*10^{-3}$
75	257.3	257.5	0.2	82.2	$0.02*10^{-1}$	0.27×10^{-4}
45	266.9	267.9	1	58.1	$0.11*10^{-1}$	$0.19*10^{-3}$
38	258	258	0	41.4	0	0
Pan	517.3	517.3	0	26.9	0	0

In the second run, the masses retained on the sieve plate were: 37.1 grams as mass retained in sieve plate of 300 µm, 2.2 grams as mass retained in sieve plate of 250 µm, 25.9 grams as mass retained in sieve plate of 180 µm, 19 grams as mass retained in sieve plate of 125 µm, 4.1 grams as mass retained in sieve plate of 90 µm, 0.1 grams as mass retained in sieve plate of 75 µm, 0.7 grams as mass retained in sieve plate of 45 µm, 0 gram as mass retained in sieve plate of 38 µm and 0 gram as mass retained in the pan. In the third run, the masses retained on the sieve plate

were:7.1, 2.6, 43.7, 27.8, 6.4, 0.3, 1.8, 0.2, and 0 gram corresponding to the sieve plate of 300, 250, 180,125,90,75,45, 38 µm and the pan. In the fourth run, the masses retained on the sieve plates were:12.8, 2.5, 59.3, 12.5, 2.2, 0.1, 0.7, 0.1 and 0 gram corresponding to the mass retained in the sieve plate of 300, 250, 180, 125, 90, 75, 45, 38 µm and the pan. The sauter mean diameter find in a sieving analysis of 90 grams were: 181.2, 183.9, 168.3, 192.4 µm.

The variation of the different sizes of solid particles of samples can be explained by the fact that for this sample 3, solid particles a very distributed in their sizes. The average size of the sauter mean diameter of sample 3 was calculated to a value of 160.7 µm.

4.1.4. Sample 4

The setting up of the sieve plates for the sieving analysis for the determination of the size of the solid particle for sample 4 was the same as setting up of sample 1 and sample 2. The procedure performed in the sieving analysis for sample 1 and sample 2 applied to the sieving process for sample 4. The sauter mean diameter in this sample irrespective the mass under investigation to size the sample produced sauter mean diameter quite closer, for example, the sauter mean diameter for the 10 grams for the first, second, third and fourth run were found to be equal to 326.6, 331, 331.3, 332.9 µm respectively. In the sieve analysis for 20 grams, all four runs produced the sauter mean diameter of 334.1, 327.3, 344.5, and 345.4 µm each.

Table 4.10 below shows the sieve analysis for sample 4 evaluated from the first run of 10 grams, data obtained from the sieve plates system. The apparatus is described in figure 3.1.

Table 4. 10: Sieve analysis for the first run of 10 grams for sample 4 to evaluate the size of solid particles

Size of sieve(µm)	Mass of empty sieve(g)	Mass of sieve + sample(g)	Mass of sample(g)	d_i(µm)	Mass fraction f_i	f_i/d_i
600	322.9	322.9	0	424.3	0	0
425	309.1	309.7	0.6	505	$0.6*10^{-1}$	$1.19*10^{-4}$
300	288.5	295.8	7.3	357.1	$7.3*10^{-1}$	$0.02*10^{-1}$
212	284.6	286.3	1.7	252.2	$1.7*10^{-1}$	$6.74*10^{-4}$
150	266.6	267	0.4	178.3	$0.4*10^{-1}$	$2.24*10^{-4}$
106	272.4	272.4	0	126.1	0	0
75	256.8	256.8	0	89.2	0	0
pan	245.4	245.4	0	53	0	0

In the sieve analysis for 90 grams, the sauter mean diameter for each run was represented by the value of 353, 345.4, 343.4, 340.4 µm. The average sauter mean diameter that become the size of the solid particle of sample 4 was calculated and find to a value of 338 µm.

The determination of the size of the samples collected in the Discipline of Chemical Engineering was very useful in a way that the application of these value representing the size of the solid particles of samples is an important property of that is used in the many equations, the accuracy and the precision will reduce the rate of uncertainty in the calculation of parameters for the fluidization process. That way, the emphasis was on producing many experimental data in the running of the sieving analysis.

4.2. Measurement of the density for the samples

The behavior of the fluidization of the solid particles strongly depend on its physical properties such as the size and density of solid particles. These two physical properties allow the solid particles to be classified into Geldart classification where their fluidization behaviour can be predicted. This gives rise to the importance of measuring the density of the samples collected in the Discipline of Chemical Engineering. Before step on the fluidization, from the physical properties of the samples, the size of solid particles of the samples can be a group in Geldart chart where necessary correlation can be used subject on the type of fluidization the samples obey.

4.2.1. Sample 1

The density of the solid particle of sample 1 was measured in the main laboratory of the Discipline of Chemical Engineering following the methodology described in chapter 3 section 3.2. After the collection of distilled water at a particular time, the density of distilled water was found to be equal to 0.972 g/ml at 27 ºC.

The density of solid particle of the sample was measured using a pycnometer where the volume was always corrected using distilled water, in this regard, the corrected volume of the pycnometer without a solid particle of the sample was weighed to a value of 307 ml. Four runs were performed for the measurement of the density of sample 1, where the masses of the solid particle of sample 1 were taken randomly. In the first run, the mass of solid particle of sample 1 was weighed to a value of 155.4 grams, in the second run, the mass of the sample 1 was 96.5 grams, the third run the mass of the sample 1 was 153.3 grams and the fourth run, the mass of sample 1 was weighed

to a value of 243 grams. As described in chapter 3, Section 3.2, the densities in the first, second third, and fourth run remained unchanged to a value of 2.6 g/ml.

4.2.2. Sample 2

The methodology for measuring the density of solid particles of samples applied to all solid particles of a sample that have been collected.

Table 4.11 below shows the mass of pycnometers and the corrected volume of pycnometers. Results obtained after test.

Table 4. 11: Corrected volume of 250 ml pycnometers

Mass pycnometers(g)	Mass pycnometers + distilled water(g)	Mass of distilled water(g)	The corrected volume of pycnometers(ml)
99.1	387.1	288	296.3
106.5	405.4	298.9	307.5
102.5	407	304.5	313.3

Table 4.12 below shows the masses of pycnometers and distilled water. Results obtained after test.

Table 4. 12: The masses of pycnometers and distilled water for determination of density of the solid particle of sample 2

Mass of pycnometer(g)	Mass pycnometer + sample 2(g)	Mass sample 2(g)	Mass of pycnometer, sample 2 and distilled water(g)	Mass of distilled water(g)
99.2	205.1	105.9	452	246.9
106.6	223	116.4	476.9	253.9
102.7	212.4	109.7	474.7	262.3

The density of distilled water estimated at 27 ^{o}C did not change to the density of sample 1. The volume of pycnometers was corrected using distilled water, the first pycnometer was corrected to a volume of 296.3 ml, the second corrected to a value of 307.5 ml and the third pycnometer was

corrected to a value of 313.3 ml as referring the table 4.11; the masses of the solid particle of sample 2 weighed randomly, the first mass of solid particle of sample 2 was recorded at 105.9 grams, the second mass of solid particle of sample 2 was calculated to 116.4 grams and the third mass of solid particles of sample 2 was recorded to 109.7 grams. The density of sample 2 was measured from different pycnometer using different masses of solid particles of sample 2. It was recorded that the density of the sample in the three pycnometers to be the same as a value of 2.5 gm/ml.

From the measurement of the densities of a solid particle of samples, the last solid particle of a sample that has been considered in the measurement was the sample 2, and there was the usage of 3 pycnometers of different sizes because when the densities the sample 1, sample 3 and the sample 4 were measured in the experiment, only one pycnometer was available. The density of samples 1, 3, and 4 was measured using one pycnometer. Then thereafter, the measurement of the densities of solid particles except for the density of sample 2, the pycnometers with different size could be found in the analytical laboratory in the Discipline of Chemical Engineering. This is the main reason for measuring the density of solid particles of sample 2 in three different pycnometers having different volumes.

Table 4.13 below shows the densities of sample 2 and distilled water. Results obtained after test.

Table 4. 13: Densities of sample 2 and distilled water evaluated in a 25 ml measuring cylindrical tube calibrated at 27 degrees Celsius at a value of 0.972 gm/ml

The volume of distilled water(ml)	The volume of sample 2(ml)	The density of solid particles of sample 2(g/ml)
254	42.3	2.5
261.2	46.3	2.5
269.9	43.4	2.5

4.2.3. Sample 3

The density of solid particles of sample 3 did not change from the measurement of sample 1. The distilled water was measured at 26.8 degrees Celsius and was found to be equal to 0.992 g/ml. It was necessary to correct the volume of the pycnometer before use for accurate measurement in the density of solid particles of sample 3. In this case, the volume of pycnometers used was corrected to a value of 305.5 ml. The masses of solid particles of sample 3 was weighed and for the first run, the mass of solid particle of sample 3 was 56.2 grams, in the second run was 46.5 grams and the third run was 26.1 grams. After the measurement of the density in each run, the solid particle of sample 3 had different densities; 2.5 g/ml in the first run, 2.4 g/ml in the second

run, and 2.2 g/ml in the third run. The density of solid particles of sample 3 was considered to the average in the densities of all runs. 2.4 g/ml was the density of sample 3.

Noting that the density of distilled water was a property taken with more consideration since the collection of distilled water was occurring at a different time and the distilled water had to satisfy to the calibration property of the measuring device such as the calibration property of the cylindrical tube used to measure the density of distilled water at a particular time.

4.2.4. Sample 4

The density of distilled water in this regard was measured in a gradual cylindrical tube of 25 ml, this apparatus served in the measurement of distilled water in all types of samples collected. Because the distilled water had been collected at a particular time, its property such as temperature had to coincide with the calibration property of the apparatus used in the measurement. In this case, the gradual cylindrical tube was calibrated at 27 degrees Celsius. The density of distilled water find was 0.972 gm/ml. Several runs on the measurement of the density of distilled water were performed until the property of the distilled water became similar to the calibration property of the measuring apparatus. Three masses of sample 4 were taken for three runs; 82.5 g/ml, 114.5 g/ml, and 88.2 g/ml respectively. And the densities for the runs were: 1.7 g/ml, 1.6 gm/ml and 1.6 g/ml in each run. The density of a solid particle of sample 4 was taken at an average of the densities in each run, and the density of the sample 4 was 1.6 g/ml.

The procedure in the measurement of the density of the sample followed the methodology described in chapter 3 in the evaluation of the density of solid particles.

Table 4.14 below shows the sizes of solid particles of samples and their densities. Results obtained after test.

Table 4. 14: the sizes of solid particles of samples and their densities

Solid Particles	Sample 1	Sample 2	Sample 3	Sample 4
Size(µm)	277.2	427.7	160.7	338
Density(g/ml)	2.6	2.5	2.4	1.6

4.2.5. Classification of samples according to the Geldart group

From Figure 2.1, it is necessary to point out that after the determination of two properties of a solid particle of samples, samples were able to be classified into the Geldart group. For sample 1, the size and density find after calculation was 277 µm and 2.6 g/ml. By using the chart described

in figure 2.1, this sample was located into group B as described by Geldart chart, the density of solid particles plays a great role in the classification of the sample according to the Geldart group, since the classification of solid particles of samples depends strongly on the density of solid particle even if the flowing medium is considered in the fluidization.

For sample 2, the size and density calculated were 428 µm and 2.5 g/ml, after locating the sample on the Geldart chart, sample 2 was classified as group B. The density difference of the solid particle of sample 2 to the density of the flowing medium, in this case, dry air was depended on the density of solid particle of the sample because of the insignificant in the magnitude of the flowing medium to the density of the solid particle of sample 2.

The physical property of sample 3 was found to be 161 µm in the size of the solid particle of the sample and 2.4 g/ml as the density of the solid particle of a sample. The prediction of the fluidization characteristics of this sample followed the same trend of the fluidization of sample 1 and sample 2 as described above. This similarity in the tendency on the fluidization of sample 3 to other samples was pointed out on the physical property of sample 2. The categorization of this sample on the Geldart chart demonstrated that sample 3 belongs to group B and its fluidization could be well predicted.

Sample 4 was located on the Geldart chart as on the same procedure in classifying the samples into the Geldart group. In this manner, the size and density of the solid particle of sample 4 were 338 µm and 1.6 g/ml respectively. These two physical properties of the solid particle of sample 4 were necessary enough to categorize the sample into the chart, and sample 4 falls into group B.

It was notified that the categorization of the samples in the Geldart chart was strongly dependent on the size and density of the solid particle.

4.3. Fluidization behavior of solid particles of samples using a conventional fluidized bed

After the categorization of the samples according to Geldart chart, it has seemed necessary to investigate the fluidization behavior of the solid particle of the samples. Each sample was under fluidization process and parameters such as flow rate of the air from the rotameters, the height of the bed, and the pressures on the fluidized bed were recorded for further analysis. Each sample demonstrated its behavior which was strongly dependent on the physical property of the samples.

4.3.1. The behavior of sample 1

4.3.1.1. Fluidization of sample 1 using pressure transducers

the size and density of sample 1 were 277.190 µm and 2.613 g/ml respectively. With these two physical properties, sample 1 was categorized as group B in the Geldart chat. In this fluidization process of sample 1 using pressure transducers model S-20, P# 10471134, the first test was to fluidize the sample at the lowest height of the bed of solid particles. In this regard, a 5 cm was chosen at first as the initial height in the investigation. According to the pressure profiles from pressure transducers placed at different regions of the fluidized bed, especially the pressure profile on the bed of solid particles indicated that 5 cm as initial height could not produce a predictable result as referred to published results on the pressure profile from researchers, barring in mind that the rotameter used in this process was one of the smallest rotameter on the line. To produce some predictable pressure profile in different parts of the fluidized bed, the emphasis was to increase the height of the bed of the solid particle of the sample to a height of 10 cm. 1790.1 grams of solid particles of sample 1 was weighed on a scale and subjected under fluidization. This weight of sample 1 represented 10 cm as initial height. The weighed mass of sample 1 represented an initial voidage of 0.82.

Table 4.15 below shows the initial height, voidage, and sphericity of samples, data used in the apparatus described in figure 3.5, sample 3 is not shown because the sample could not fluidize in a conventional fluidized bed column.

Table 4. 15: showing the initial height, voidage, and sphericity of samples

	Initial height, H_o (m)	Initial voidage, ϵ_o	Sphericity, Φ
Sample 1	0.1	$8.36*10^{-1}$	$3.21*10^{-1}$
Sample 2	0.5*10^-1	$8.17*10^{-1}$	$1.18*10^{-1}$
Sample 4	0.1	$7.34*10^{-1}$	$1.69*10^{-1}$

The pressure profile in the air distributor chamber, on the bed of the solid particle of the sample and above the bed of solid materials, show that the measurement of pressure from pressure transducers model S-20, P#10471134 was predictable at 10 cm. Because the air distributor chamber was filled with packed cylindrical hollow material in ceramic, the pressure profile in this region was remaining linear for a good distribution of superficial velocity above the perforated plate. From the graph of the pressure above the air distributor chamber vs the superficial velocity as shown in figure 8.12, the observation done from the experimental data was, on the plotting of pressure drop vs the superficial velocity, at a superficial velocity of 0.028 m/s, all bed of solid

particles started to fluidized, at this condition, the minimum fluidization velocity was found to be 0.028 m/s with a minimum fluidization voidage of 0.839.

When referring to the figure of the bed expansion of sample 1 during fluidization, the bed of solid particle started to expand when a superficial velocity was above 0.03 m/s, the all bed of solid materials began to be under minimum fluidization condition when reached a superficial velocity of 0.028 m/s as a minimum fluidization velocity and the all bed of solid materials reached a minimum fluidization height of 11.2 cm. The bed of solid particles of sample 1 remained fixed at a pressure above 0.25 kPa to a pressure of 0.55 kPa and dropped before fluidization to a pressure of 0.52 kPa. From the principal of a fixed bed, the relationship of the pressure drop and superficial velocity before minimum fluidization showed a linear relationship; thus the Ergun correlation and other correlation applied to our experimental data. The pressure drop calculated from the Ergun correlation was fitted to the experimental data by adjusting the correcting factor to the diameter of the solid particle that was called the sphericity. Because the devices in the pressure measurement in different regions of the fluidized bed were highly precise, by fitting the calculated pressure drop to the experimental predicted the sphericity of the solid particle. At this exercise, a sphericity of 0.346 was found to be the sphericity of the solid particle of sample 1.

Table 4.16 below shows the sphericities of samples after fitting the Ergun equation to the experimental pressure drop, the process measurement devices used are pressure transducers of model S-20, P#10471134, and the inverted U-tube manometers, sample 3 are omitted in the table due it fluidization behavior in a conventional fluidized bed.

Table 4. 16: Measured sphericity of samples after fluidization in a conventional fluidized bed

	Sample 1	Sample 2	Sample 4
Φ from pressure transducers	$3.21*10^{-1}$	$1.18*10^{-1}$	$1.69*10^{-1}$
Φ from inverted manometers	$2.98*10^{-1}$	$0.81*10^{-1}$	$1.85*10^{-1}$

Table 4.17 below shows the minimum fluidization parameters obtained from the fluidization of samples, sample 3 is not shown in the table above due to its fluidization behavior in a conventional fluidized bed.

Table 4. 17: Minimum fluidization parameters of samples, the pressure measured using pressure transducers and inverted U-tube manometers

Pressure Transducers S-20, P#10471134	Sample 1	Sample 2	Sample 4
u_{mf} (m)	$0.28*10^{-1}$	$1.5*10^{-1}$	$0.4*10^{-1}$
ϵ_{mf}	$8.53*10^{-1}$	$8.69*10^{-1}$	$7.34*10^{-1}$
H_{mf} (m)	$1.12*10^{-1}$	$0.7*10^{-1}$	$1.09*10^{-1}$
Inverted U-tube manometers	Sample 1	Sample 2	Sample 4
u_{mf} (m)	$0.35*10^{-1}$	$1.19*10^{-1}$	$0.4*10^{-1}$
ϵ_{mf}	$8.53*10^{-1}$	$8.69*10^{-1}$	$8.3*10^{-1}$
H_{mf} (m)	$1.12*10^{-1}$	$0.7*10^{-1}$	$1.08*10^{-1}$

After the pressure was dropped from 0.55 kPa to a minimum fluidization condition, we have observed that at a pressure of 0.52 kPa, by the increment of the superficial velocity beyond the minimum fluidization velocity, the pressure was kept unchanged, and when looking the relation of pressure drop and superficial velocity measured on the bed of the solid particle of the sample when the bed of the solid expanded for minimum fluidization, there is a deviation of pressure above or below the pressure of 0.52 kPa, this could be explained by the fact that the controllers were very sensitive in displaying pressure because 0.52 kPa were keeping reproduced much time; then from the graph, we can deduce that the pressure of 0.52 kPa remained unchanged during fluidization. The bed of solid particle of sample 1 was keeping increasing after minimum fluidization condition when the superficial velocity was increased beyond the minimum fluidization velocity.

The minimum fluidization velocity was calculated using the Kunii and Lenvespiel equation for small solid materials, and in this work, the minimum fluidization velocity was computed to a value of 0.31 m/s with a voidage at the fluidization condition using the drag force equation for pressure drop in the region of fluidization; and the minimum fluidization voidage calculated was 0.819.

Table 4.18 below shows the predicted minimum fluidization parameters. Results obtained after test.

Table 4. 18: The predicted minimum fluidization parameters from Kunii and Lenvenspiel equation using sphericity computed from pressure transducers and inverted U-tube manometers

	Experimental u_{mf} (m/s)	Empirical u_{mf} (m/s) using Φ from pressures transducers	Empirical u_{mf} (m/s) using Φ from the inverted U-tube manometers
Sample 1	$0.28*10^{-1}$	$3.08*10^{-1}$	$2.65*10^{-1}$
Sample 2	$1.5*10^{-1}$	$1.13*10^{-1}$	$0.53*10^{-1}$
Sample 4	$0.4*10^{-1}$	$0.74*10^{-1}$	$0.62*10^{-1}$

	Calculated ϵ_{mf}	Experimental ϵ_{mf}
Sample 1	$8.19*10^{-1}$	$8.53*10^{-1}$
Sample 2	$7.68*10^{-1}$	$8.69*10^{-1}$
Sample 4	$6.59*10^{-1}$	$0.83*10^{-1}$

Table 4.19 below shows the initial voidages and voidages after hysteresis. Results obtained after test.

Table 4. 19: the initial voidages of samples and their voidages after hysteresis

	ϵ_o	ϵ_o after the first run
Sample 1	$8.36*10^{-1}$	$8.51*10^{-1}$
Sample 2	$8.17*10^{-1}$	$8.42*10^{-1}$
Sample 4	$7.34*10^{-1}$	$8.27*10^{-1}$

4.3.1.2. Fluidization of Sample 1 Using an Inverted U-tube Manometer

After the utilization of the pressure transducers as measuring devices for pressures in different regions of the fluidized bed, a set of 4 tubes in glasses purchased from a local supplier were used in the construction of the inverted U-tube manometers from the workshop in the Discipline of Chemical Engineering at the University of KwaZulu-Natal. An inverted U-tube manometer was connected in the region of the air distributor chamber where a pressure head was measured from one leg of the tube glass of the inverted U-tube manometer; the other leg was mounted in the region of the bed of the solid particles, in this particular manner, the pressure head was measured from the tube glass. The pressure difference between the two regions; the air distributor chamber and the bed of the solid particles represented the pressure drop in the region of the bed of solid particles. When looking at figure 8.11 in appendices, the graph showing the expansion of the bed demonstrated, the bed of solid particles fluidized when minimum fluidization of 0.035 m/s was reached. Using an inverted U-tube manometer for sample 1 as measuring devices to measure the pressure drop in different regions of the fluidized bed column, the minimum fluidization velocity interpreted from the graph did not differ with the bed expansion. The interception of the fitted lines on the graph of bed expansion in the lower and upper part demonstrate that at a superficial velocity of 0.035 m/s, the bed of the solid particles was under fluidization condition, this let to say that the minimum fluidization velocity was found to be 0.035 m/s. During fluidization, the pressure drop remained unchanged at a pressure drop of 0.30 kPa. Graphically, the minimum fluidization condition started from a bed height of 0.112 m.

It was showing that the analysis of the experimental data from using the inverted U-tube manometer fall in the same way with experimental from pressure transducers, the minimum fluidization parameters were analyzed in the same way. A linear regression on the plotting of the height of the bed and the superficial velocity was conducted to easily read the minimum fluidization velocity. The minimum fluidization voidage and height were kept the same to a value of 0.839 and 0.112 m respectively.

The pressure drop calculated from the Ergun correlation was fitted to the experimental data where the correcting factor to the diameter of the solid particle of the sample was adjusted. When utilizing inverted U-tube manometers in the process of measuring pressure on the fluidized bed, the sphericity find was 0.133.

The empirical minimum fluidization velocity was calculated by using the correlation described by Kunii and Levenspiel, the voidage at the condition of fluidization was calculated using the drag force equation for pressure drop. The minimum fluidization velocity and voidage were found to be 0.046 m/s and 0.819 respectively. The initial voidage did not coincide with the voidage after

the reading of the rotameter was in the decreasing, and the voidage was found to be 0.836 that differ to an initial voidage of 0.82.

4.3.2. The behavior of sample 2

4.3.2.1. Fluidization of sample 2 using pressure transducers

Because the target was to investigate the fluidization behavior of different samples at 5 cm, then sample 2 was under fluidization of 5 cm as initial height. 928.5 grams of sample 2 was weighed from a scale that represented 0.05 m as initial height when the bed of solid particles is fixed. The sample was sieved to a sauter mean diameter of 427.729 µm and a density of 2.515 g/ml. The pressure profile from the reading of pressure transducers model S-20, P# 10471134 above the perforated plate, on the bed of solid material of the sample represented the pressure drop on the region. This type of sample shows a better profile in pressure in the air distributor chamber during fluidization, an increase in superficial velocity during fluidization in the air distributor chamber does demonstrate a linear increase in pressure because the chamber was packed with hollow cylindrical material in ceramic. With the initial height and voidage of 0.05 m and 0.817, the bed of solid particles was under fluidization conditions when the pressure drop reached 0.4 kPa. By referring to the plotting of the pressure drop and superficial velocity, graphically, the minimum fluidization can be easily interpreted to a superficial velocity of 0.150 m/s, at the condition, the all bed of solid materials fluidized when the height was attained 0.07 m with a minimum fluidization voidage of 0.869. The bed of solid particle of the sample remained unchanged to its initial height when a superficial velocity from 0.065 to 0.150 m/s was applied to the fluidized bed during fluidization. From a fixed bed to a fluidized bed, the pressure above the perforated plate increased from 0.05 kPa to 0.40 kPa before fluidization, thereafter the pressure remained unchanged after minimum fluidization condition. From the graph produced in the measurement of the pressure above the perforated plate, experimentally the minimum fluidization velocity was recorded to 0.150 m/s. The expansion of the bed before fluidization was due to solid particles in small sizes being slightly shifted upward.

The measuring devices, in this case, was the pressure transducers model S-20 was the most accurate measuring devices used in the experiment because there were such parameters that needed to be measured, the correcting factor to the diameter of the solid particle of the sample was measured experimentally by fitting the calculated pressure drop from Ergun correlation to the experimental pressure drop. The Ergun equation fitted well to a sphericity adjusted to a value of 0.118. The measured minimum fluidization velocity and voidage were compared to the calculated minimum fluidization parameters. The use of the Kunii and Levenspiel for the small

solid particle correlation, the minimum fluidization velocity was calculated and found to be 0.053 m/s with a minimum fluidization voidage of 0.768.

4.3.2.2. Fluidization of sample 2 using an inverted U-tube manometer

In the same condition of the experiment, the measuring devices were replaced with the inverted U-tube manometers producing a pressure drop relation with superficial velocity. The minimum fluidization velocity and voidage were 0.119 m/s and 0.869 respectively. Noting that the interpretation of minimum fluidization velocity was difficult to be read on the graph. A linear regression on the expansion of the bed was performed, an intercept of the lower part and upper part of the expansion, a superficial velocity was able to be interpreted as a minimum fluidization velocity. When referring to the figure 8.16 in the appendices, the plot is showing that if a linear regression is done on the lower and upper part of the bed expansion, it is graphically observed that the all bed of solid particle started to fluidized at a superficial velocity of 0.119 m/s as a minimum fluidization velocity. It is noticeable from figure 8.16 when the bed reached 0.06 m in height, the bed of the solid particle fluidized. In this regard as compared to the pressure drop profile when utilizing pressure transducers, the produced pressure drop profile for this sample 2 deviated much. The calculated pressure drop from the Ergun equation did not fit well to the experimental data when the inverted U-tube manometer was used. From the empirical correlation described by Kunii and Lenvenspiel, the minimum fluidization velocity was calculated to 0.053 m/s quite below the measured value. And the voidage at this condition was calculated from the drag force equation of pressure drop, the value found was 0.768. Hysteresis on the pressure drop measured during fluidization, it was observed that the bed of the solid particle did not come to its initial position, the fact was that the initial voidage was different and below the voidage when the bed of the solid particle comes to the rest position after decreasing of rotameter reading and the voidage at this present position was found to be 0.842.

4.3.3. The behavior of sample 3

Amongst the samples that were collected in the Discipline of Chemical Engineering at University of KwaZulu-Natal, sample 3 was sieved to sauter mean diameter of the solid particle of 161 µm, its density was calculated using a laboratory method described in chapter 3 section 3.2.3, it has been observed sample 3 was having the smallest sauter mean diameter compared to other samples, and was described as a powder with a density of 2.535 g/ml. This powder sample was tested in a conventional fluidized bed using initials height of 5 and 10 cm. By fluidizing this sample, at 5 cm

as the initial height of the bed of solid particles, the bed of the solid particles has lifted as a plug, when the rotameter was closing, the bed of solid particle just disintegrated, when the valve of the rotameter was open after the disintegration of the bed of solid particle, the fluidized bed was filled with dust showing no sign of the bed of solid particle in motion. The sample could not be fluidized in a conventional fluidized bed; this could be explained by their physical proprieties. By looking the size of solid particles of sample 3 and its density, the sample will be classified in a Geldart group B but looking the description of the sample, it was powder, the sieve size could be a real size of aggregates of solid particles of the sample and not a size of a single solid particle. The sample could be in the form of powder with a size of 161 µm but showing different characteristics than other samples such as the predominant of forces existing between solid particles. The fluidization of sample 3 will be further tested in other fluidization enhanced by external forces such as vibro-fluidization.

4.3.4. The behavior of sample 4

4.3.4.1. Fluidization of sample 4 using pressure transducers

Solid particles of sample 4 were sieved to a sauter mean diameter of 337.960 µm with a density of a sample of 1.616 g/ml. For the investigation in the behavior of sample 4 on the fluidization, a mass of 691.2 grams was weighed and subjected under the fluidization process. This mass represented an initial height of 3.7 cm. after several runs in fluidizing of this sample, the pressure profile produced after the reading of pressure from pressure transducer located in the air distributor chamber did not show any linearity, the pressure profile on the bed of solid material did not correspond to the literature, especially in the region where the bed of the solid material was fixed. Instead of using a lower superficial velocity, For the same height of 3.7 cm, a higher superficial velocity was chosen. It was observed that the pressure profile on the bed of solid material was still not corresponding to the literature with no sign on identifying the minimum fluidization state of the bed. Because none of the reading from rotameter 1 and 2 in the fluidization of sample 4 did produce any predictable results that could correspond to the literature; an increase in the initial height of the bed of solid material was decided. 10 cm in height of the solid particle was under fluidization, this height was representing a weighed mass of 1632.7 grams. The initial voidage of the solid particles of the sample once in the fluidized bed was 0.734, thereafter the sample was under the fluidization process.

It was observed that the pressure profile in the plenum chamber during fluidization was linear. By the increase of the superficial velocity to the fluidized bed, we have observed the bed being fixed while the air was flowing into the bed of solid material from 0.015 m/s to 0.039 m/s and

started its expansion from a height of 10.75 cm. The experimental interpretation of finding the minimum fluidization parameters is by interpolating values from the plot of the pressure transmitted by pressure transducer placed on the bed of the solid materials, from the graph it can be deduced that at an air velocity of 0.04 m/s, the pressure on the bed of materials remained unchanged during fluidization. While The bed of solid materials was subjected under fluidization condition, the bed of solid materials remained fixed as superficial velocity was increased at a pressure of 0.21 kPa to 0.58 kPa and remained unchanged as airflow rate was increased. This increase in the air velocity beyond the minimum fluidization velocity promotes the expansion of the bed of solid materials. The minimum fluidization velocity graphically was found to be 0.04 m/s and the minimum fluidization voidage and height of 0.83 and 10.75 cm respectively.

As previously demonstrated in the measurement of the correcting factor to the diameter of the solid particle of the sample, the sphericity was measured experimentally by fitting the calculated pressure drop from the Ergun equation to the experimental pressure drop in the adjustment of the sphericity and the sphericity found was 0.169.

This sphericity was used in the calculation of the minimum fluidization velocity from the correlation described by Kunii and Levenspiel. And for this sample, the calculated minimum fluidization velocity was calculated to a value of 0.074 m/s quite above the measured minimum fluidization velocity. And the voidage at this condition was calculated from the drag force equation and find to be 0.659, quite below the measured minimum fluidization voidage.

4.3.4.2. Fluidization of sample 4 using an inverted U-tube manometer

As fluidization was occurring, the expansion of the bed of the solid materials in the fluidized bed was recorded at the same time with the reading of the pressure in different regions of the fluidized bed. As described previously, one leg of the tube in a glass of an inverted U-tube manometer was connected in the air distributor chamber where pressure head was collected and the other was connected in the region of the bed of the solid materials, the pressure drop in the bed of solid material was the difference in pressure in the two different legs. The fluidization process started at a pressure drop of 0.15 kPa to a pressure drop of 0.50 kPa while fixed. From this maximum pressure of 0.15 kPa, the bed of solid particles started to fluidized and the minimum fluidization velocity was measured graphically at value 0.04 m/s. At fluidization condition, the bed reached a height of 10.75 cm and the measured voidage at minimum fluidization velocity was found to be 0.83. The minimum fluidization velocity can be visualized by referring to figure 8.21 in appendices showing the expansion of the bed when pressure drops were measured using an inverted U-tube manometer. From the plot, it is observed by linearizing the expansion of the bed,

graphically speaking, the superficial velocity and the height of the bed were 0.04 m/s and 10.75 cm respectively. To validate the expression of the Ergun correlation to the experimental data, calculated pressure drops were fitted to the experimentally measured pressure drop, by adjusting the sphericity of the solid particle of the sample. After the fitting, the sphericity of the solid particle was found to be 0.185.

The empirical correlation of the minimum fluidization velocity described in Kunii and Levenspiel (Kunii and Levenspiel, 2013), the calculated the minimum fluidization velocity from the equation that is applicable for small solid particles. The calculated minimum fluidization velocity was 0.062 m/s quite above the minimum fluidization velocity find experimentally. Because the pressure at fluidization remained unchanged, the voidage at minimum fluidization condition was calculated from the pressure drop using the drag force equation. The voidage calculated from the drag equation at minimum fluidization condition was 0.659 quite below the measured minimum fluidization voidage. After hysteresis on the pressure drop measured from the inverted U-tube manometer, it was observed that after the first run of the fluidization of the sample, the voidage when the bed was read in decreasing manner and stop while the rotameters was closed was not equal to the initial voidage, in this case for an initial voidage of 0.734, the voidage after the run of hysteresis was found to be 0.827. this result proved that the bed of solid particles did not come to its initial position.

4.4. Fluidization behavior of solid particles of sample 3 and sample 4 using a vibro-fluidized bed

4.4.1. The behavior of sample 3

The fluidization of sample 3 in a conventional fluidized bed was found to be a difficult task by the fact the bed of the solid particles of sample 3 was lifted as a plug when the rotameter valve was open and the air was allowed to flow through the conventional fluidized bed. This was due to the physical properties of sample 3. The sample was sieved with a size of 161 µm. The sample was of the form of powder, the main reason for the sample not behaving in fluidizing like other samples, because the sample was a powder, and the forces existing between solid particles have affected the fluidization of the sample. These forces were having more influence on the attraction of the solid particles creating small spaces in between them, for this cause, when airflow was injected into the conventional fluidized bed, the bed of solid particles just lift as a plug, by increasing the airflow to the fluidized bed, the bed of solid particles disrupted and formed dust in the conventional fluidized bed as discussed in section 4.4.3.

The experiment was aimed at investigating the behavior of the fluidization of nanoparticle's solid particles by studying the behavior of samples collected in the main laboratory of the Discipline of Chemical Engineering in the fluidization process and observing the applicability of published correlations such as Ergun correlation. In this case; fluidization enhances by vibration was tested to two samples, sample 3 and sample 4.

4.4.1.1. Fluidization of sample 3 assisted by vibration using pressure transducers

After applying the vibration on the fluidized bed containing sample 3, it was observed the fluidization occurring for sample 3 when selecting a panel controller reading of 8 corresponding to 250 rpm. As stated above, the resistance of the sample to not fluidized in a conventional fluidized bed was overcome by applying a vibration on the fluidized bed. The forces existing in between the solid particles were disrupted and creating more space in the bed of solid particles and allowed the air to flow, thus enhancing the fluidization of sample 3 in a vibro-fluidized bed. The sample was in the form of aggregate, if it was the contrary, the sample could be categorized as part of Geldart group B where the fluidization could be similar to the other samples belonging to the group B. In this case the sample could not be fluidized in a conventional fluidized bed demonstrating that sample 3, irrespective its size was not belonging to group B but was forming aggregates of particles of the size of 161µm. The sample was tested in a vibro-fluidized bed where the vibration was kept constant as the airflow was increasing from 0.5 cm/s to 3.5 cm/s. When the pressure drop was reached 0.40 kPa, in increasing the airflow rate, this pressure drop in the bedchamber was seems to be recorded often from the controller. The height of the expanded bed of solid particles could not be recorded due to the position of the bed of solid particles in the fluidized bed when vibration was followed by the airflow to the fluidized bed. At maximum superficial velocity, the bed of the solid particles was fully fluidized, at that point, the vibration was turned off and the bed of the solid particles kept it fluidization stat for a time. The process measurement devices used in this category of the experiment was the pressure transducers. When referring to the figure 8.29, it is shown that the pressure drop on the bed of solid particles of sample 3 in the bedchamber, it was observed that the fitting of the Ergun equation in the region of a fixed bed while the sample is under fluidization state could predict the sphericity of sample 3 with uncertainty. Linear regression was performed in the region of the fixed bed where pressure drop in the region did not follow the trend of the regression line. The error of the pressure drop in the low superficial velocity to the fitted regressed line was higher compared to the error at a high superficial velocity in the fixed bed region.

4.4.1.2. Fluidization of sample 3 assisted by vibration using an inverted U-tube manometer

The process measurement in this case of the experiment was the inverted U-tube manometers. In the presence and absence of vibration, the pressure in different parts of vibro-fluidized bed; the plenum chamber, and the bedchamber during fluidization; inverted U-tube manometers were connected to the measuring pressure tap from the plenum and bedchamber of the vibro-fluidized bed. The pressure measurement during fluidization was very important, especially in the case where the fluidized bed was under vibrations causing fluctuations to the pressure measuring devices. In this manner, the vibro-fluidized bed was connected to the inverted U-tube manometers to measure the pressure in different parts of the vibro-fluidized bed. The influence of vibration on the vibro-fluidized bed was playing a major part in the fluidization of sample 3. Disruption of the bed of solid particles and dust formation during fluidization the sample 3 were not of concern when fluidization was under vibration with air flowing to the fluidized bed. The fluidized bed was under vibration at panel reading of 8 (250 rpm), and the rotameter valve was opened to allow the air to flow, vibration did interrupt forces existing between solid particles and the same behavior of sample 3 as described in this section was observed. Contrary to the previous section, the inverted U-tube manometers measured the pressure drop in the bedchamber from 0.05 to 0.23 kPa where the reading of the pressure drop kept displaying most the time at fluidization state. It was with difficulty to predict the sphericity of sample 3 in the region of a fixed bed while the sample was under fluidization state. The expectancy in the fixed bed region when superficial velocity is increasing before fluidization occurs was a linear relation of the measured pressure drop with superficial velocity on the bed of solid particles. The measured pressure drop at lower superficial velocity demonstrated a deviation on the fitted pressure drop when referring to figure 8.30.

4.4.2. The behavior of sample 4

Before the use of the vibro-fluidized bed in the fluidization of nanoparticles; aluminum oxide and silicon dioxide nanoparticles, it has been decided to test the vibro-fluidized bed with samples collected in the main laboratory of the Discipline of Chemical Engineering at University of Kwazulu Natal. Sample 4 was among the samples chosen to test the vibro-fluidized bed. Another reason for choosing sample 4 in the vibro-fluidization is that the sample was behaving differently when using 5 cm as an initial height of the bed of solid particles, it was observed that at 5 cm, the sample could not show any predictable fluidization behavior.

4.4.2.1. Fluidization of sample 4 assisted by vibration using pressure transducers

The sample was tested without and with vibration on the fluidized bed, and the vibration parameter selected in the experiment was the frequency, this parameter was the only vary parameter during fluidization of sample, the fluidized bed was subjected to a frequency of 0 rpm, 250 rpm, and 270 rpm; the other parameter such as amplitude was kept constant during vibro-fluidization. The process measurement devices in this case used to measure the pressure drop were pressure transducers.

4.5.2.1(a). Fluidization with no vibration

In fluidizing the sample without vibration, it was observed that the range of the pressure drop above the air distributor plate during the vibro-fluidization with no vibration, was between 0.07 kPa and 0.23 kPa. The bed of solid particles started to show the condition of fluidization at a superficial velocity of 0.025 m/s at 0 rpm frequency with pressure measured using pressure transducers with an initial bed height of 10 cm. By graphical observation, it was demonstrated that after a superficial velocity of 0.025 m/s, the pressure on the bed of solid particles remained constant as the air velocity was increasing in the vibro-fluidized bed of outside diameter of 0.16 m and 0.49 m as height. From the relationship of pressure drop measured using pressure transducers above the air distributor plate with the air velocity, it is shown that the sphericity that is a parameter used for empirical correlation of the pressure drop while still fixed during fluidization and for the prediction of minimum fluidization velocity using theory described by Kunii and Levenspiel, should be measured from the experiment, in this regard, the calculation of pressure drops from Ergun equation was fitted to the experiment by adjusting the sphericity as the only unknown parameter in the equation. In doing so, by measuring precisely the pressure drop using pressure transducers, the only parameter that needs to be calculate was the sphericity that was found by fitting the Ergun frictional pressure drop to the measured pressure drop. This measure of sphericity from the experiment was also obtained from the measured pressure drop by linear regression in the fixed bed region after fluidization. The sphericity obtained after the fitting of the Ergun correlation was 0.140, looked the same with the value of 0.144 obtained from linear regression.

4.5.2.1(b). Fluidization with vibration

The vibration was applied to the fluidized bed, to test the vibro-fluidization of sample 4 and investigate the effect of the vibro-fluidized bed on the minimum fluidization parameters of the sample without and with vibration. Because a test was done on the fluidization without vibration on the fluidized bed of 0.16 m as outside diameter and 0.49 m as height, to observe the effect of the vibration on the minimum fluidization parameters, a vibration was applied to the fluidized bed, a 250 rpm as a frequency in the vibro-fluidized bed column. Concern was mainly objected to the vibration and its effects on the fluidization parameters when used in different situations as with no and with vibration. It was observed that during fluidization of the sample in the vibro-fluidized bed, a range of pressure drops above the air distributor plate between 0.08 kPa and 0.21 kPa was observed. And the sample started to fluidized at a superficial velocity of 0.020 m/s, and the pressure drop remained constant until further increased in the superficial velocity. In the fluidization of sample 4 using the vibro-fluidized bed with a frequency of 250 rpm, it was observed that the bed of solid particles fluidized faster compared to the fluidization in the vibro-fluidized bed with no vibration, and the bed of solid particles in the vibro-fluidized bed with 250 rpm as frequency applied to the fluidized bed, fluidized as an all at a superficial velocity of 0.038 m/s. In further increase of superficial velocity behind 0.038 m/s, it was observed a formation of a big bubble of air forming in the bed of the solid particle as fluidizing. As mention in the previous section in the fluidization of sample 4 using no vibration on the measurement of the sphericity using the measured pressure drop from the experiment, the measure of the sphericity was done in the pressure drop from the experiment from the fluidization of the sample with the vibration of 250 rpm; the main purpose of doing this measurement in the two circumstances; measurement of the sphericity from the experiment using pressure drop in a vibro-fluidized bed with 0 frequency and 250 rpm as the frequency was to investigate if vibration would affect the sphericity of the solid particles, has it is known that the sphericity of solid particles remained the same irrespective the type of fluidization. A linear regression on the fixed bed region during fluidization was performed to calculate the only unknown parameter of the coefficient carried by the velocity in the Ergun correlation that was a sphericity. After the linear regression, it has demonstrated that the sphericity measured in the fluidization with vibration did not differ with sphericity measure during fluidization with no vibration. The sphericity measured during fluidization with vibration was 0.140 when linearizing the pressure drop in the region of fixed bed during fluidization.

4.4.2.2. Fluidization of sample 4 assisted by vibration using an inverted U-tube manometer

It was noted that besides the pressure transducers as measuring devices, inverted U-tube manometers were selected in the experiment to measure the pressure during the fluidization of

samples using different configurations of a fluidized bed. In that matter, the pressures profiles were deduced from measurement using different measuring methods of the pressure. This was increasing the rate of accuracy on the pressure measured during fluidization. The inspection of the pressure measurement in the vibro-fluidized bed was conducted with inverted U-tube manometers in the absence and presence of the vibration.

4.5.2.2(a). Fluidization with no vibration

In the same circumstances of fluidization of sample 4 with no vibration, the inverted U-tube manometers were utilized to measure the pressure drop in the bedchamber. The only challenged face during the measurement of the pressure using the inverted U-tube manometer in the vibro-fluidized bed of 0.16 m and 0.49 m as height was when the bed of solid particles was still fixed before fluidization, any increased of the rotameter reading could not produce a corrected reading on the tubes of the inverted U-tube manometers, this was because the increase of the airflow from the rotameter was not sufficient for the inverted U-tube manometer to read the pressure. This was explainable when the superficial velocity was increased during fluidization when the bed was still fixed, the inverted U-tube manometers were producing the same values in a certain range of the rotameter reading before fluidization, resulting in a profile quite not the same compared to other measuring devices such as pressure transducers. But the pressure drop in the bedchamber reached the plateau, it was observed that the pressure drop above the air distributor plate remained constant, and the superficial velocity where the pressure drop above the air distributor chamber remained unchanged was noted to a velocity of 0.26 m/s. The pressure drops were in the range between 0.05 to 0.22 kPa, and drop to 0.20 kPa where it remained constant during fluidization. The inverted U-tube manometers in this case of measuring pressure in the vibro-fluidized bed could be explained by the fact the configuration of the fluidized bed diffed to the conventional bed. The vibro-fluidized bed did not contain any material as packed material in the plenum chamber but the conventional fluidized bed has cylindrical material packed in the plenum chamber what could affect the measurement of the pressure using inverted U-tube manometer in the two circumstances of fluidization.

4.5.2.2(b). Fluidization with vibration

In measuring the pressure drop above the air distributor plate, the range during fluidization with vibration was found to be between 0.05 kPa and 0.26 kPa, the pressure drop when it reached the plateau, the bed of solid particles started to be under fluidization condition, the superficial velocity

where the pressure drop above the air distributor plate remained unchanged was find to be 0.20 m/s, in this circumstances, the inverted U-tube manometers read pressure drop in the bedchamber as well in the plenum chamber. It was noted that the reading of pressure drop in the bedchamber when the bed was still fixed during the fluidization was recorded with difficulty as the vibration was affecting the reading of the pressure due to the vibration of the connection tubing from the pressure tap to the inverted U-tube manometer leg. In the hysteresis of the pressure drop in the bedchamber, the increasing pressure drop did not match well with the decreasing pressure drop measurement which was not the case when the pressure drop was measured using pressure transducers, the cause was not on the fluidized bed but was due to the fact the vibration of the fluidized bed cause disturbances in reading pressure drop when measured using inverted U-tube manometers; the connections tubing from the pressure tap in the fluidized bed where vibration was causing small fluctuation in the tube of the inverted U-tube manometers. The reading of the pressure in the tube of the inverted U-tube manometers became difficult to visualize.

4.5. The behavior of nanoparticles in fluidization associated with eternal forces

The objectiveness of investigating the characteristics behavior of aluminum oxide nanopowder, 13 nm primary particle (TEM), 99.8% trace metals basis and silicon dioxide nanopowder, 10-20 nm particle size (BET), 99.5% trace metals basis in fluidization associated with external forces were of merger concern. In an appropriate turn, acoustic sound fluidization and vibro-fluidization of aluminum oxides and silicon dioxides nanoparticles were run in the main laboratory to observed the minimum fluidizations of the nanomaterials.

4.5.1. Acoustic sound fluidization of aluminum oxides nanoparticles

After the powder nanoparticles of aluminum oxides have been under fluidization enhanced with acoustic sound, it was observed the bed of nanomaterials expanded rapidly when the valve of the rotameter was open to permit the fluidizing medium to flow through the line. The initial height of the bed of nanoparticles was set at 15 cm and was reduced to 8 cm due to the formation of agglomerates of nanoparticles in the bed and loss of dust of nanoparticles at top of the fluidized bed. The recording of the measured variables such as bed expansion of nanoparticles, pressure in the plenum chamber of the fluidized bed, pressure on the bed of nanoparticles, and pressure above the bed of nanoparticles were reproduced after many runs. In the fifth run of acoustic sound fluidization, the bed of nanoparticles was at 8 cm. It was observed a small reading in the pressures

in different parts of the fluidized bed when aluminum oxides nanoparticles were under fluidization. The rotameter reading was open and increased with an increment of 1.

4.5.1.1. Determination of fluidization parameters

The pressure drop on the bed of aluminum oxide nanoparticles recorded after acoustic sound fluidization demonstrated a minimum fluidization velocity at a value of 0.03 m/s; the pressure drop remained unchanged when the pressure transducers recorded a pressure of 0.012 kPa. It was observed that the expansion of the bed of aluminum oxide nanoparticles started to occurred from the top of the bed to the bottom; the bed did not show any behavior as the bed remained fixed while the superficial air velocity was injected to the acoustic sound fluidized bed. And the all bed of the aluminum oxide nanoparticles fluidized entirely at a height of 9.3 cm. The initial voidage of the aluminum oxide nanoparticles in the acoustic sound fluidized bed was calculated using the Richardson and Zaki equation. During the acoustic sound fluidization of this nanoparticle, it was observed the aluminum oxide nanoparticles demonstrated fluidization of the form of agglomerate particulate fluidization thus the Richardson and Zaki accommodated the calculation of parameters such as initial voidage, minimum fluidization voidage, voidage after minimum fluidization and the terminal velocity. The plot of the velocity and the height of the bed of aluminum oxide nanoparticle from a linearized Richardson and Zaki equation shows a y-intercept representing the terminal velocity of 0.192 m/s, and an initial voidage was calculated from the plot to be 0.513.

Figure 4.1 below is demonstrating the profile of aluminum oxides nanoparticles on the portions of nanoparticles in a fluidized bed column associated with an acoustic sound at 100 Hz, the pressure drops were measured using pressure transducers, graph drawn using MatLab software.

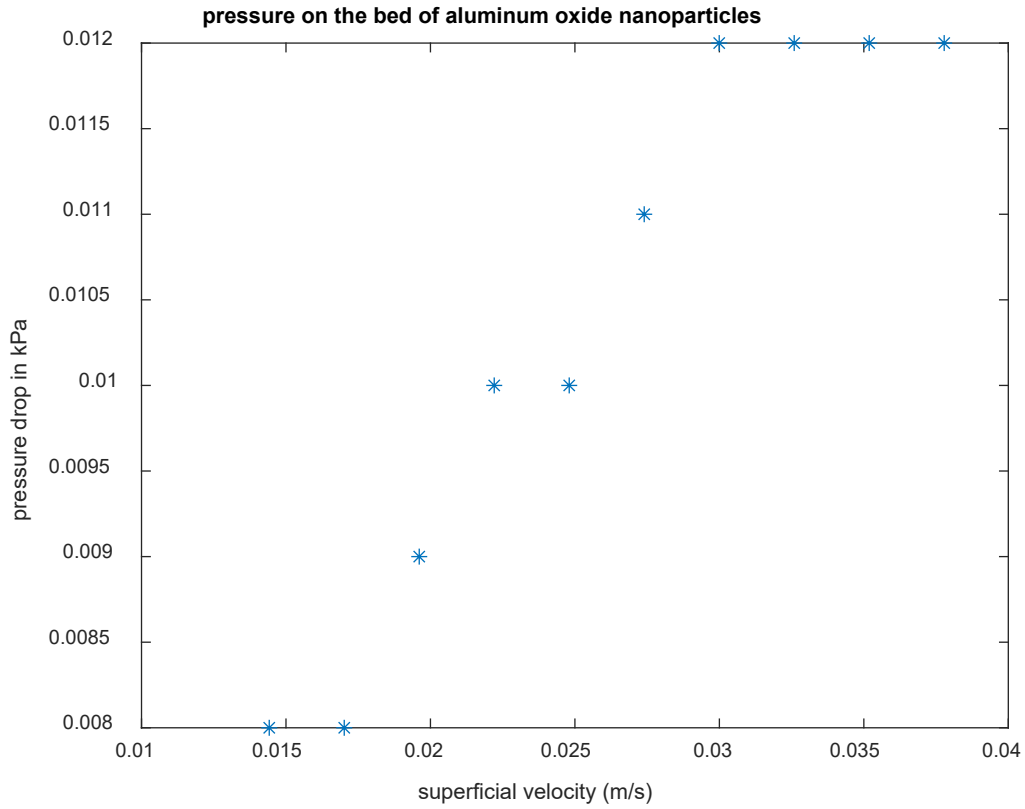

Figure 4. 1**: the pressure drop on the bed of aluminum oxide nanoparticles in acoustic sound fluidization with a frequency of 100Hz**

Figure 4.2 below shows the profile of the combination of Richardson and Zaki equation with the bed expansion linearized, the graph is drawn using MatLab software.

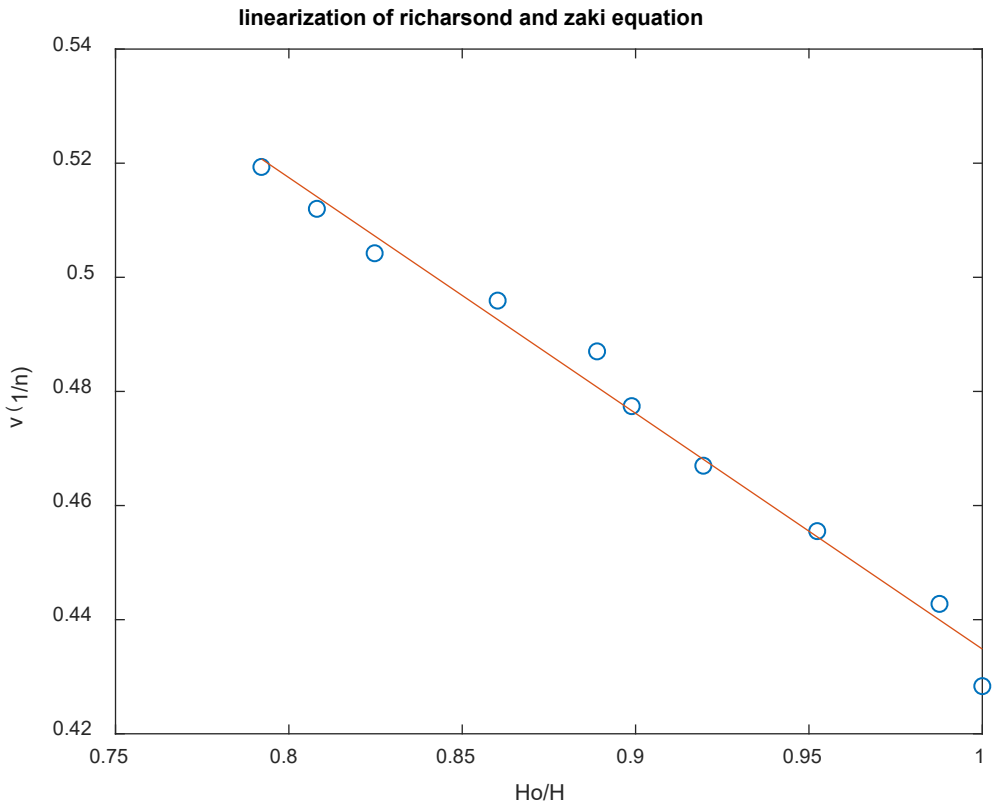

Figure 4. 2**: a linearized Richardson and Zaki equation from the acoustic sound fluidized Bed of aluminum oxide nanoparticle with a y-intercept as the terminal velocity and the slope as the initial voidage at an index of 5**

4.5.1.2. Determination of the size of the agglomerates nanoparticles using Stokes' Law

Aluminum oxide nanoparticles fluidized in a modified fluidized bed with acoustic sound, and the fluidization was of the form of agglomerate particulates fluidization. the agglomerate formed during the acoustic sound fluidization were distributed in the bed of the aluminum oxide nanoparticles, it was observed that the main cause of the fluidization of this nanoparticle in the acoustic sound fluidization was due to the formation of agglomerate, and the mean size of the agglomerate was estimated using the Stokes' Law. The mean diameter of the agglomerates was estimated at a value of 128 μm using Stokes' Law.

4.5.1.3. Determination of the size of agglomerates nanoparticles using scanning electron microscopy analysis (SEM)

After the acoustic sound fluidization of aluminum oxide nanoparticles, the forming agglomerate nanoparticles formed during fluidization were analyzed through the scanning electron microscopy analysis to visualize the structure of the agglomerate aluminum oxide nanoparticles and to determine the size distribution of the agglomerate formed. It was observed the agglomerate aluminum oxide nanoparticles were observed to be spherical. The maximum and minimum size of the agglomerate found were 21.59 µm and 9.783 µm respectively.

Figure 4.3 below shows the picture of the SEM image of aluminum oxide nanoparticles agglomerate in acoustic sound fluidization, the image was used to estimate the size of agglomerate.

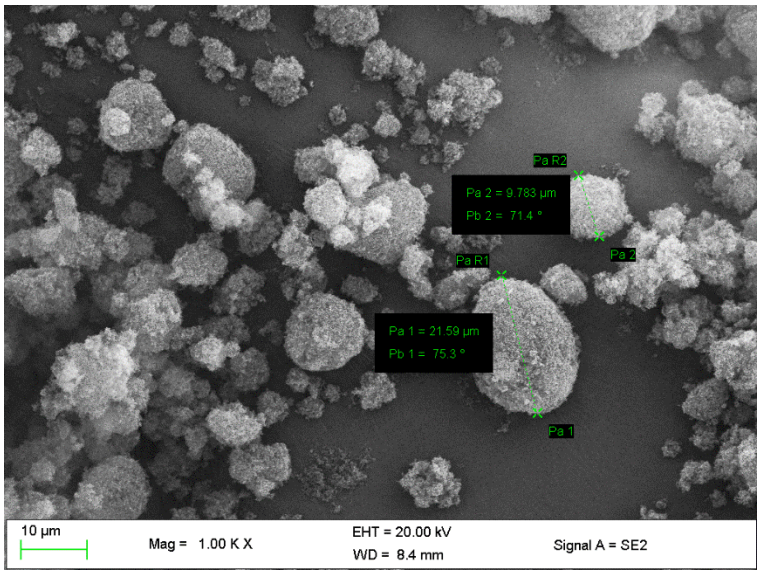

Figure 4. 3**: the SEM image of agglomerate formed during acoustic sound fluidization of aluminum oxide nanoparticles, picture taken at Microscopy and Microanalysis Unit at University of KwaZulu-Natal-Westville campus**

4.5.2. Vibro-fluidization of aluminum oxides nanoparticles

The vibration from the two motors mounted on a vibrating plate where a fluidized bed was positioned, the applied vibrations were at a frequency of 2 and 4 Hz. The fluidized bed was simulated with vibration before the fluidizing medium was allowed to pass in the line. The expansion of the bed of nanoparticles was initiated by the flowing of the air. After the second run, the nanoparticles were forming agglomerate and fluidizing at the same time. It was observed that the expansion of the bed was so height and the behavior of the aluminum oxide under vibro-fluidization demonstrated an agglomerate particulate fluidization. The increase of the pressure on the bed while the vibro-fluidization was occurring was recorded and a pressure profile was produced. Due to the primary size of the aluminum oxide nanoparticles, the complexity arises if

the initial voidage could be determined using methodology performed in the conventional fluidization of samples collected in the main laboratory of the Discipline of Chemical Engineering. Because there was the formation of agglomerate during the vibro-fluidization of aluminum oxides nanoparticles and the loss dust of nanoparticles, it has necessitated the combination of the model voidage to the ratio of the initial height to the bed expansion with the mathematical representation of the superficial velocity for liquid fluidization.

4.5.2.1. Determination of the fluidization parameters

The initial voidage was calculated from a linearized Richardson and Zaki equation; the behavior of the aluminum oxide nanopowders under vibro-fluidization was of agglomerate particulates fluidization as its bed of nanoparticles expanded so higher at a frequency of 2Hz. In linearizing the Richardson and Zaki correlation, the graphical representation of the superficial velocity exponent to the fraction of the Richardson and Zaki index with the ratio of the initial height to the bed expansion produced a straight line where y-intercepted represented the terminal velocity and the initial voidage was calculated from the slop of the linearized graph.

The Richardson and Zaki index considered in the experiment was 5. From the slop of figure 4.2, the initial voidage of aluminum oxide nanoparticles in a vibro-fluidized bed was calculated at a value of 0.5134. The superficial velocity was reaching 0.0105 m/s when the pressure on the bed of nanoparticles remained unchanged, it was observed that the pressure stayed unchanged when the pressure transducers recorded a pressure of value of 0.009 kPa. By using the minimum fluidization velocity, the bed expansion reached its minimum fluidization height when the bed of nanoparticles was at 11.7 cm. Graphically, the minimum fluidization voidage was interpreted by plotting the superficial velocity with the voidage as the bed expanded after minimum fluidization has reached. The minimum fluidization voidage was graphically read at a value of 0.56.

4.5.2.2. Determination of the size of the agglomerates of the nanoparticle using Stokes'Law

As vibro-fluidization was occurring, the formation of agglomerate was observed, the complexity of the configuration of nanopowders in colliding and creating big size particles is explained by the fact vibrations were applied to the bed of nanoparticles. It was with evidence to calculate the size the agglomerate formed during vibro-fluidization. A mathematical calculation of the size of the agglomerate was an approximate way of estimating the size of the agglomerates as stated by other researchers. Using Stokes'Law, the average diameter of the agglomerate of aluminum oxide

nanopowders was calculated using the terminal velocity find from the linearized Richardson and Zaki equation, the average diameter of the agglomerate was 48 µm. In situ observation of arrangement of the agglomerate in the fluidized bed during vibro-fluidization was observed when agglomerate of aluminum nanoparticles in small size tend to locate in the upper layer of the bed of aluminum oxide nanoparticles and the agglomerate in larger sizes were located at bottom of the bed of nanoparticles.

After, aluminum oxide nanoparticles were exposed in a vibro-fluidized bed at an increased frequency of 4 Hz to investigate the behavior of nanopowders aluminum oxide at a higher frequency. It was observed that at a frequency of 4 Hz, the aluminum oxide nanopowders behaved differently when the frequency was applied at moderate. The minimum fluidization velocity at a frequency of 4 Hz was lower compared to the minimum fluidization velocity at moderate frequency. When vibration was applied at a higher frequency of 4 Hz, the bed expansion of aluminum oxide nanopowders reached a bed height of 13 cm at maximum superficial velocity while at a frequency of 2 Hz, the bed of aluminum oxide nanoparticles expanded and reached a bed height of more than 13 cm when a maximum superficial velocity was applied. It was deduced that the Richardson and Zaki equation was accommodated when aluminum oxide nanoparticles under vibro-fluidization at a lower frequency of 2 Hz as the expansion of the bed was higher.

Figure 4.4 below shows the profile of the Richardson and Zaki equation in a fluidized bed column linked to a vibration system, the graph is drawn using MatLab software.

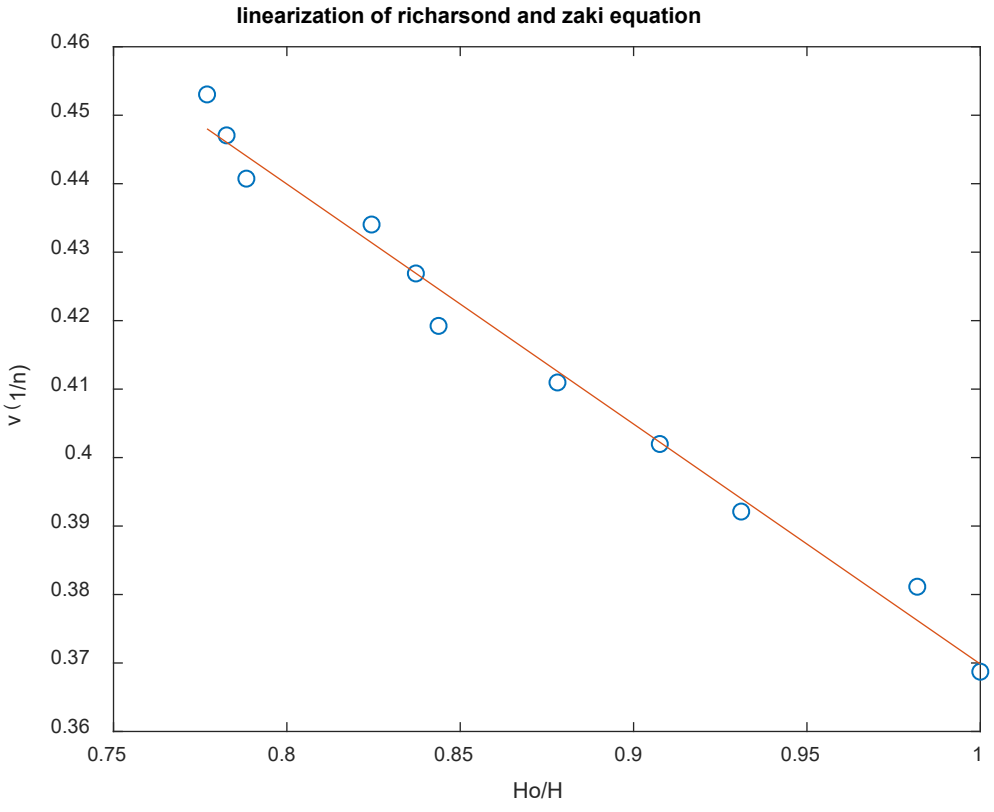

Figure 4. 4**: showing a linearized Richardson and Zaki equation from a vibro fluidized bed**

Figure 4.5 below shows the profile of aluminum oxides nanoparticles on a portion of nanoparticles during fluidization linked with vibration, the graph is drawn using MatLab software.

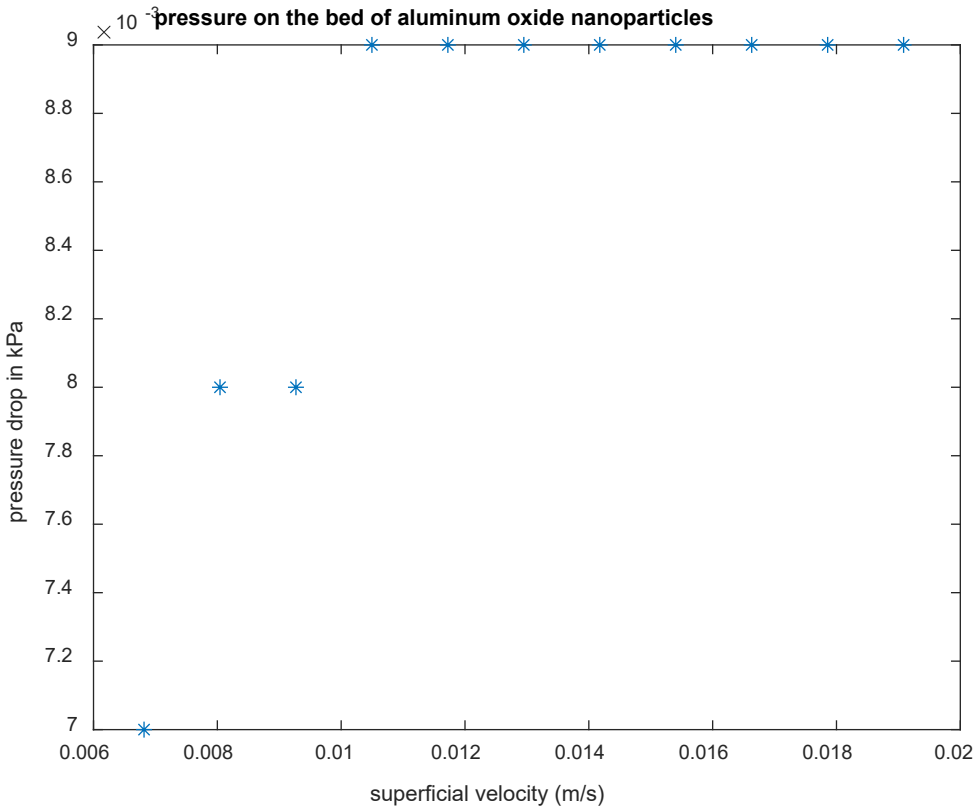

Figure 4. 5**: Pressure on the bed of Al_2O_3 nanopowder during vibro-fluidization at 2Hz**

4.5.2.3. Determination of the size of agglomerates nanoparticles using scanning electron microscopy analysis (SEM)

The size of the agglomerate formed during the vibro-fluidization of aluminum oxide nanoparticles was measured from the SEM analysis, during the analysis, the shape and structure of the agglomerates were visualized and measured. Noting that single nanoparticle created agglomerates which were able to break the complexity of the nanoparticle in fluidization. For common sense, the size of this agglomerate was important to study and investigate their size and structure as this allowed the fluidization of aluminum oxide nanoparticles to occur. The maximum and minimum size of agglomerate of aluminum oxide nanoparticles in vibro fluidization was found to be 25.57 µm and 11.39 µm respectively.

Figure 4.6 below shows the picture of the SEM image of aluminum oxide nanoparticles agglomerate, the image was used to estimate the size of the agglomerate.

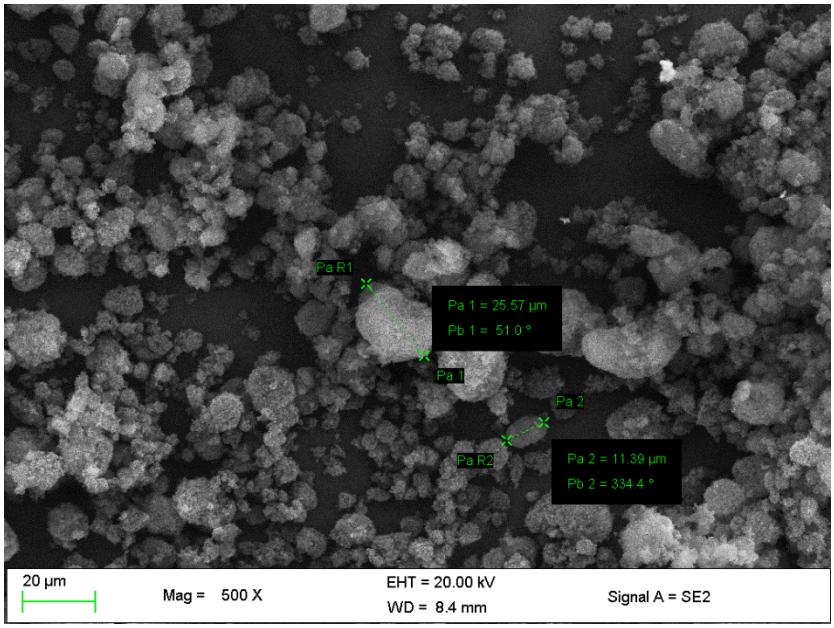

Figure 4. 6**: the SEM image of agglomerates formed during the vibro-fluidization of aluminum oxide nanoparticles, picture taken at Microscopy and Microanalysis Unit at the University of KwaZulu-Natal-Westville campus**

4.5.3. Acoustic sound fluidization of silicon dioxide nanoparticles

The introduction of acoustic sound on the fluidization of silicon dioxide nanoparticles of 10-20 nm did not help much in the fluidizing the nanoparticles. It was observed increasing the flow rate of the fluidizing medium to the fluidized bed, the bed of silicon dioxide formed channeling, this would be caused by the fact that the inter-particles forces existing between nanoparticles had much influence and dominated. By filling the silicon dioxide into the fluidized bed, nanoparticles stick on the wall of the fluidized bed, this tendency of nanoparticles sticking in the wall can be explained from the dominancy of the capillary force in the nanopowder.

Figure 4.7 below shows the bed expansion of aluminum oxides nanoparticles in a vibro-fluidized bed, the graph is drawn using MatLab software.

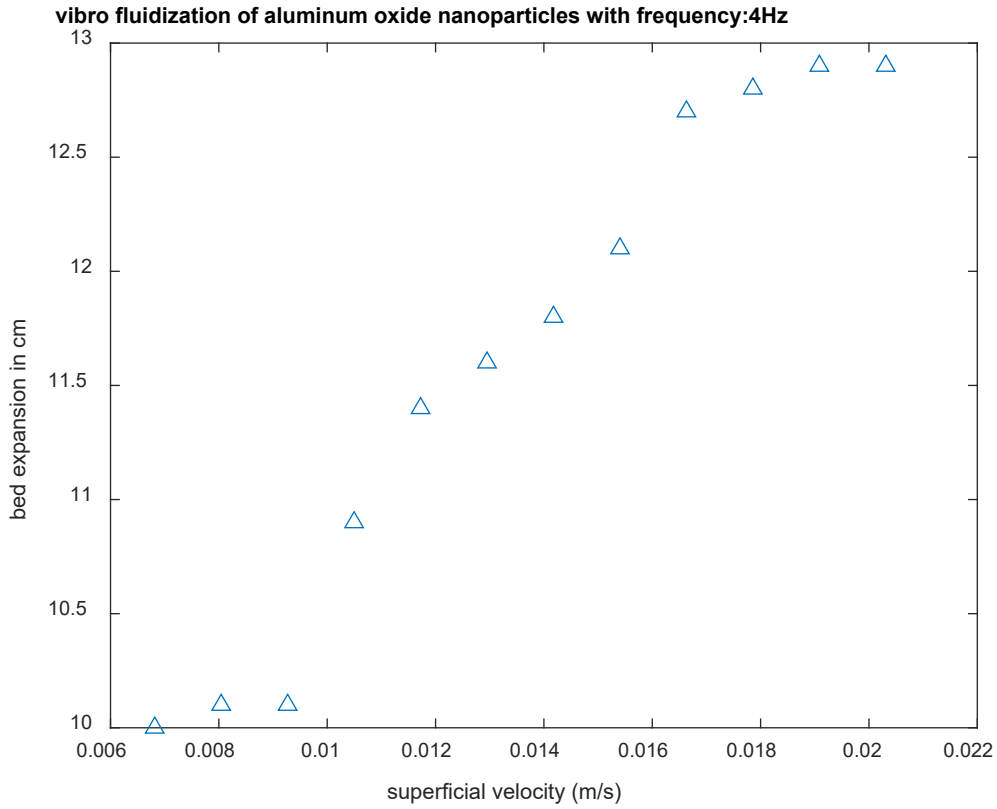

Figure 4. 7**: Bed expansion of Al_2O_3 nanopowder in vibro-fluidized bed at 4Hz**

4.5.4. Vibro-fluidization of silicon dioxide nanoparticles

The attempt of fluidizing silicon dioxide in a vibro-fluidized bed proves the complexity of this material and the inter-particles forces existing between nanoparticles. The measure of the expansion of the bed of silicon dioxide nanoparticles was highly described with difficulty due to the complexity of the movement of nanoparticles in the vibro-fluidized bed. By opening the rotameter, the pressure in the plenum chamber and on the bed of silicon dioxide could be easily measured using the pressure transducers connected to the vibro-fluidized bed. The bed of silicon dioxide fluidized by the influence of vibration on the fluidized bed at a frequency of 4 Hz. The entire bed of nanoparticles fluidized when the pressure change on the bed of silicon dioxide remained unchanged at a value of 0.013 kPa.

4.5.4.1. Determination of the size of agglomerate of nanoparticles using scanning electron microscopy analysis (SEM)

The SEM analysis of agglomerates of silicon dioxide nanoparticles formed during vibro-fluidization has demonstrated how the structure and shape of agglomerate are existing during vibro-fluidization. The visualization of the agglomerate shows an irregular shape of agglomerate and their size was easily observed during the scanning. The picture below shows the SEM image and size of agglomerates of silicon dioxide nanoparticles during vibro-fluidization. it was found the maximum and minimum size of agglomerates was 13.52 µm and 6.414 µm respectively.

Figure 4.8 below shows the picture of the SEM image of silicon dioxide agglomerates nanoparticles, the image was used to estimate the size of the agglomerates.

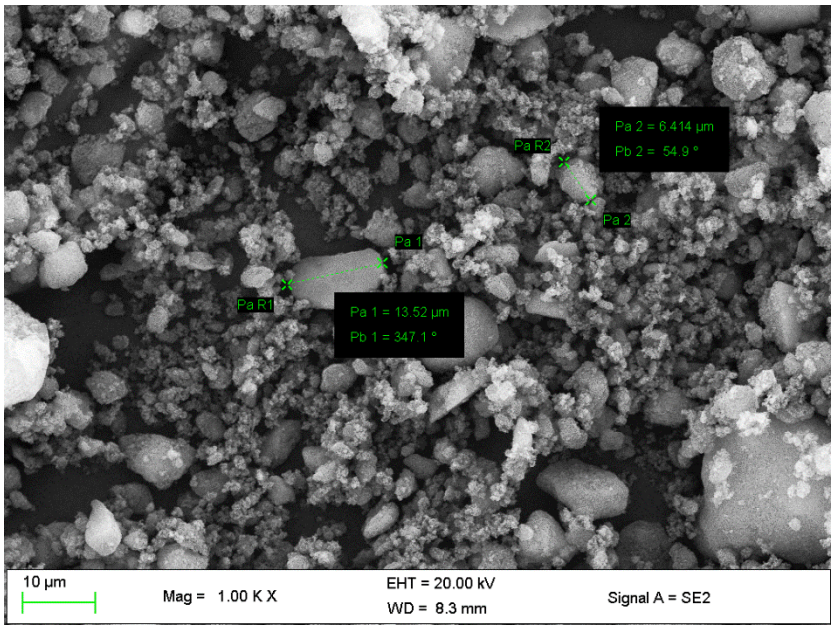

Figure 4. 8**: the SEM image of silicon dioxide agglomerate nanoparticles formed during vibro-fluidization, an image captured at Microscopy and Microanalysis Unit at the University of KwaZulu-Natal-Westville campus**

4.6. Sedimentation behavior of nanoparticles

4.6.1. Batch settling test for silicon dioxide nanoparticles

It was observed that some nanoparticles settled a few seconds after immersing silicon dioxide nanoparticles in water; this is explained by the presence of the natural agglomerate formed during the packaging of silicon dioxide nanoparticles. At immersion time, few agglomerate were tracked to observe their settling velocity in water. The settling time of nanoparticles was recorded to calculate the settling velocity of nanoparticles. The suspension was filled with nanoparticles having different sizes; this was just by the observation of the color of the suspension. The pictures taken during the batch-settling test of silicon dioxide nanoparticles have proven the settling of the

suspension in water as the color of the water started changing at the interface after 2 hours these can be seen from the figure 4.9. After 2 hours of immersing silicon dioxide in water, two distinguished zones have formed during batch settling test; a clear zone on the top of the suspension and a colored zone where suspension of silicon dioxide nanoparticles was located. It was evident that these suspensions have settled, as two-zone were distinguishable during batch settling test. The clear zone increased after 4 hours of observation.

Figure 4.9 below shows the images of the behavior of sodium dioxide nanoparticles in a batch settling test.

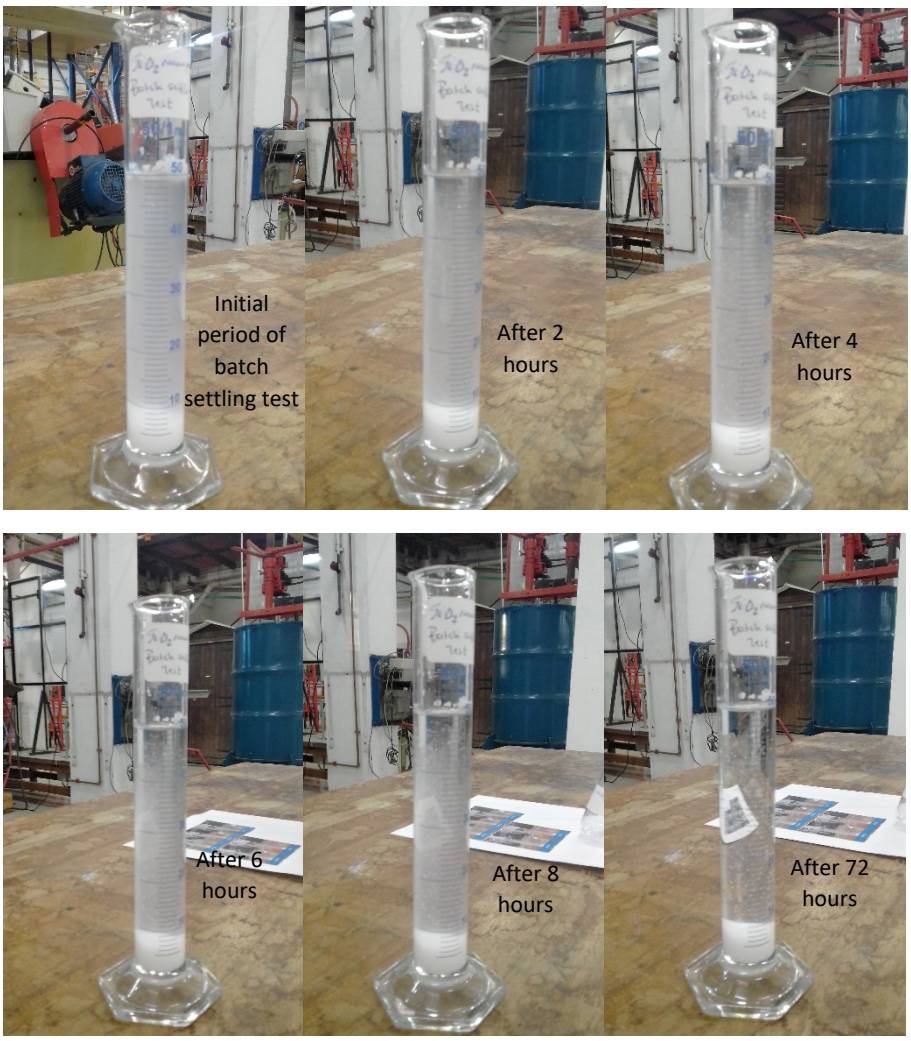

Figure 4. 9**: the behavior of silicon dioxide in water from the initial period of batch settling test and after 8 hours of immersion with an interval of 2 hours and 72 hours**

It was noticeable that after 8 hours of immersing silicon dioxide in water, two distinguishable zones were still observable during batch settling test. Suspensions of silicon dioxide nanoparticles were in the water but the clear zone has increased. After 8 hours of batch settling test of silicon dioxide nanoparticles, the suspensions were allowed to stay in water for 72 hours to observe their

behavior in water; it was seen that the suspensions were settled after 72 hours of batch settling test.

At the start of the batch settling test of silicon dioxide nanoparticles, the recorded time for the settling of nanoparticles were: 6.93 seconds, 36.36 seconds, 3.28 seconds, and 10.42 seconds. These times were recorded to investigate the nanoparticles just settled at the beginning of the batch settling test. The test was performed in a measuring cylindrical tube with a height of 12 cm. Based on the above measurements, the settling velocities of different nanoparticles were calculated and were found to be relative to the recorded time at beginning of the batch settling test: 0.0197, 0.0033, 0.0364, and 0.0115 m/s respectively. Using the settling velocities of nanoparticles, the size of the settled agglomerate was calculated using Stokes' Law. It was found that nanoparticles just settled a few seconds during batch settling tests were: 146.112, 59.814, 198.652, and 111.901 μm. Batch settling test was allowed to stay for 2 hours, 4 hours, 6 hours, 8 hours, and 72 hours. The procedure was to observed the changes in the suspension of nanoparticles in water. After 2 hours of the batch settling test, it was noticeable that nanoparticles in the size of 4.253 μm have settled this influenced the presence of the clear zone in the batch settling tube. The clear zone increased after 4 hours, 6 hours, 8 hours, and 72 hours after 3.007, 2.455, 2.126, and 0.709 μm have settled. It was noticeable that the clear zone increased after 72 hours of observation with no presence of suspended nanoparticles.

The primary size of silicon dioxide nanoparticles was analyzed through a transmission electron microscopy analysis to verify the size of the supplier, and it was found the silicon dioxide nanoparticles were distributed in different ranges of size with a minimum and maximum size of 9.71 and 19.69 nm respectively. In this manner, the settling velocity of the primary size of nanoparticles was calculated from the size distribution of nanoparticles using Stokes'Law.

Figure 4.10 below shows the figure predicting the behavior of silicon dioxide nanoparticles from Stokes' Law.

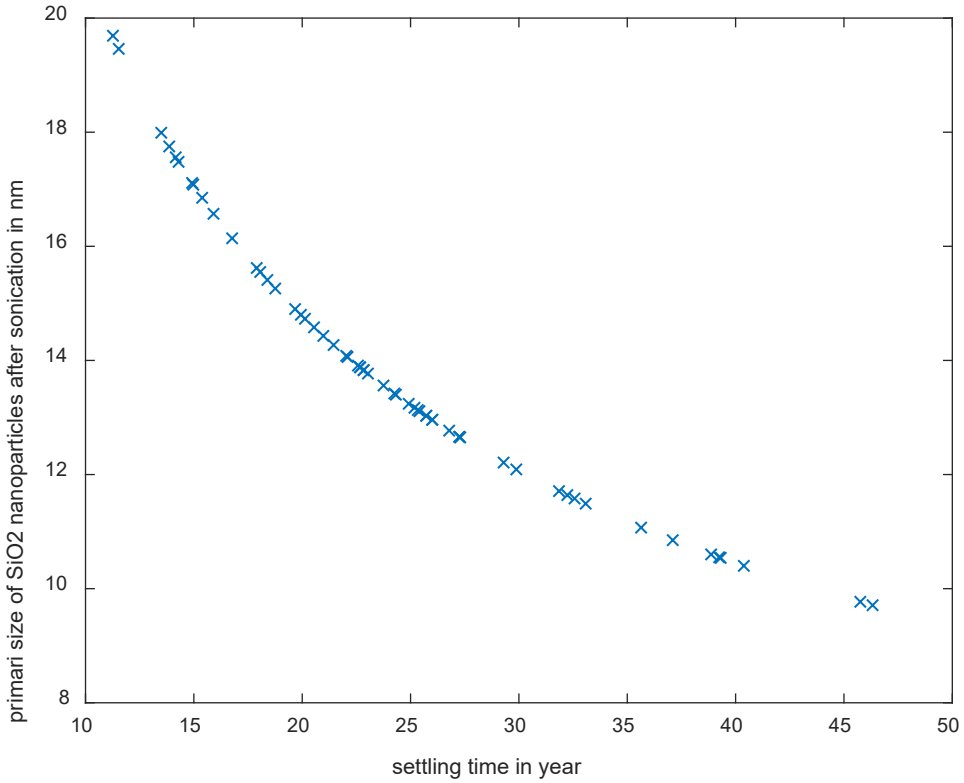

Figure 4. 10**: the settling velocity of the primary size of silicon dioxide nanoparticles after sonication**

From Figure 4.10, it was with evidence that the nanoparticles with a minimum in size will settle longer compared to the maximum and it will take 45 years for the minimum size to settled and less than 15 years for the maximum size. During batch settling test of silicon dioxide nanoparticles, after 72 hours, the images in figure 4.9 taken were proven 2.126 µm settled, it was observed that silicon dioxide nanoparticles settled as agglomerates during batch settling test.

4.6.2. Batch settling test for aluminum oxide nanoparticles

The sedimentation behavior of aluminum oxide nanoparticles was investigated in the same manner as for silicon dioxide nanoparticles. A batch settling test was performed by immersing a small number of aluminum oxide nanoparticles in water and observation of nanoparticles was obtained after capturing the images of the batch settling test after 5 minutes,10 minutes,15 minutes, and 2 hours. From the images shown in figure 4.11, it was clearly showing that aluminum oxide nanoparticles could settle in 2 hours of batch settling test.

Figure 4.11 below shows the behavior of aluminum oxide nanoparticles in the batch settling test.

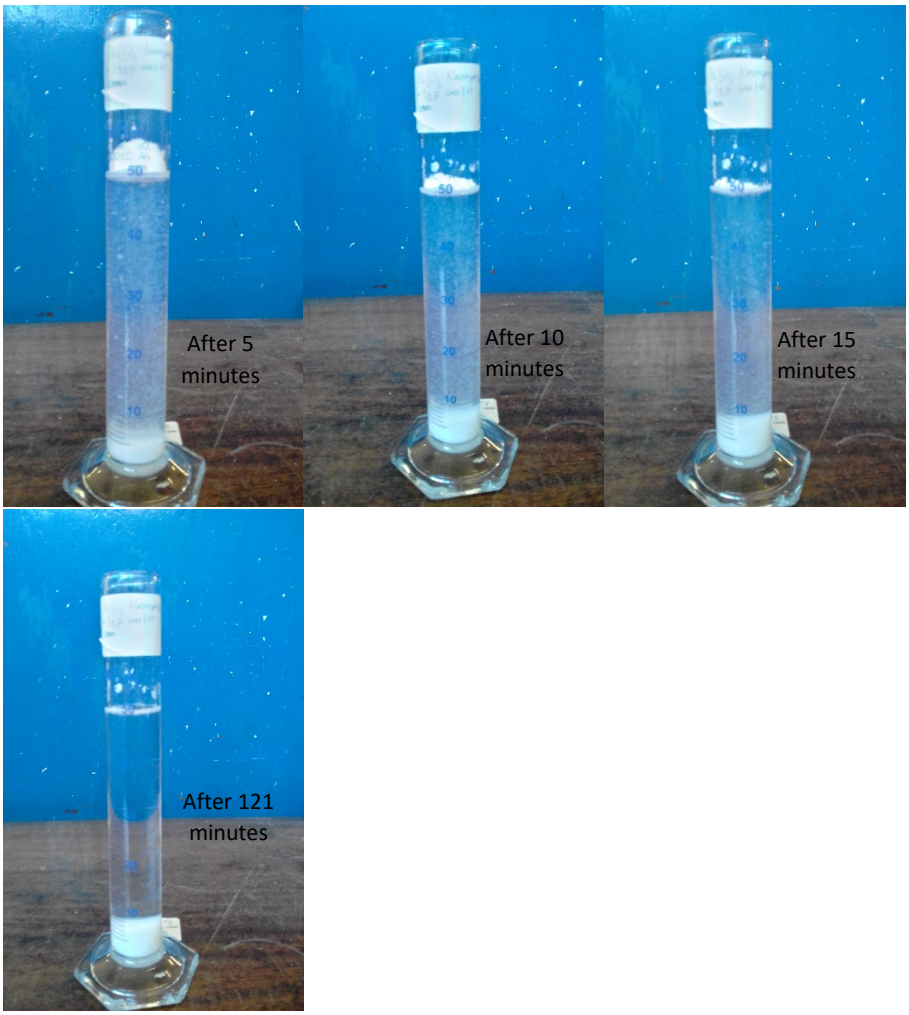

Figure 4. 11: showing the images of batch settling test for aluminum oxide nanoparticles

The images demonstrated that the settling of aluminum oxide nanoparticles was occurring in the form of agglomerate, which initiated the settling of aluminum oxide nanoparticles in water. As seen on the image after 2 hours of batch settling test, the interface is covered by a small number of aluminum oxide nanoparticles forming a ring, these nanoparticles could not be settled after 72 hours of observation, they have remained floating in the interface. The settling of aluminum oxide nanoparticles was demonstrated by the decaying of the concentration of the suspension in water from 5 minutes to 2 hours of batch settling test. This was observed by recording the settling velocity of aluminum oxide nanoparticles in water during the period of observation.

5. CONCLUSION

It was intended to investigate the fluidization and sedimentation behavior of 5, 7, and 12 nm silicon dioxide and aluminum oxide nanoparticles, these nanoparticles could not be found from any local supplier for an experiment. Instead of the proposed nanoparticles, 13 nm aluminum oxide and 10-20 silicon dioxide nanoparticles were purchased from a local supplier for the research on the fluidization and sedimentation behavior of nanoparticles. The third technique proposed to enhance the fluidization of nanoparticle was the addition of foreign particles, in this case, the particle of Geldart group A was an option. The third method was not considered as it was an addition of a solid particle of Group A, an intensive experiment on the fluidization on the samples of solid particles located in the Discipline of Chemical Engineering was considered. In this manner only two methods of fluidization of 13 nm aluminum oxide and 10-20 nm silicon dioxide nanoparticles were considered; fluidization enhanced by mechanical vibration and fluidization associated with acoustic sound. The pressure transducers of model S -20 were appropriate in the measurement of the pressures in the plenum chamber, on the bed of nanoparticles, and above the bed of nanoparticles.

The sphericities of solid particles of samples were measured by fitting the Ergun equation to the measured pressure drop, these in return were inserted to the empirical equation for the prediction of the minimum fluidization velocity of each sample and compared with the experiment, its sample demonstrated its behavior on the fluidization. The measured parameters from the measurement from pressure transducers of model S-20 and inverted U-tube manometers did not differ much in the process measurement of the samples.

The fluidization enhanced my mechanical vibration and acoustic sound of 13 nm aluminum oxide nanoparticles and 10-20 nm silicon dioxide nanoparticles demonstrated different behavior. The acoustic sound fluidization of 13 nm aluminum oxide with a frequency of 100 Hz in a 0.12 m of diameter was observed and the pressure profile on the bed of 13 nm aluminum oxide nanoparticles was obtained in 10 cm of a bed of nanoparticles. It was observed the formation of agglomerate during the acoustic sound of these nanoparticles distributed within the bed of an acoustic sound fluidized bed. In the vibro- fluidized bed, the 13 nm aluminum oxide demonstrated a lower minimum fluidization velocity measured during the experiment, and different vibration frequencies were applied to the vibro-fluidised bed of 13 nm of aluminum oxide; 2 Hz and 4 Hz. It was observed the bed of nanoparticle expanded much when 2 Hz was applied on the vibro-fluidised bed then 4 Hz and the minimum fluidization velocity at 4 Hz was found much lower compared to the minimum fluidization velocity at a lower frequency, thus the vibration influenced the fluidization behavior of 13 nm aluminum oxide nanoparticles. The 10-20 nm diameter silicon dioxide nanoparticles were fluidized by stimulating the fluidized bed with the vibration, in this

case, the nanoparticles showed a complex character in the bed when fluidized such as, the difficulty in recording the expansion of the bed of nanoparticles. It was observed that due to the high density of the silicon dioxide nanoparticles and the distribution of the primary size of the silicon dioxide nanoparticles, the frequency of the vibration during vibro-fluidisation required a high frequency for all bed of nanoparticle to be under fluidization.

During the batch-settling test of silicon dioxide nanoparticles, it was observed; nanoparticles were still in suspension for 8 hours and the suspensions were disappeared after 72 hours of sedimentation. The size of settled nanoparticles and suspensions were calculated using the sedimentation theory. The settling time for the primary size of nanoparticles was estimated to be longer for a minimum size of nanoparticles compared to the maximum size with a magnitude of 400000 and 100000 hours respectively. Aluminum oxide nanoparticles demonstrated the behavior different from the silicon dioxide nanoparticles. in terms of their settling period, aluminum oxide nanoparticles could settle in 2 hours of batch settling test.

6. RECOMMENDATIONS

In the vibro-fluidization of samples, the effect of vibration should be added to the Ergun equation for a better prediction of minimum fluidization parameters.

The size of the agglomerates of aluminum oxide and silicon dioxide nanoparticles formed during fluidization enhanced by vibration and acoustic sound should be measured with accuracy when the advanced technique is applied, an in situ measurement on the size of agglomerates using a digital camera should produce an accurate measurement.

7. REFERENCES

Ali, S. S., Al-Ghurabi, E. H., Ibrahim, A. A. & Asif, M. 2018. Effect of adding Geldart group A particles on the collapse of fluidized bed of hydrophilic nanoparticles. *POWDER TECHNOLOGY -LAUSANNE-,* 330**,** 50-57.

Blott, S. J. & Pye, K. 2006. Particle size distribution analysis of sand-sized particles by laser diffraction: an experimental investigation of instrument sensitivity and the effects of particle shape. *Sedimentology,* 53**,** 671-685.

Cocco, R., Karri, S. R. & Knowlton, T. 2014. Introduction to fluidization. *Chem. Eng. Prog,* 110**,** 21-29.

Eberhard, L., Schindler, H., Hellmann, D., Schmitter, M., Rammelsberg, P. & Giannakopoulos, N. 2012. Comparison of particle-size distributions determined by optical scanning and by sieving in the assessment of masticatory performance. *Journal of oral rehabilitation,* 39**,** 338-348.

Fabre, A., Clemente, A., Balas, F., Lobera, M. P., Santamaría, J., Kreutzer, M. T. & Van Ommen, J. R. 2017. Modeling the size distribution in a fluidized bed of nanopowder. *Environmental Science: Nano,* 4**,** 670-678.

Geldart, D. 1973. Types of gas fluidization. *PTEC</cja:jid> Powder Technology,* 7**,** 285-292.

Geldart, D. 1986. *Gas fluidization technology,* Chichester; New York, Wiley.

Hoo, C. M., Starostin, N., West, P. & Mecartney, M. L. 2008. A comparison of atomic force microscopy (AFM) and dynamic light scattering (DLS) methods to characterize nanoparticle size distributions. *Journal of Nanoparticle Research,* 10**,** 89-96.

Khlebtsov, B. & Khlebtsov, N. 2011. On the measurement of gold nanoparticle sizes by the dynamic light scattering method. *Colloid Journal,* 73**,** 118-127.

Konert, M. & Vandenberghe, J. 1997. Comparison of laser grain size analysis with pipette and sieve analysis: a solution for the underestimation of the clay fraction. *Sedimentology,* 44**,** 523-535.

Kunii, D. & Levenspiel, O. 2013. *Fluidization engineering*, Elsevier.

Li, J., Kong, J., He, S., Zhu, Q. & Li, H. 2018. Self-agglomeration mechanism of iron nanoparticles in a fluidized bed. *Chemical Engineering Science,* 177**,** 455-463.

Matsuda, S., Hatano, H., Lin, H. & Tsutsumi, A. Fluidization Characteristics of Nanoparticles. Asian Pacific Confederation of Chemical Engineering congress program and abstracts Asian Pacific Confederation of Chemical Engineers congress program and abstracts, 2004. The Society of Chemical Engineers, Japan, 41-41.

Morooka, S., Kusakabe, K., Kobata, A. & Kato, Y. 1988. Fluidization state of ultrafine powders. *Journal of Chemical Engineering of Japan,* 21**,** 41-46.

Raganati, F., Chirone, R. & Ammendola, P. 2018. Gas-solid fluidization of cohesive powders. *CHERD Chemical Engineering Research and Design,* 133**,** 347-387.

Rizvi, S. A. & Saleh, A. M. 2018. Applications of nanoparticle systems in drug delivery technology. *Saudi Pharmaceutical Journal,* 26**,** 64-70.

Tahmasebpoorthese Authors Contributed Equally to This Work, M., De MartíN, L., Talebi, M., Mostoufi, N. & Van Ommen, J. R. 2013. The role of the hydrogen bond in dense nanoparticle–gas suspensions. *CP Physical Chemistry Chemical Physics,* 15**,** 5788-5793.

Tamadondar, M. R., Zarghami, R., Boutou, K., Tahmasebpoor, M. & Mostoufi, N. 2016. Size of nanoparticle agglomerates in fluidization. *The Canadian Journal of Chemical Engineering,* 94**,** 476-484.

Taubner, H., Roth, B. & Tippkötter, R. 2009. Determination of soil texture: Comparison of the sedimentation method and the laser-diffraction analysis. *Journal of Plant Nutrition and Soil Science,* 172**,** 161-171.

Valverde, J. M. & Castellanos, A. 2006. Fluidization of nanoparticles: A modified Richardson-Zaki law. *AIChE journal,* 52**,** 838-842.

Valverde, J. M. & Castellanos, A. 2008. Fluidization of nanoparticles: a simple equation for estimating the size of agglomerates. *Chemical Engineering Journal,* 140**,** 296-304.

Wang, X. S., Rahman, F. & Rhodes, M. J. 2007a. Nanoparticle fluidization and Geldart's classification. *Chemical Engineering Science,* 62**,** 3455-3461.

Wang, X. S., Rahman, F. & Rhodes, M. J. 2007b. Nanoparticle fluidization and Geldart's classification. *CES Chemical Engineering Science,* 62**,** 3455-3461.

Xu, C. C. & Zhu, J. 2008. Prediction of the minimum fluidization velocity for fine particles of various degrees of cohesiveness. *Chemical Engineering Communications,* 196**,** 499-517.

Zhang, W. & Zhao, M. 2010. Fluidisation behaviour of silica nanoparticles under horizontal vibration. *Journal of Experimental Nanoscience,* 5**,** 69-82.

Zhu, C., Liu, G., Yu, Q., Pfeffer, R., Dave, R. N. & Nam, C. H. 2004. Sound assisted fluidization of nanoparticle agglomerates. *PTEC</cja:jid> Powder Technology,* 141**,** 119-123.

Zhu, C., Yu, Q., Dave, R. N. & Pfeffer, R. 2005. Gas fluidization characteristics of nanoparticle agglomerates. *AIC AIChE Journal,* 51**,** 426-439.

8. APPENDICES

8.1. Appendix A1: Tables

Table 8. 1: the sieve analysis for the first run for 10 grams of sample 1

Size of sieve(µm)	Mass of empty sieve(g)	Mass of sieve + sample(g)	Mass of sample(g)	d_i(µm)	Mass fraction f_i	f_i/d_i
600	322.8	324.2	1.4	424.264	0.141	0.00033
425	309.1	310.4	1.3	504.975	0.131	0.00026
300	288.7	290.6	1.9	357.071	0.192	0.00054
212	284.8	288.1	3.3	252.19	0.333	0.00132
150	266.8	268.6	1.8	178.326	0.182	0.00102
106	272.4	272.6	0.2	126.095	0.02	0.00016
75	257	257	0	89.163	0	0
pan	245.5	245.5	0	53.033	0	0

Table 8. 2: the sieve analysis for the first run for 20 grams of sample 1

Size of sieve(µm)	Mass of empty sieve(g)	Mass of sieve + sample(g)	Mass of sample(g)	d_i(µm)	Mass fraction f_i	f_i/d_i
600	322.8	325.4	2.6	424.264	0.129	0.0003
425	309	311.4	2.4	504.975	0.119	0.00024
300	288.5	292.1	3.6	357.071	0.179	0.0005
212	284.6	291.3	6.7	252.19	0.333	0.00132
150	266.6	270.5	3.9	178.326	0.194	0.00109
106	272.2	273	0.8	126.095	0.0398	0.00032
75	256.9	257	0.1	89.163	0.00498	5.6×10^{-5}
pan	245.4	245.4	0	53.033	0	0

Table 8. 3: the sieve analysis for the first run for 90 grams of sample 1

Size of sieve(µm)	Mass of empty sieve(g)	Mass of sieve + sample(g)	Mass of sample(g)	d_i(µm)	Mass fraction f_i	f_i/d_i
600	322.8	340	17.2	424.264	0.191	0.00045
425	309	321	12	504.975	0.133	0.00026
300	288.5	314.1	25.6	357.071	0.284	0.0008
212	284.6	310.7	26.1	252.19	0.29	0.00115
150	266.6	274.3	7.7	178.326	0.086	0.00048
106	272.2	273.4	1.2	126.095	0.013	0.00011
75	256.9	257.1	0.2	89.163	0.0022	2.5×10^{-5}
pan	245.4	245.4	0	53.033	0	0

Table 8. 4: the sieve analysis for the first run for 10 grams for sample 2

Size of sieve(µm)	Mass of empty sieve(g)	Mass of sieve + sample (g)	Mass of sample(g)	d_i(µm)	Mass fraction f_i	f_i/d_i
600	322.8	327.5	4.7	424.264	0.480	0.00113
425	309.1	312.6	3.5	504.975	0.357	0.00071
300	288.6	290.1	1.5	357.071	0.153	0.00043
212	284.6	284.7	0.1	252.19	0.010	4×10^{-5}
150	266.6	266.6	0	178.326	0	0
106	272.2	272.2	0	126.095	0	0
75	256.9	256.9	0	89.163	0	0
pan	245.5	245.5	0	53.033	0	0

Table 8. 5: the sieve analysis for the first run for 20 grams for sample 2

Size of sieve(µm)	Mass of empty sieve(g)	Mass of sieve + sample(g)	Mass of sample(g)	d_i(µm)	Mass fraction f_i	f_i/d_i
600	322.8	331.7	8.9	424.264	0.445	0.00105
425	309.1	317.4	8.3	504.975	0.415	0.00082
300	288.5	291.2	2.7	357.071	0.135	0.00038
212	284.6	284.7	0.1	252.19	0.005	2×10^{-5}
150	266.6	266.6	0	178.326	0	0
106	272.4	272.4	0	126.095	0	0
75	257.1	257.1	0	89.163	0	0
pan	245.4	254.4	0	53.033	0	0

Table 8. 6: the sieve analysis for the first run for 90 grams for sample 2

Size of sieve(µm)	Mass of empty sieve(g)	Mass of sieve + sample(g)	Mass of sample(g)	d_i(µm)	Mass fraction f_i	f_i/d_i
600	322.8	365.1	42.3	424.264	0.47	0.00111
425	309.1	337.5	28.4	504.975	0.316	0.00062
300	288.6	306.5	17.9	357.071	0.199	0.00056
212	284.7	285.9	1.2	252.19	0.013	5.3×10^{-5}
150	266.7	266.7	0	178.326	0	0
106	272.4	272.5	0.1	126.095	0.001	8.8×10^{-6}
75	256.8	256.9	0.1	89.163	0.001	1.2×10^{-5}
pan	245.4	245.4	0	53.033	0	0

Table 8. 7: the sieve analysis for the first run for 10 grams of sample 3

Size of sieve(µm)	Mass of empty sieve(g)	Mass of sieve + sample (g)	Mass of sample (g)	d_i(µm)	Mass fraction f_i	f_i/d_i
300	280.3	282.3	2	212.132	0.202	0.00095
250	286.6	287.5	0.9	273.861	0.091	0.00033
180	275	277.3	2.3	212.132	0.232	0.0011
125	275.7	278.5	2.8	150	0.283	0.00189
90	272.4	273.7	1.3	106.066	0.131	0.00124
75	256.8	256.9	0.1	82.158	0.01	0.00012
45	266.9	267.3	0.4	58.0948	0.04	0.0007
38	257.9	258	0.1	41.352	0.01	0.00024
pan	517.2	517.2	0	26.870	0	0

Table 8. 8: the sieve analysis for the first run for 20 grams of sample 3

Size of sieve(µm)	Mass of empty sieve(g)	Mass of sieve + sample(g)	Mass of sample(g)	d_i(µm)	Mass fraction f_i	f_i/d_i
300	288.5	289.7	1.2	212.132	0.061	0.00029
250	286.6	286.9	0.3	273.861	0.015	5.5×10^{-5}
180	275.1	275.7	0.6	212.132	0.03	0.00014
125	275.8	290.1	14.3	150	0.722	0.00481
90	272.4	275.5	3.1	106.066	0.157	0.00148
75	257.4	257.4	0	82.158	0	0
45	266.9	267.2	0.3	58.095	0.015	0.00026
38	257.9	257.9	0	41.352	0	0
pan	517.2	517.2	0	26.87	0	0

Table 8. 9: the sieve analysis for the first run for 90 grams of sample 3

Size of sieve(µm)	Mass of empty sieve(g)	Mass of sieve + sample(g)	Mass of sample(g)	d_i(µm)	Mass fraction f_i	f_i/d_i
300	288.5	313.5	25	212.132	0.277	0.00131
250	286.6	295.2	8.6	273.861	0.095	0.00035
180	275	300.8	25.8	212.132	0.286	0.00135
125	275.7	301.7	26	150	0.288	0.00192
90	272.5	276.1	3.6	106.066	0.04	0.00038
75	257.3	257.5	0.2	82.158	0.002	2.7×10^{-5}
45	266.9	267.9	1	58.095	0.011	0.00019
38	258	258	0	41.352	0	0
pan	517.3	517.3	0	26.87	0	0

Table 8. 10: the sieve analysis for the first run for 10 grams of sample 4

Size of sieve(µm)	Mass of empty sieve(g)	Mass of sieve + sample(g)	Mass of sample(g)	d_i(µm)	Mass fraction f_i	f_i/d_i
600	322.9	322.9	0	424.264	0	0
425	309.1	309.7	0.6	504.975	0.06	0.000119
300	288.5	295.8	7.3	357.071	0.73	0.002
212	284.6	286.3	1.7	252.19	0.17	0.000674
150	266.6	267	0.4	178.326	0.04	0.000224
106	272.4	272.4	0	126.095	0	0
75	256.8	256.8	0	89.163	0	0
pan	245.4	245.4	0	53.033	0	0

Table 8. 11: the sieve analysis for the first run for 20 grams of sample 4

Size of sieve(µm)	Mass of empty sieve(g)	Mass of sieve + sample(g)	Mass of sample(g)	d_i(µm)	Mass fraction f_i	f_i/d_i
600	322.8	322.9	0.1	424.264	0.00503	1.184×10^{-5}
425	309	310.3	1.3	504.975	0.06533	0.000129
300	288.5	303.8	15.3	357.071	0.769	0.00215
212	284.6	287.2	2.6	252.19	0.131	0.000518
150	266.6	267.1	0.5	178.326	0.0251	0.000141
106	272.2	272.3	0.1	126.095	0.005	3.985×10^{-5}
75	257.1	257.1	0	89.16	0	0
pan	245.4	245.4	0	53.033	0	0

Table 8. 12: the sieve analysis for the first run for 90 grams of sample 4

Size of sieve(µm)	Mass of empty sieve(g)	Mass of sieve + sample(g)	Mass of sample(g)	d_i(µm)	Mass fraction f_i	f_i/d_i
600	322.9	323.1	0.2	424.264	0.00223	5.255×10^{-6}
425	309.1	318.4	9.3	504.975	0.104	0.000205
300	288.5	362.4	73.9	357.071	0.824	0.00231
212	284.6	289.2	4.6	252.19	0.0513	0.000203
150	266.6	268.1	1.5	178.326	0.0167	9.377×10^{-5}
106	272.2	272.4	0.2	126.095	0.00223	1.768×10^{-5}
75	256.9	256.9	0	89.163	0	0
pan	245.5	245.5	0	53.033	0	0

8.2. Appendix A2: Graphs

The calibration of rotameters was necessary to investigate the validity of the literature calibration equations produced in the past experiment.

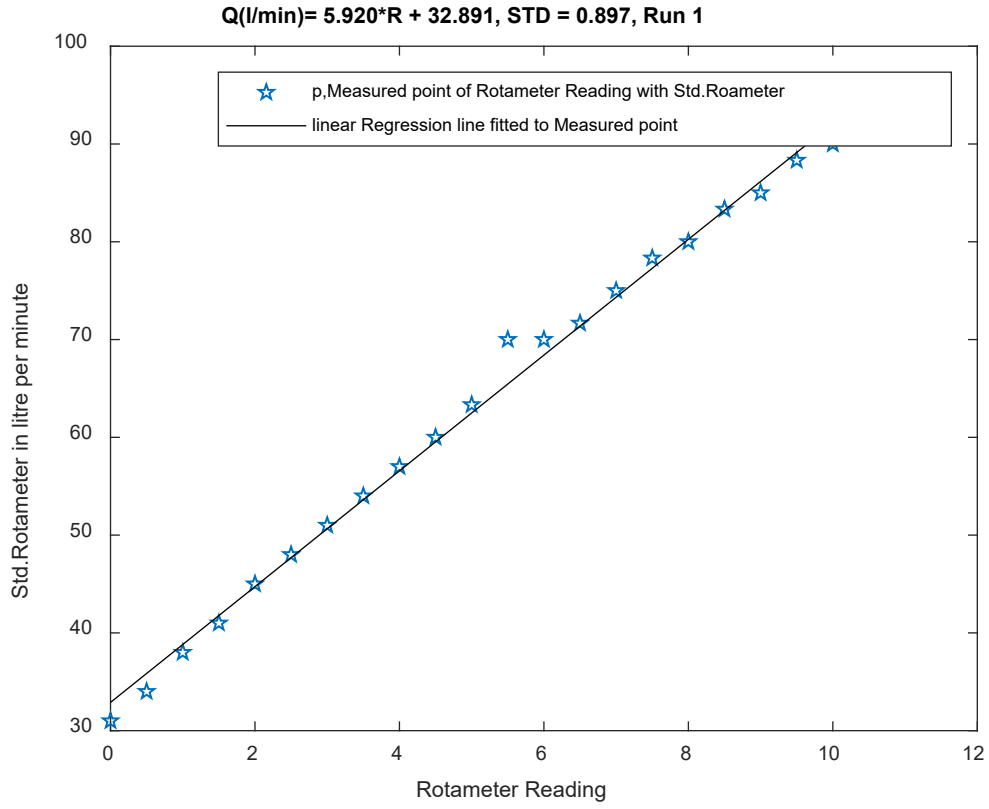

Figure 8. 1**: Calibration curve for the reading of Rotameter 1 of the first run**

Rotameter 1 has been recalibrated using a standard rotameter, after measuring the flow of the air passing through the rotameter 1 a linear relation of the standard rotameter with the reading from the rotameter 1 was plotted, a linear regression was performed to produce the calibration curves. The standard deviation on the measuring volumetric flow rate for the first run was found to be 0.897.

After performing three different runs of recalibration of rotameter 1, tree different calibration curves were produced after linear regression with a different standard deviation of the volumetric flow rate of the air. The first calibration equation produced for the first run was $Q\left(\frac{l}{min}\right) = 5.920 \times R + 32.891$, follow by the calibration equation of the second run, by linear regression the equation for the calibration find to be $Q\left(\frac{l}{min}\right) = 5.916 \times R + 32.606$ with a standard deviation of 0.902. in the third run, a linear regression was performed on the measuring of the

volumetric flowrate, the equation for the calibration has to be $Q\left(\frac{l}{min}\right) = 6.160 \times R + 31.532$ with a standard deviation of 0.932. It was decided to select the calibration curves with the smallest standard deviation. The calibration equation for the first run was selected to be used in the experiment as it has a smaller standard deviation. This calibration equation was plotted in the same graph with the literature calibration equation for observing the deviation.

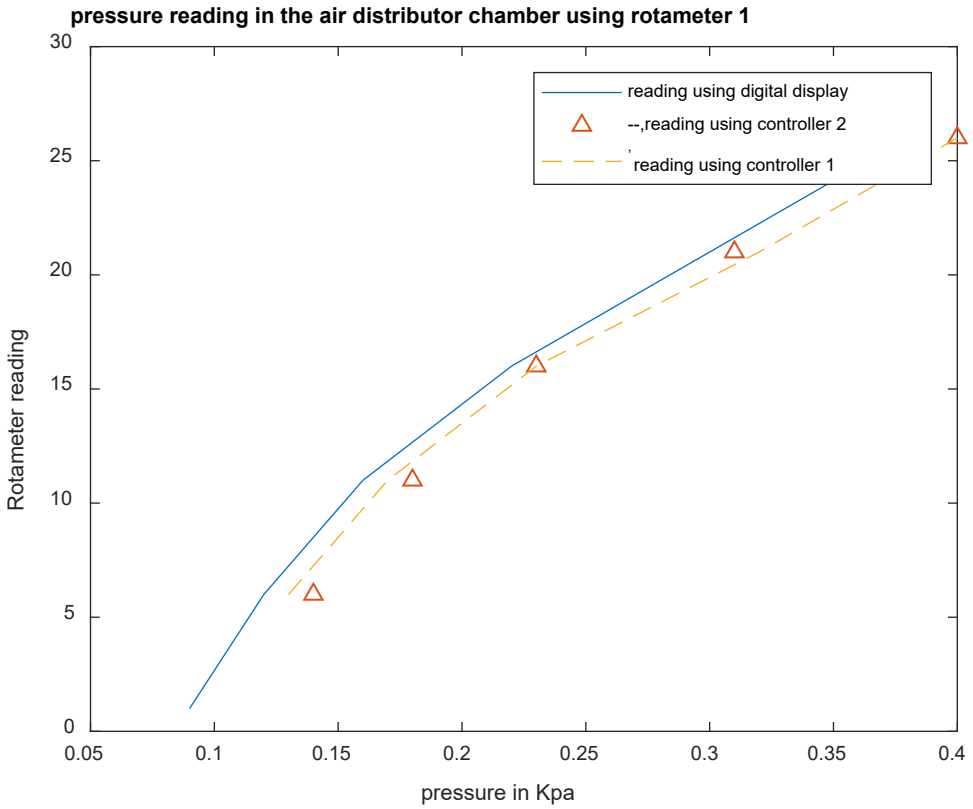

Figure 8. 2**: The sensitivity of the digital display vs controllers in the plenum**

The measuring devices used were pressure transducers of model S-20, the devices were sending a signal to the controllers for displaying the pressure. The sensitivity of the controllers was taken to locate the position of the controllers. A digital display and two controllers placed at different times in the plenum chamber to investigate the reading of the pressure using the rotameter 1. It was observed the digital display was able to read the pressure from the smallest rotameter reading while the two controllers stated reading pressure in the plenum chamber from a rotameter reading of 5.

The fluidized bed of diameter of 0.12 meter was calibrated before use, the pressure profile in the plenum chamber and the bedchamber were investigated, the pressure profile in the plenum chamber produced a linear relation with the airflow from the rotameter, the profile in the bedchamber was measured from two measuring tap where pressure transducers were connected, the pressure from the two measuring tap was showing similarity in the pressure profile.

The calibration curves in both the plenum chamber and the bedchamber are shown in the plots below:

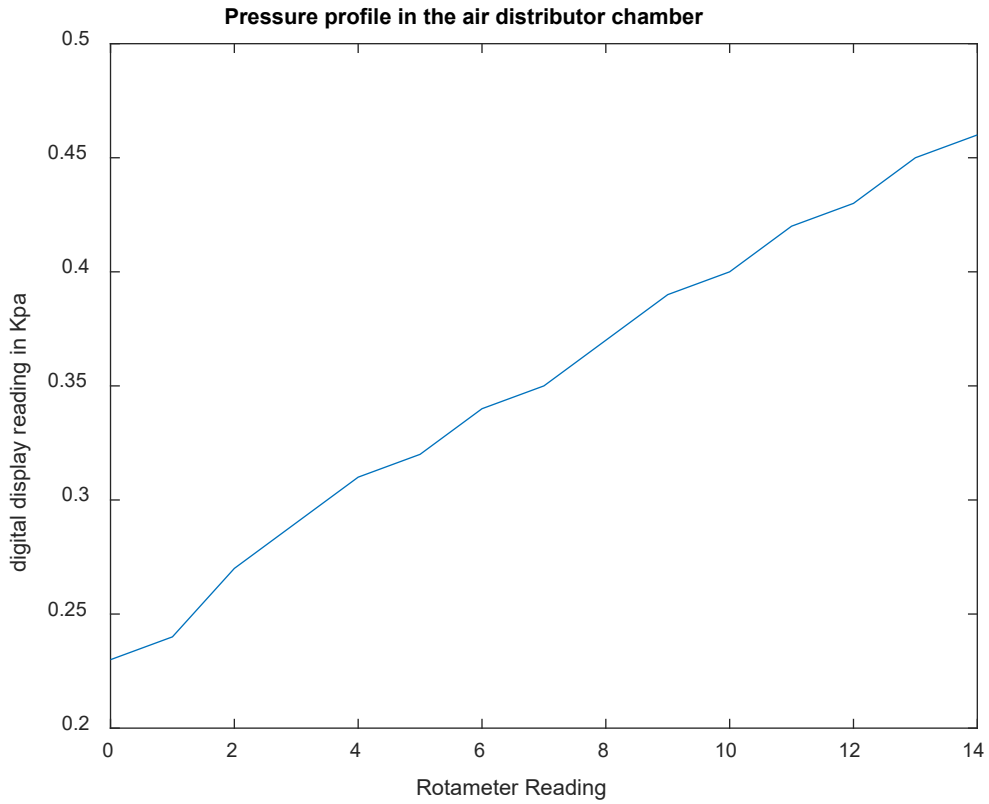

Figure 8. 3**: Pressure profile in the plenum of the conventional fluidized bed column**

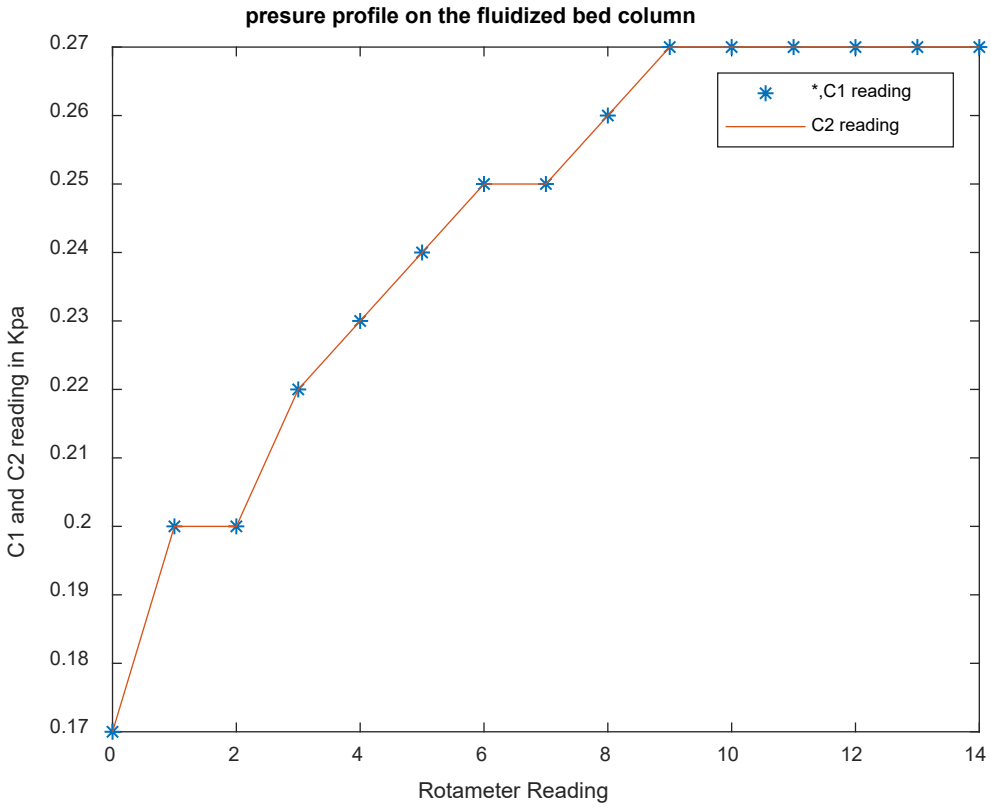

Figure 8. 4**: Pressure profile in the section above the distributor plate**

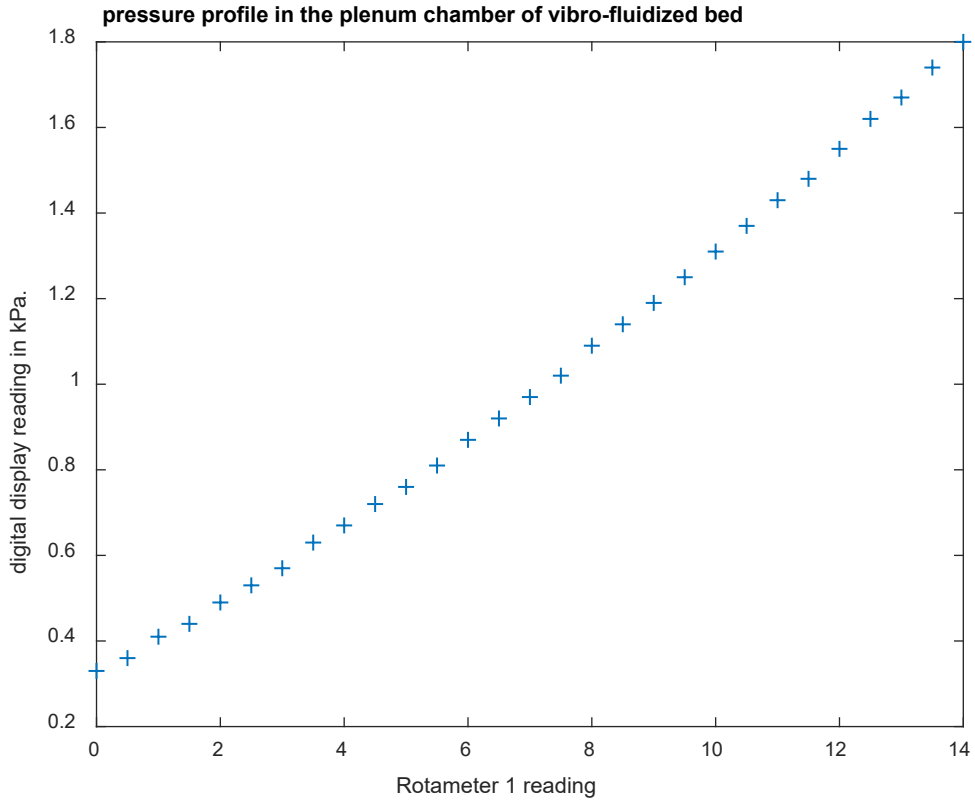

Figure 8. 5**: The increase of pressure in the plenum chamber of a Vibro-fluidized bed**

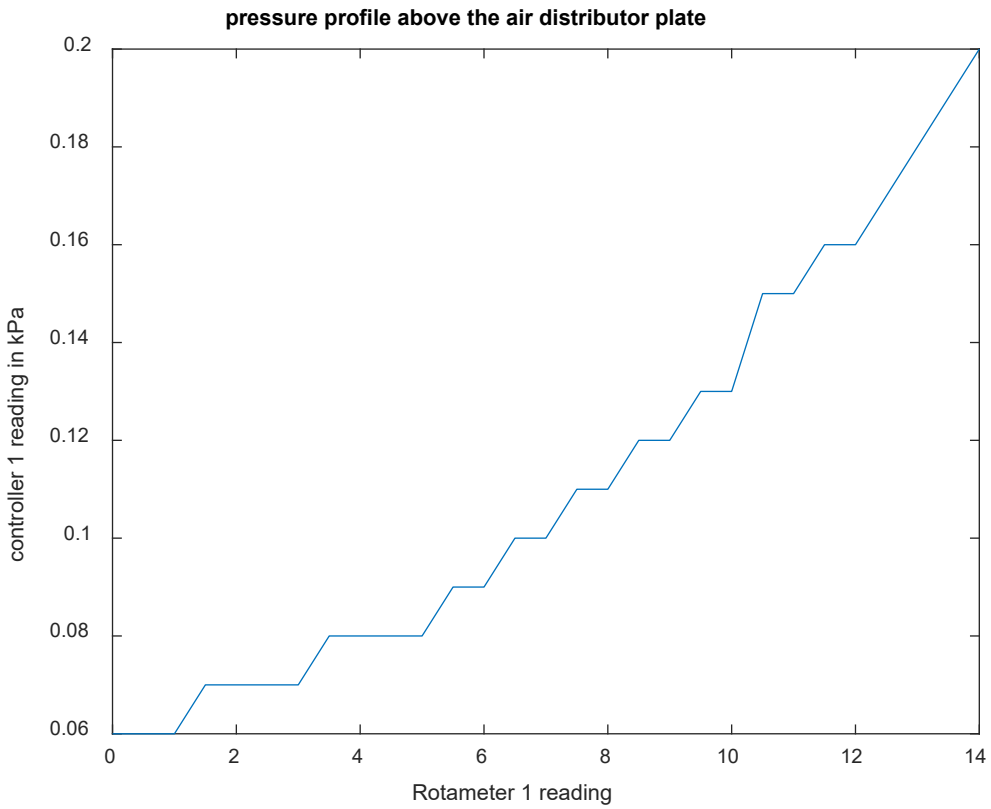

Figure 8. 6**: Pressure profile above the air distributor plate**

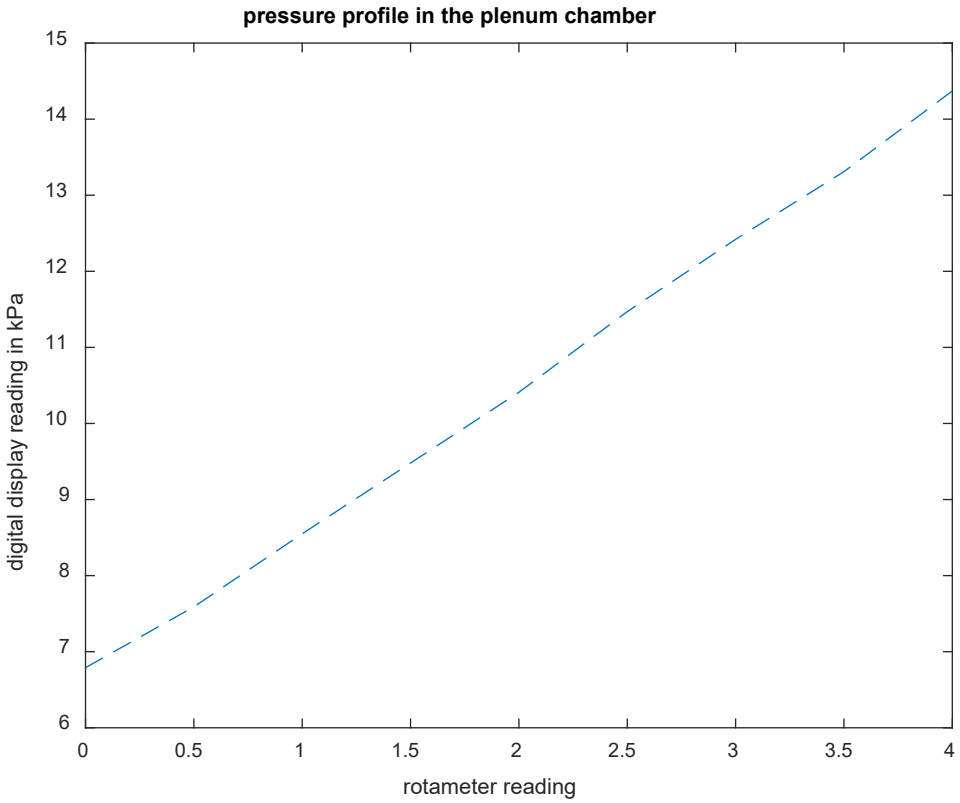

Figure 8. 7**: Pressure profile in the plenum chamber of a fluidized bed column of 50mm**

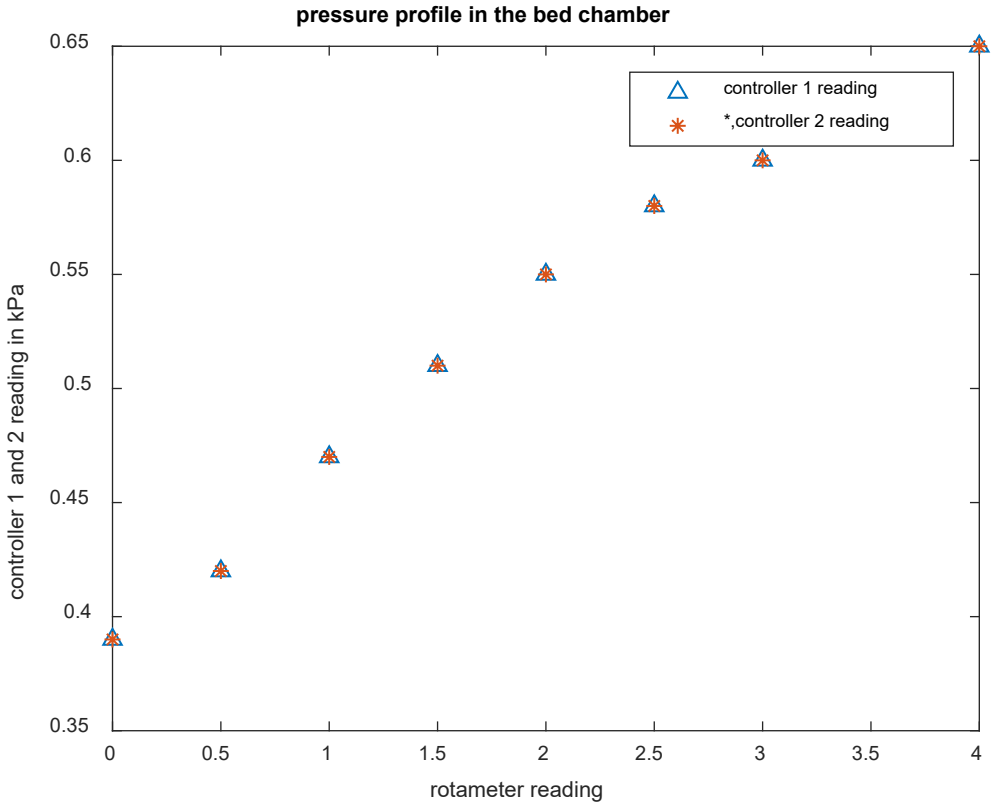

Figure 8. 8**: Pressure profile above the air distributor plate of the FB of 50mm**

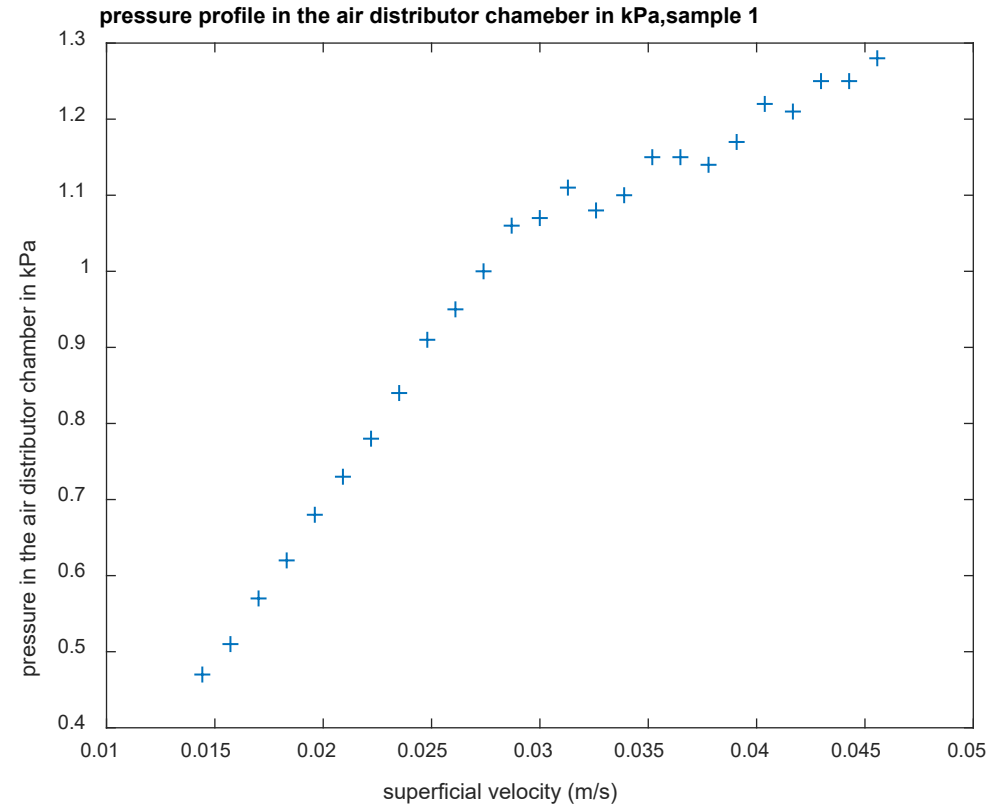

Figure 8. 9**: The increase of pressure in the plenum chamber during fluidization of sample 1**

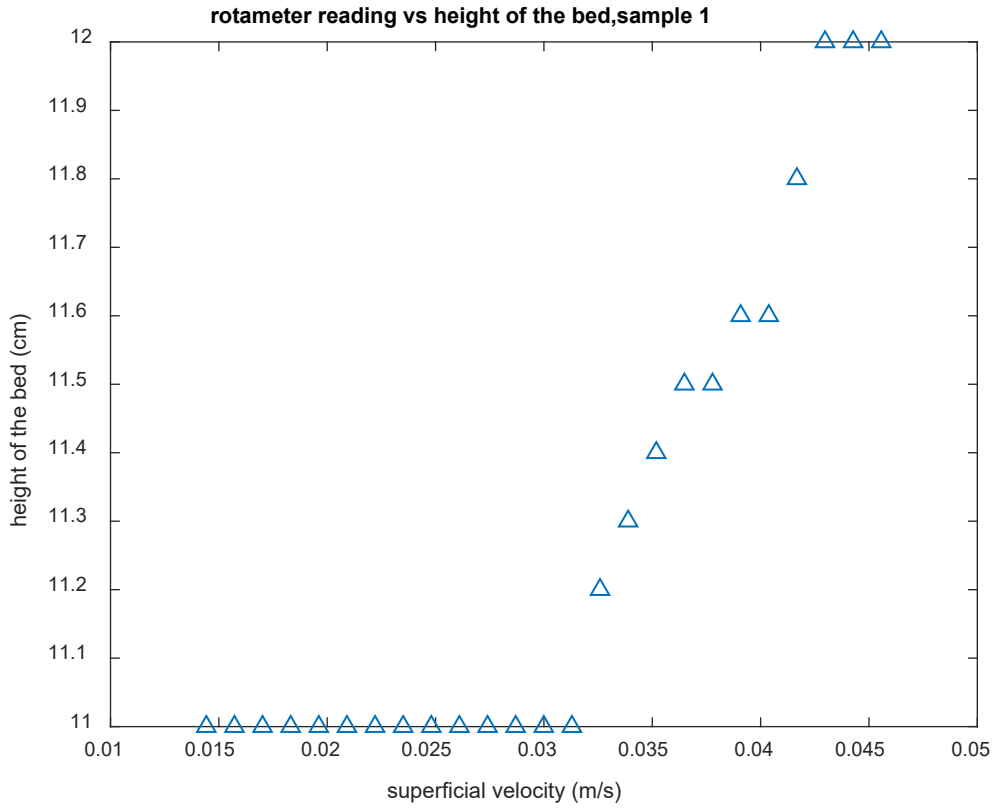

Figure 8. 10**: The bed expansion in the bedchamber of a fluidized bed of 0.12 m of diameter**

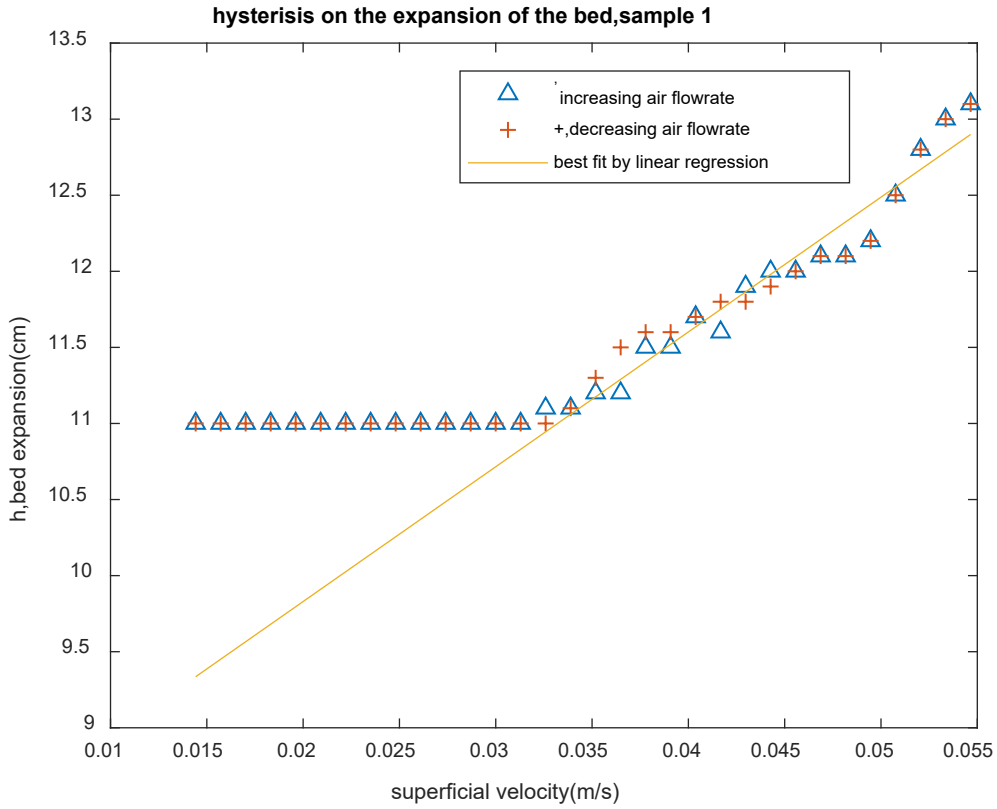

Figure 8. 11**: The expansion of the bed in the bedchamber with decreasing airflow**

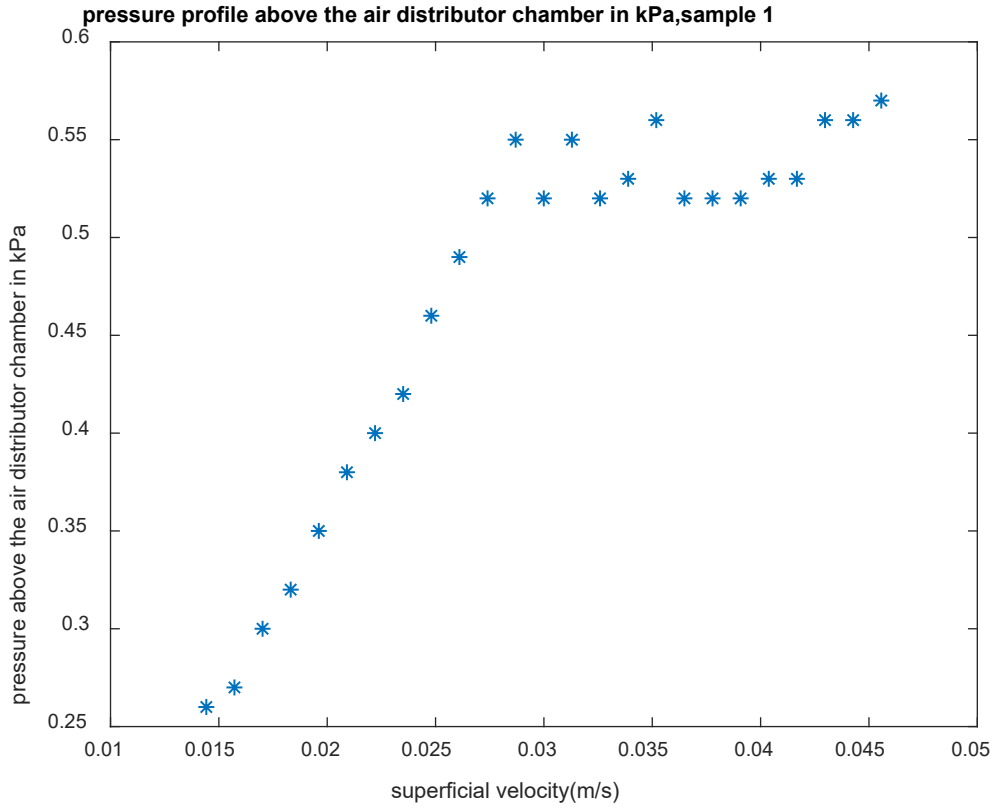

Figure 8. 12**: The pressure drop on the bed of solid measured using pressure transducers**

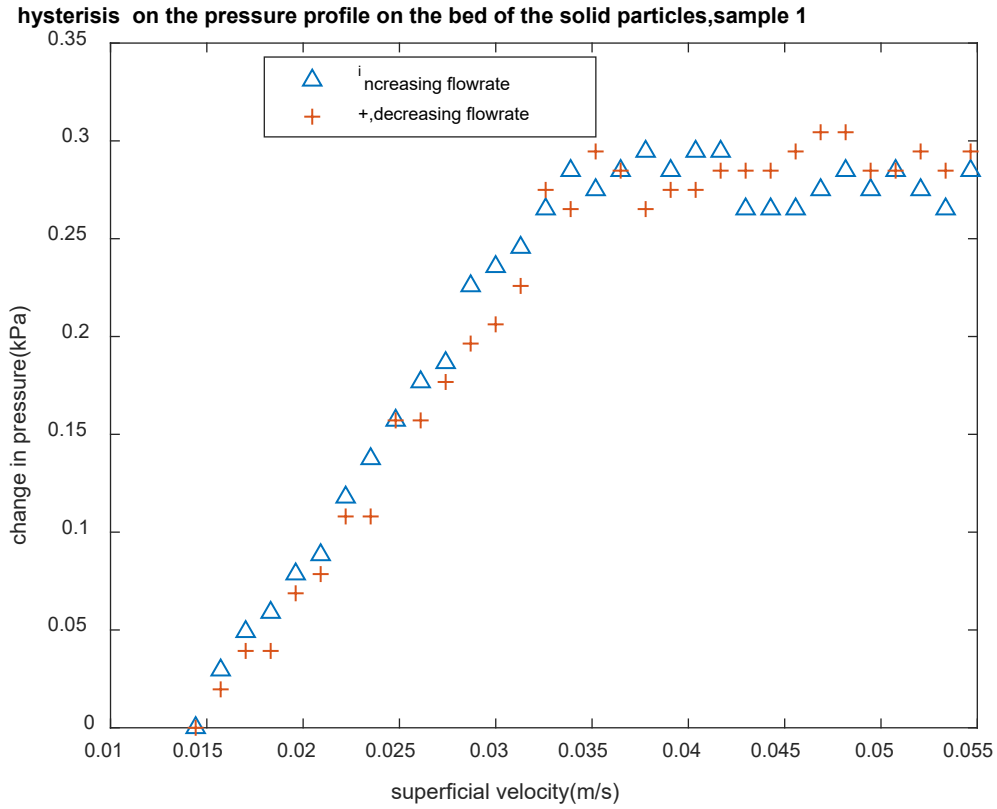

Figure 8. 13**: The pressure drop on the bed of solid measured using an inverted manometer**

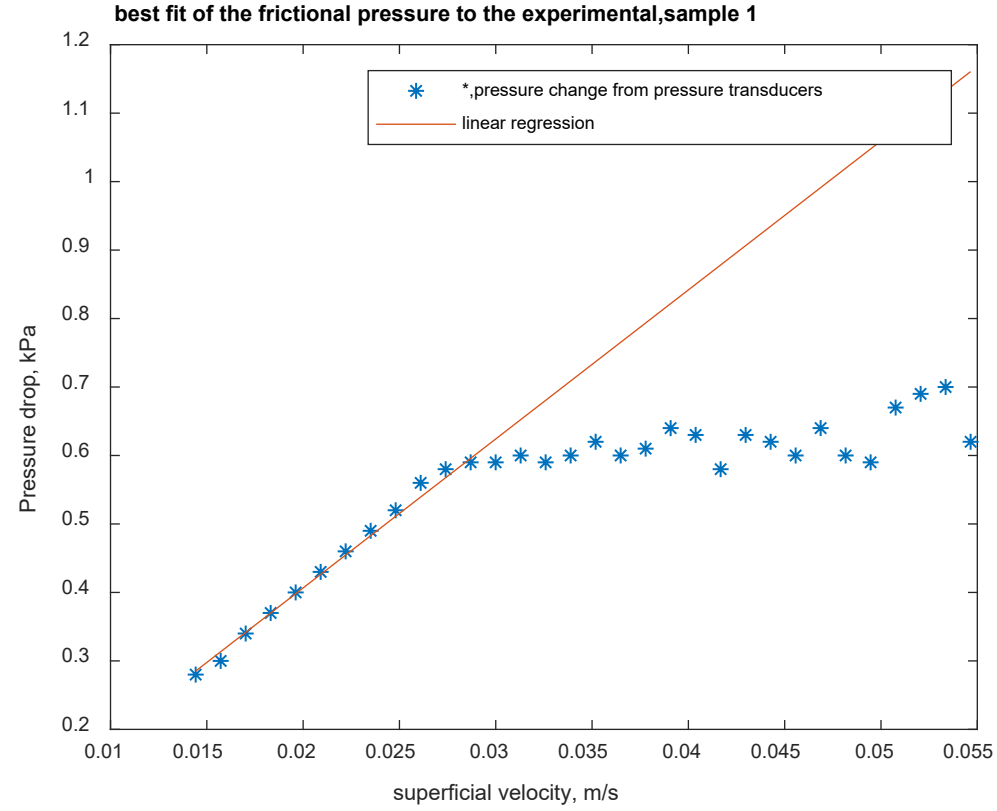

Figure 8. 14**: Fitting of the Ergun equation to the measured pressure drop**

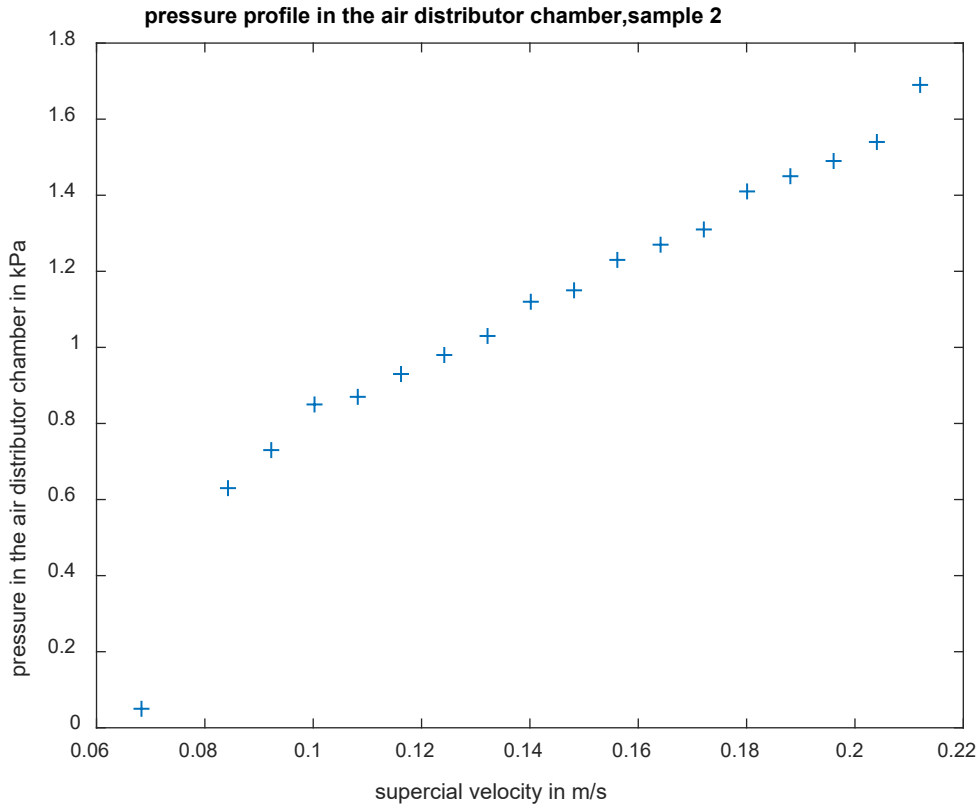

Figure 8. 15**: Increase in pressure in the plenum chamber during fluidization**

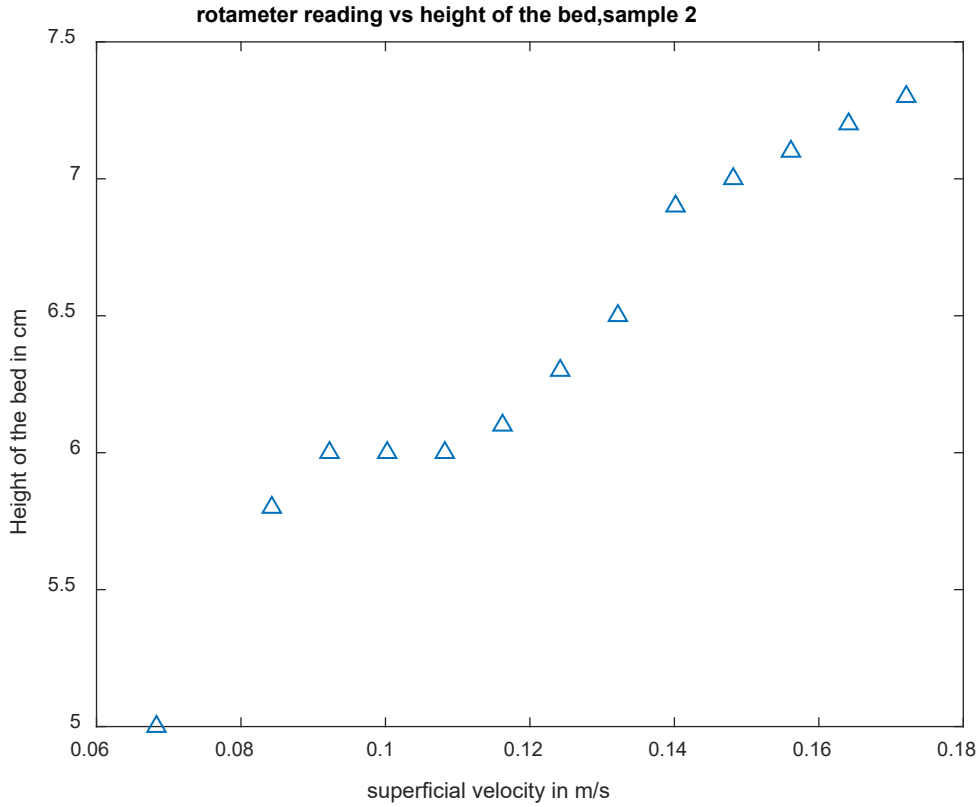

Figure 8. 16**: The bed expansion in the bedchamber of a fluidized bed of 0.12 m of diameter**

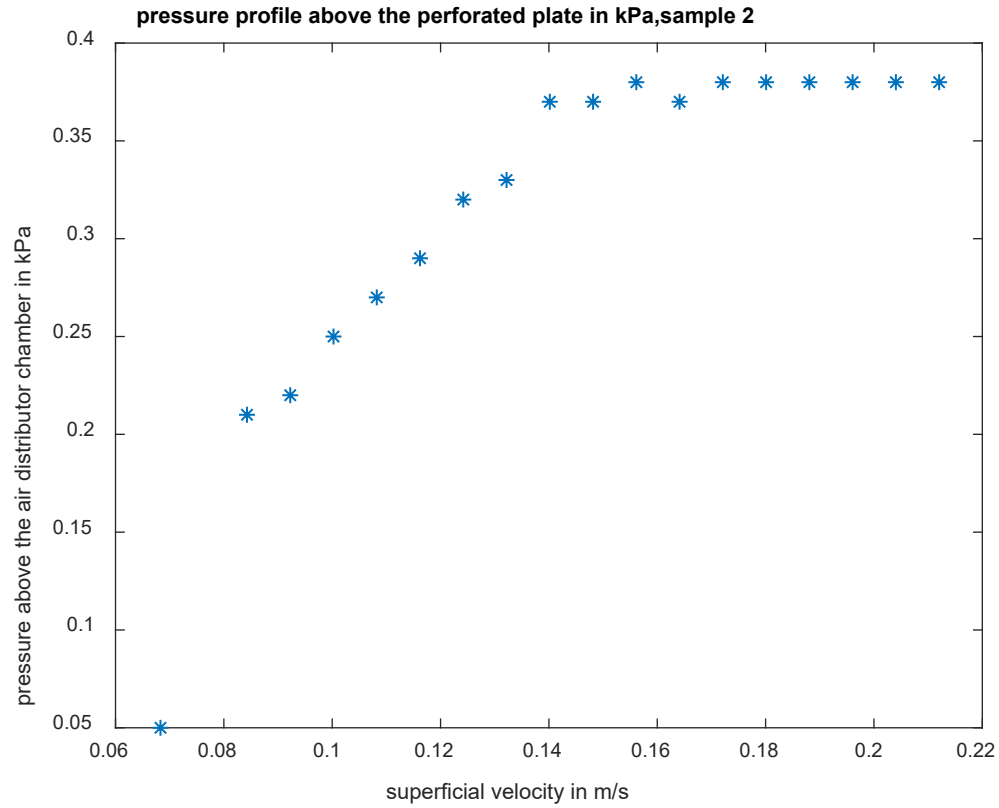

Figure 8. 17**: The pressure drop on the bed of solid measured using pressure transducers**

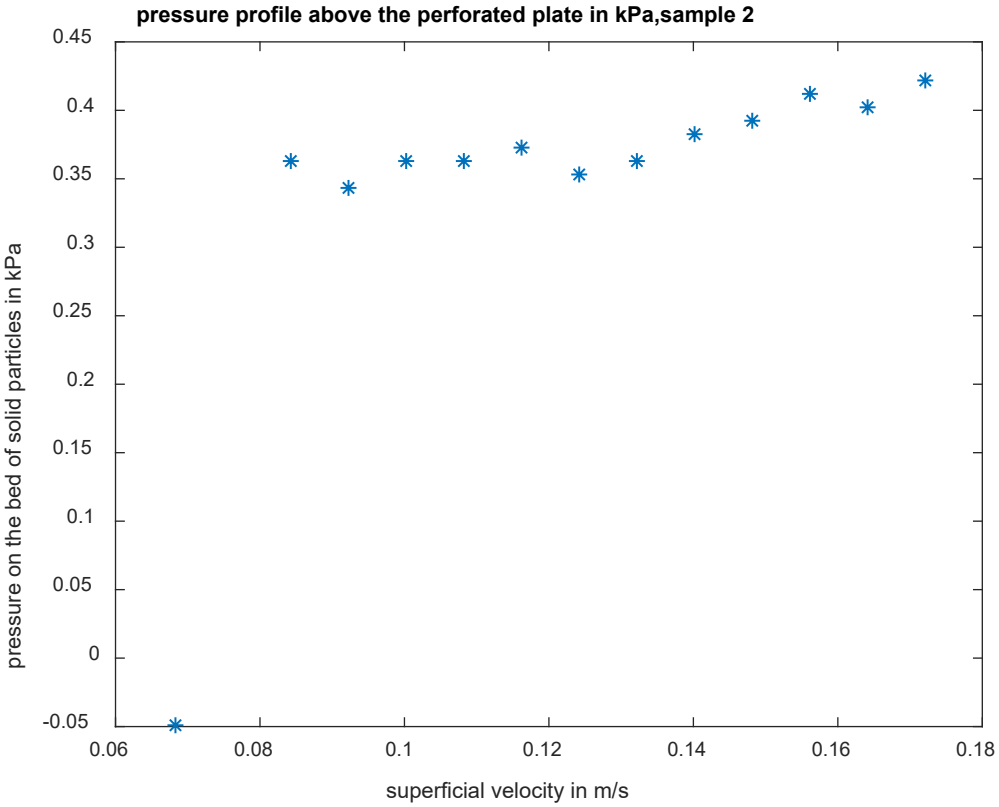

Figure 8. 18**: The pressure drop on the bed of solid measured using an inverted manometer**

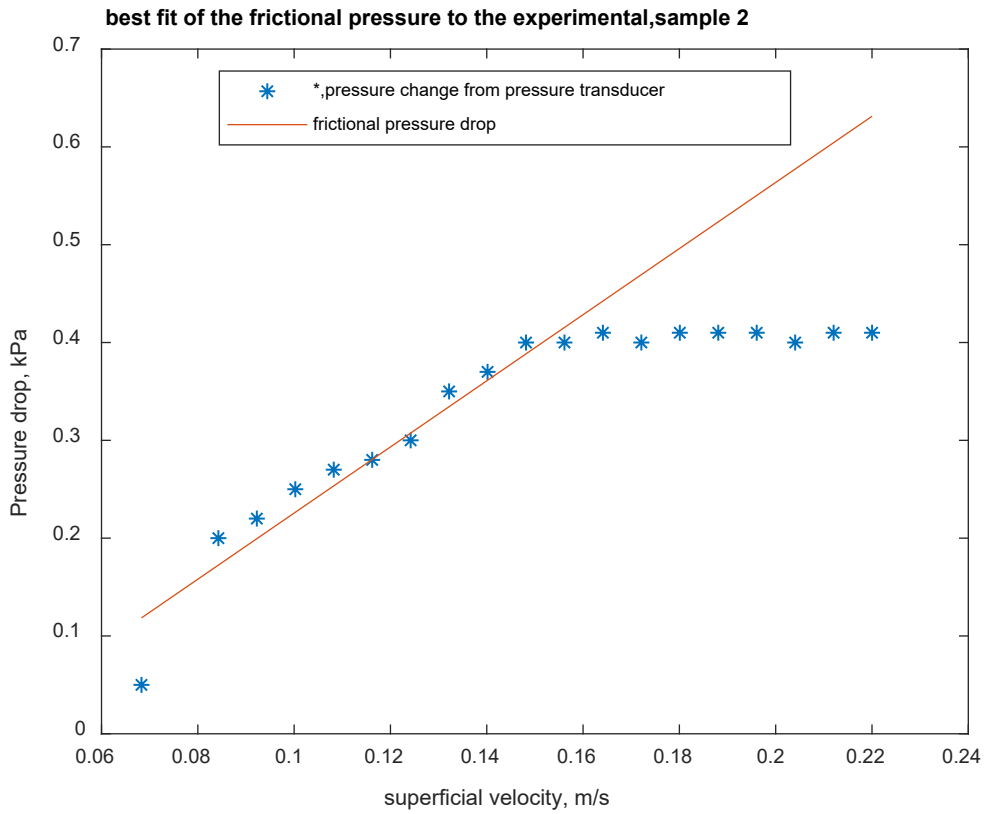

Figure 8. 19**: Fitting of the Ergun equation to the measured pressure drop**

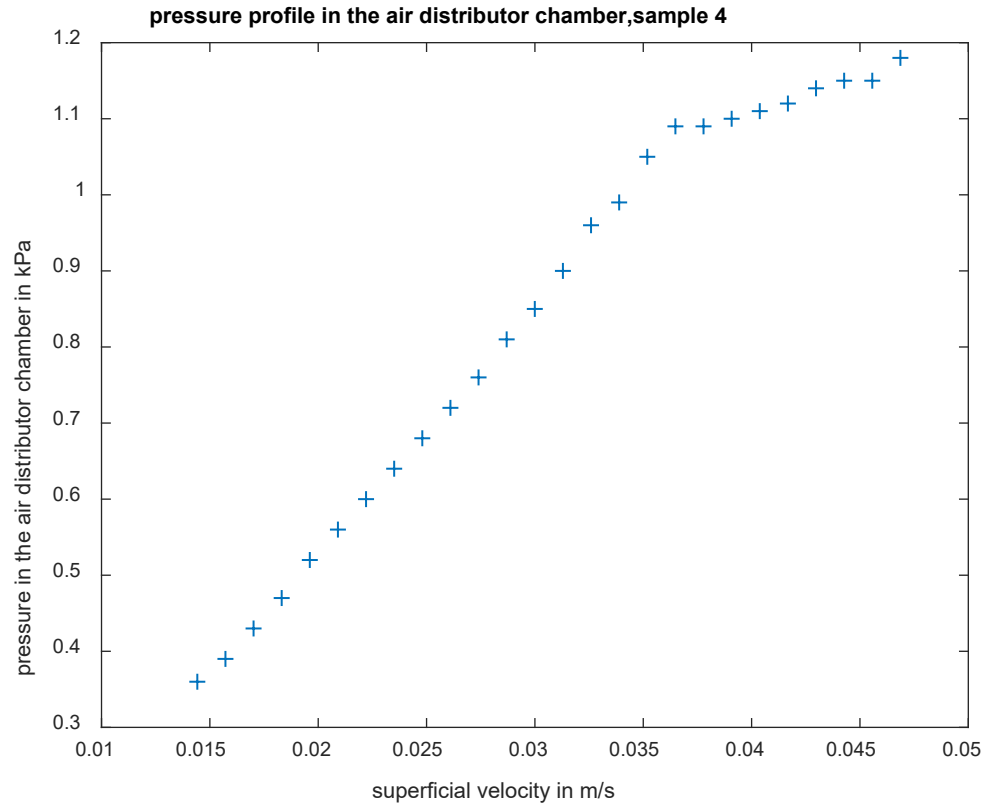

Figure 8. 20**: Increase in pressure in the plenum chamber during fluidization**

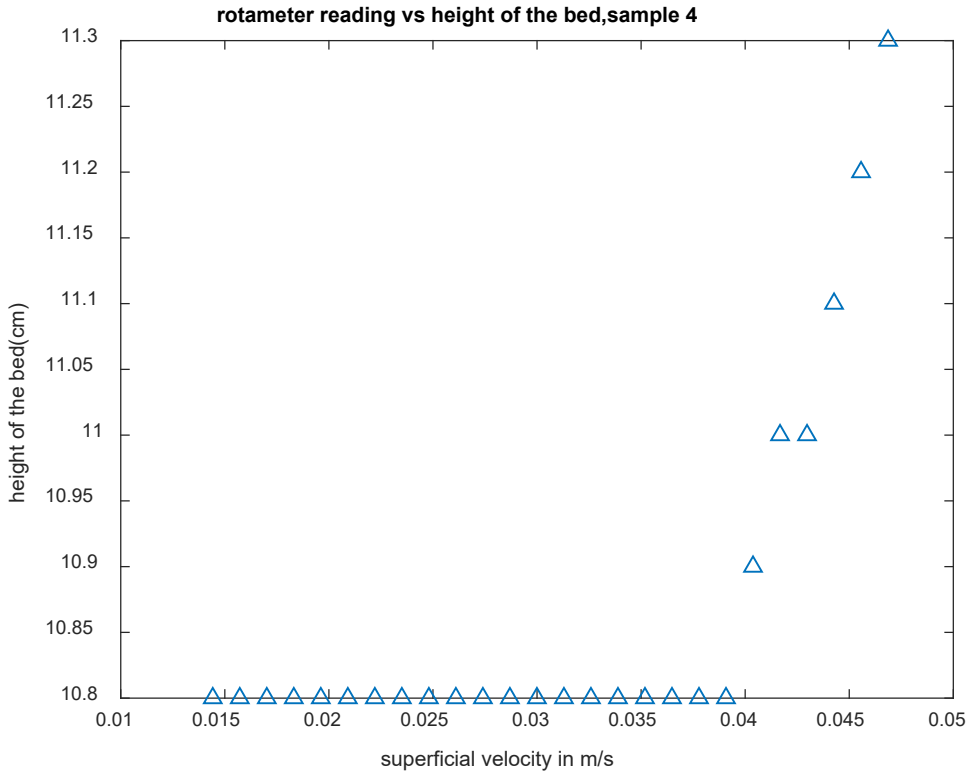

Figure 8. 21**: The bed expansion in the bedchamber of a fluidized bed of 0.12 m of diameter**

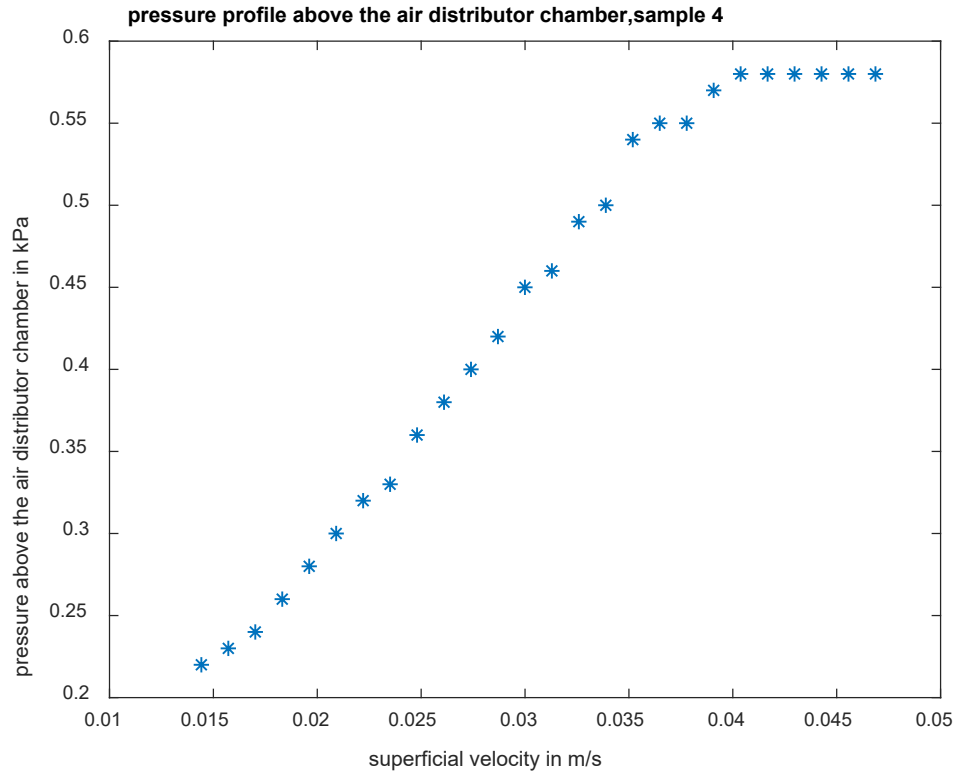

Figure 8. 22**: The pressure drop on the bed of solid measured using pressure transducers**

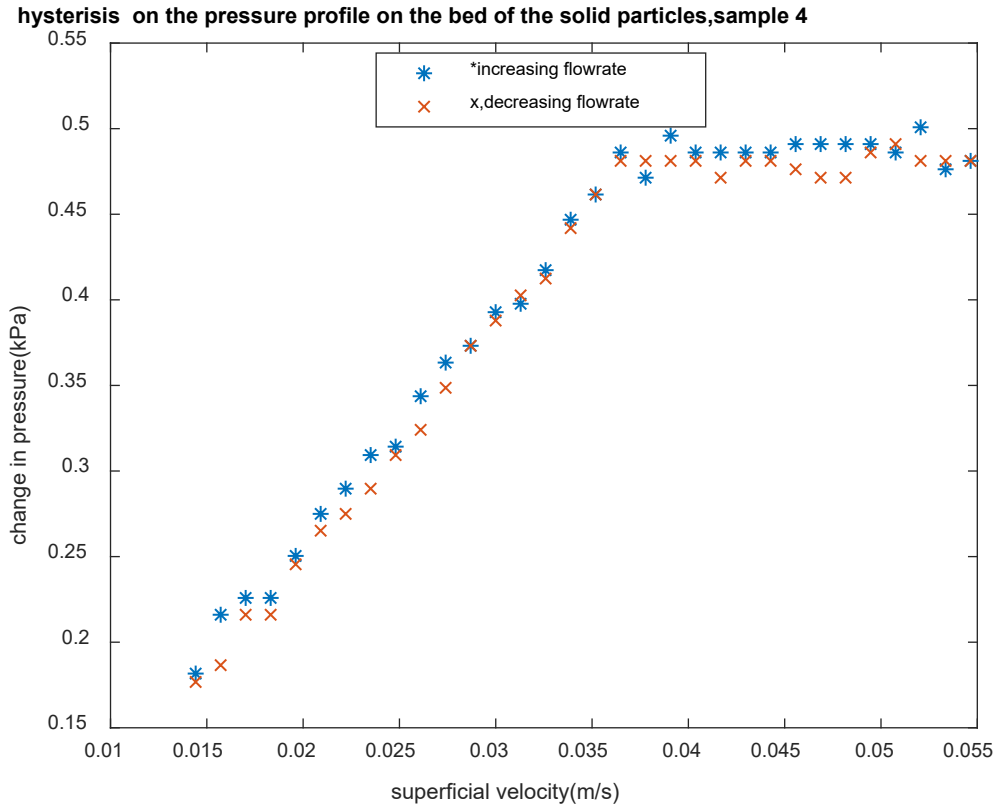

Figure 8. 23**: The pressure drop on the bed of solid measured using an inverted manometer**

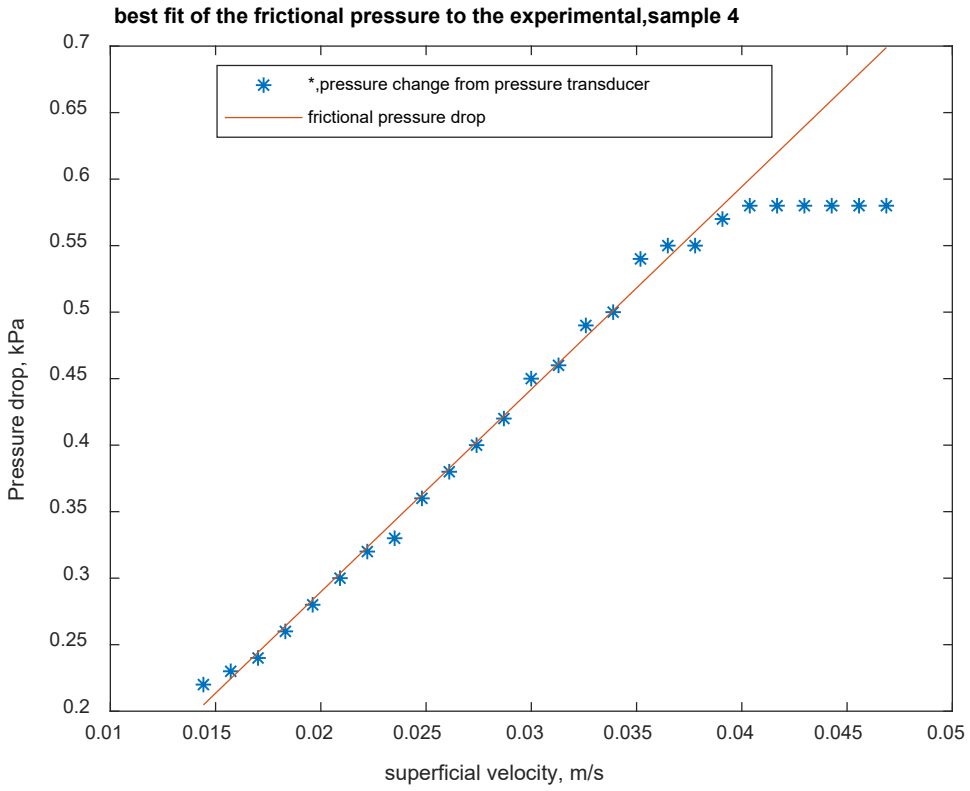

Figure 8. 24**: Fitting of the Ergun equation to the measured pressure drop**

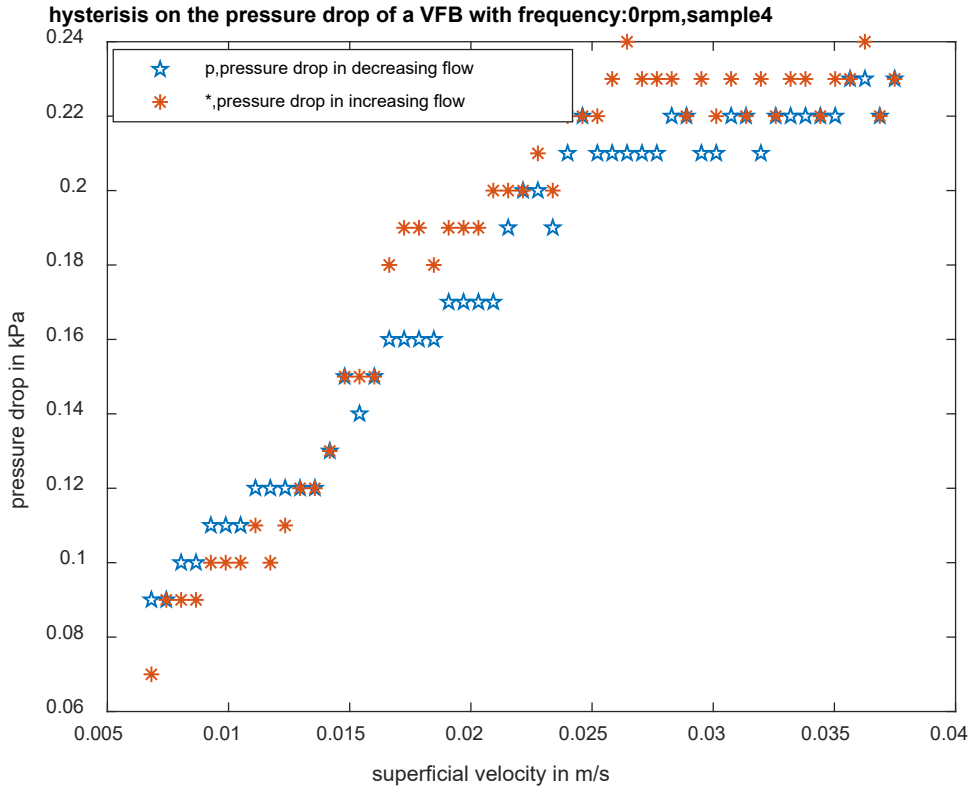

Figure 8. 25**: Pressure drop on the bed measured using pressure transducers**

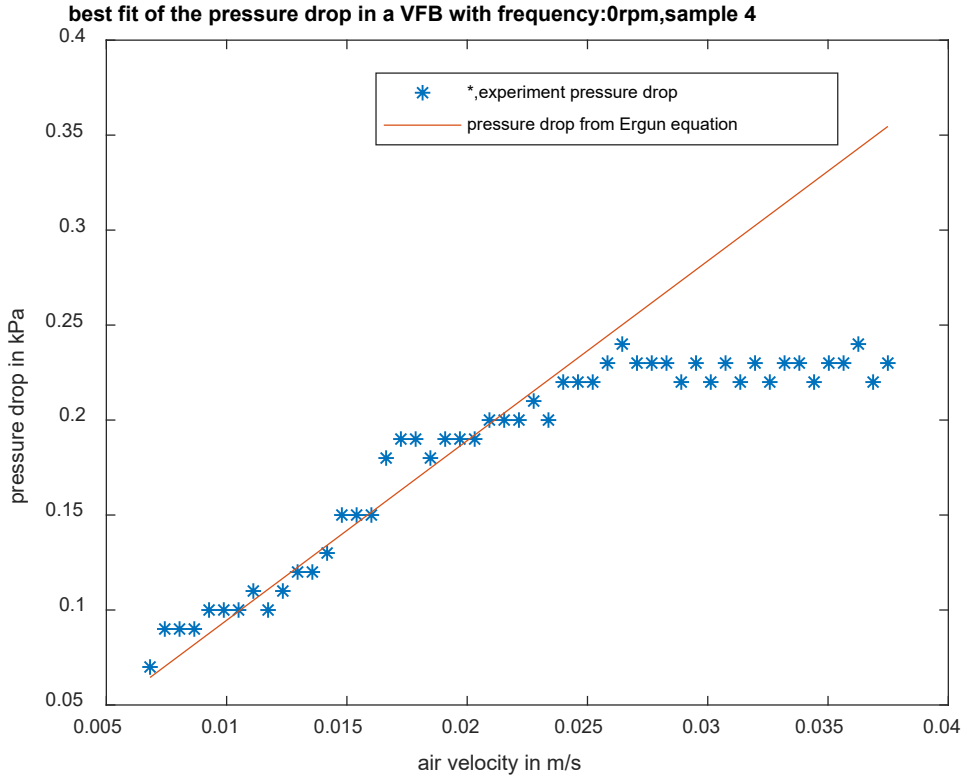

Figure 8. 26**: Fitting of the Ergun equation to the experiment pressure drop by adjusting the sphericity in a Vibro-fluidized bed**

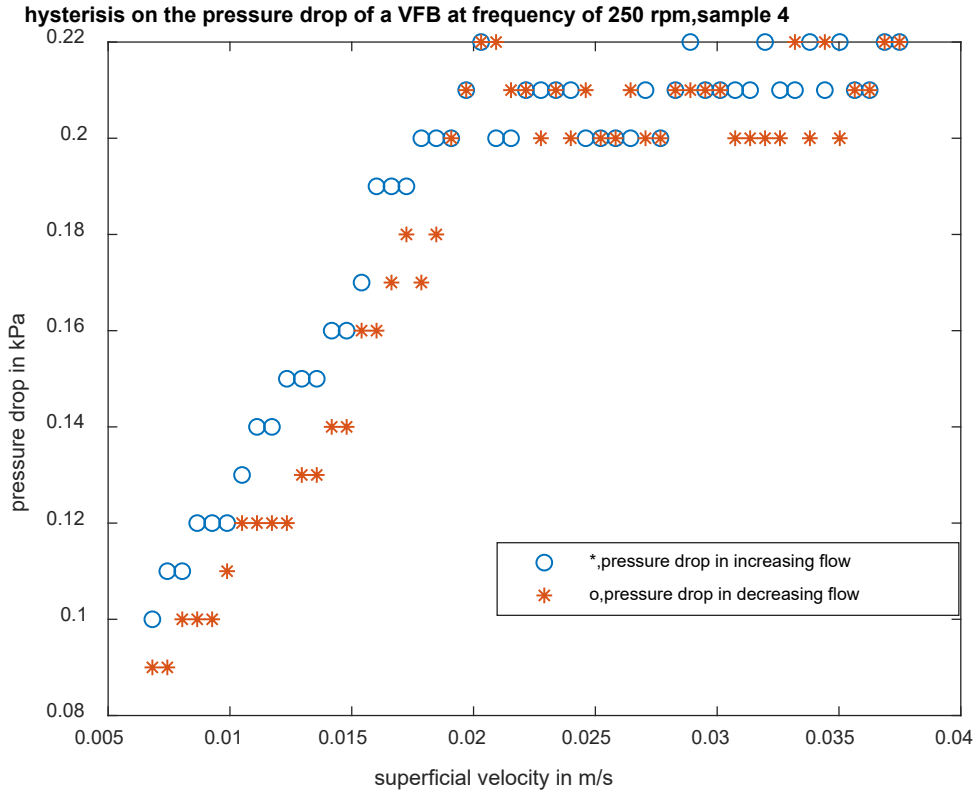

Figure 8. 27**: Pressure drop on the bed measured using pressure transducers**

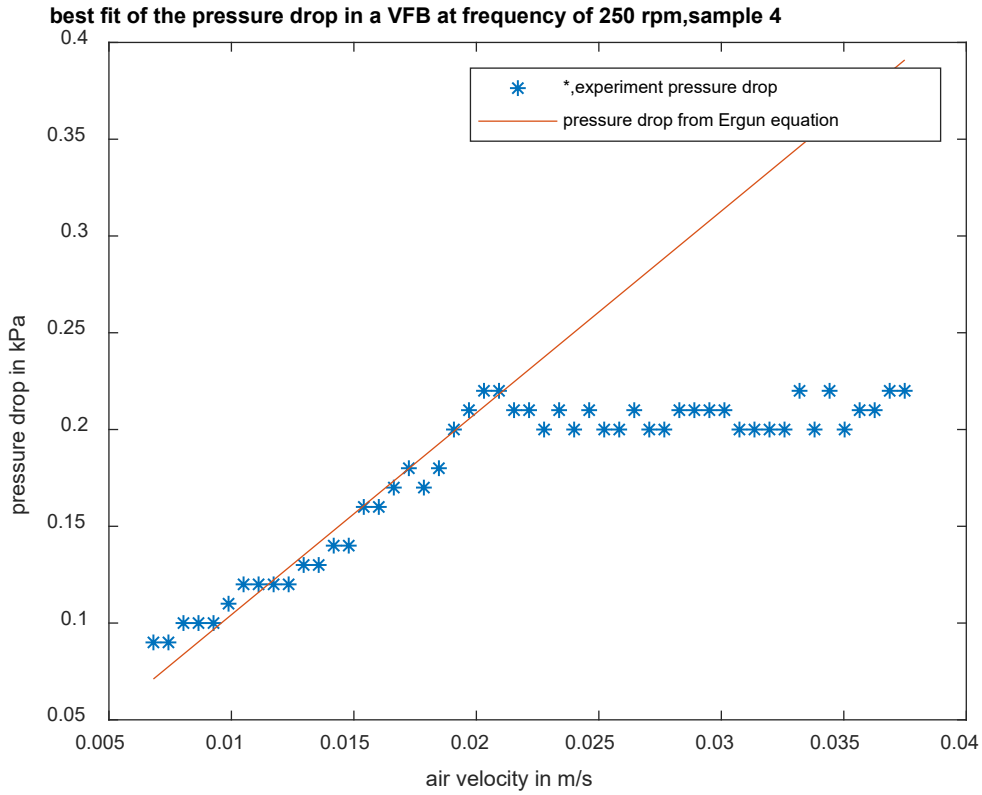

Figure 8. 28**: Fitting of the Ergun equation to the experiment pressure drop by adjusting the sphericity in a Vibro-fluidized bed**

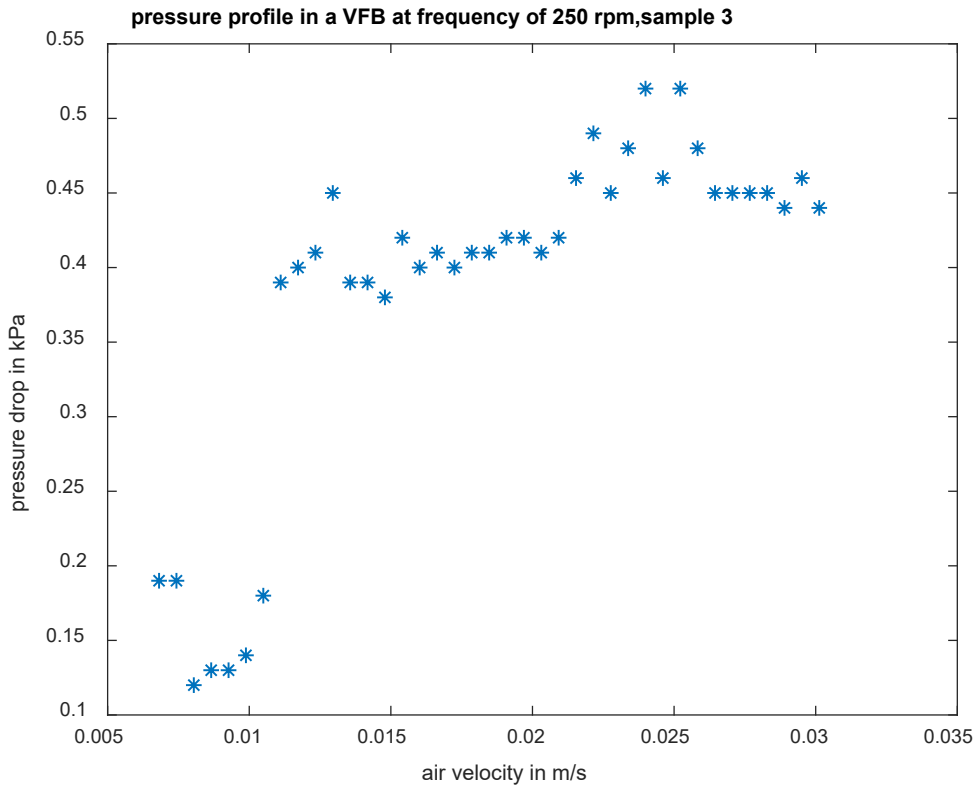

Figure 8. 29**: Pressure drop measured using pressure transducers in a VFB**

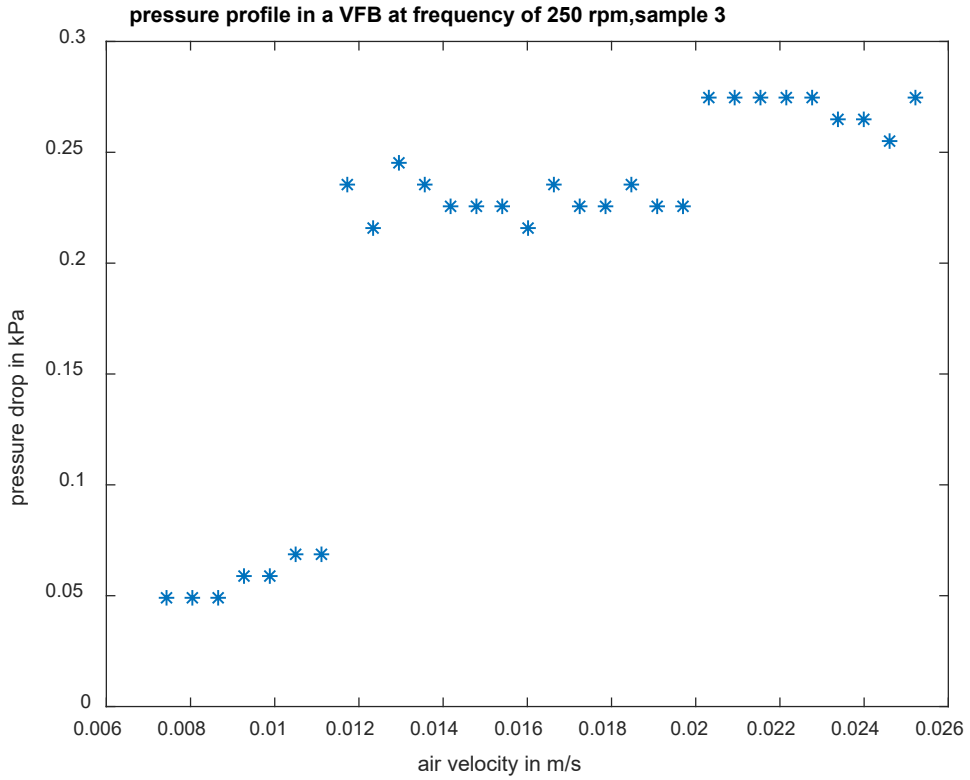

Figure 8. 30**: Pressure drop in the bedchamber of a VFB using inverted manometers**

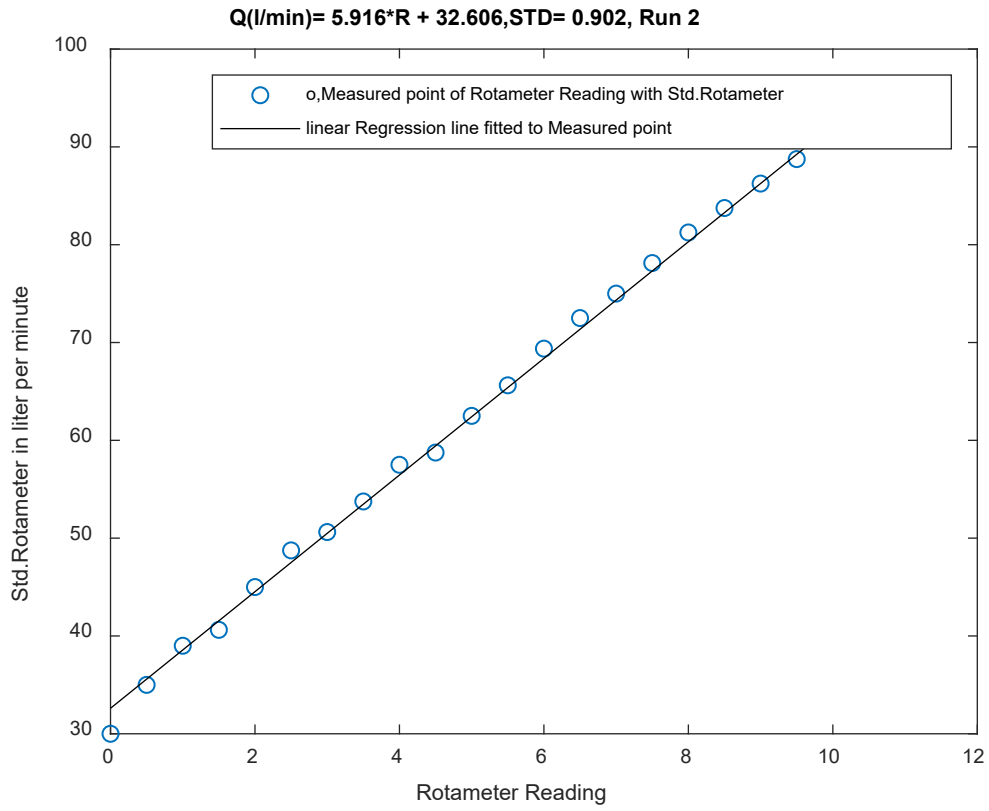

Figure 8. 31**: Calibration curve for the reading of Rotameter 1 for the second run**

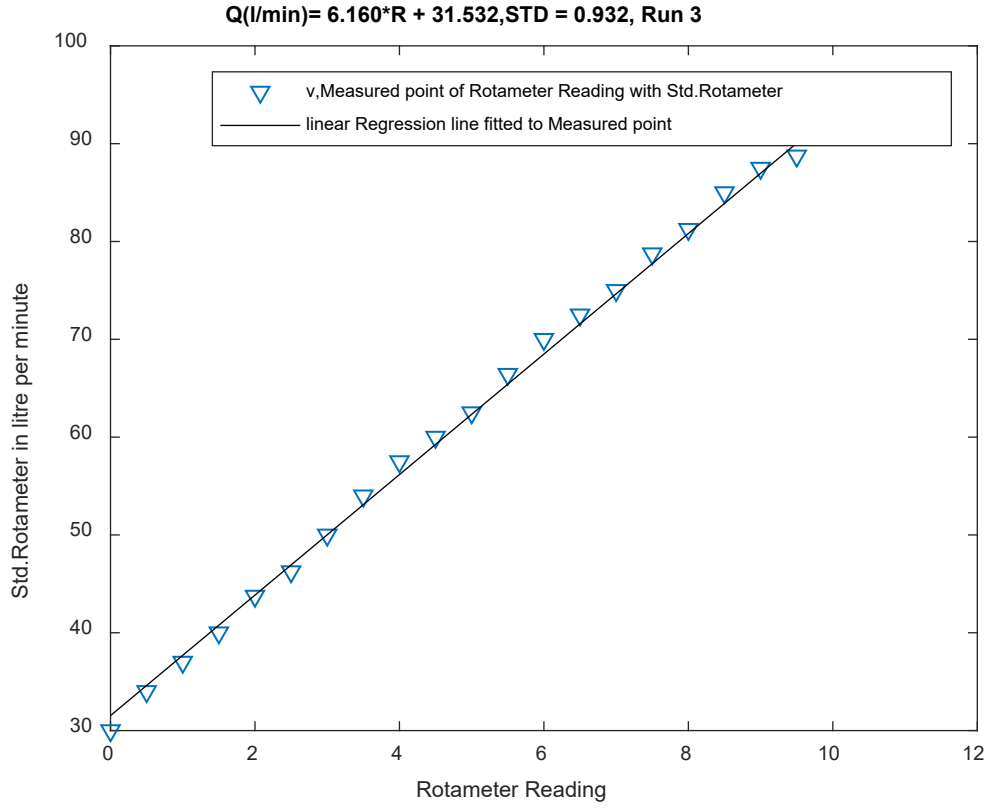

Figure 8. 32**: Calibration curve for the reading of the Rotameter 1 of the third run**

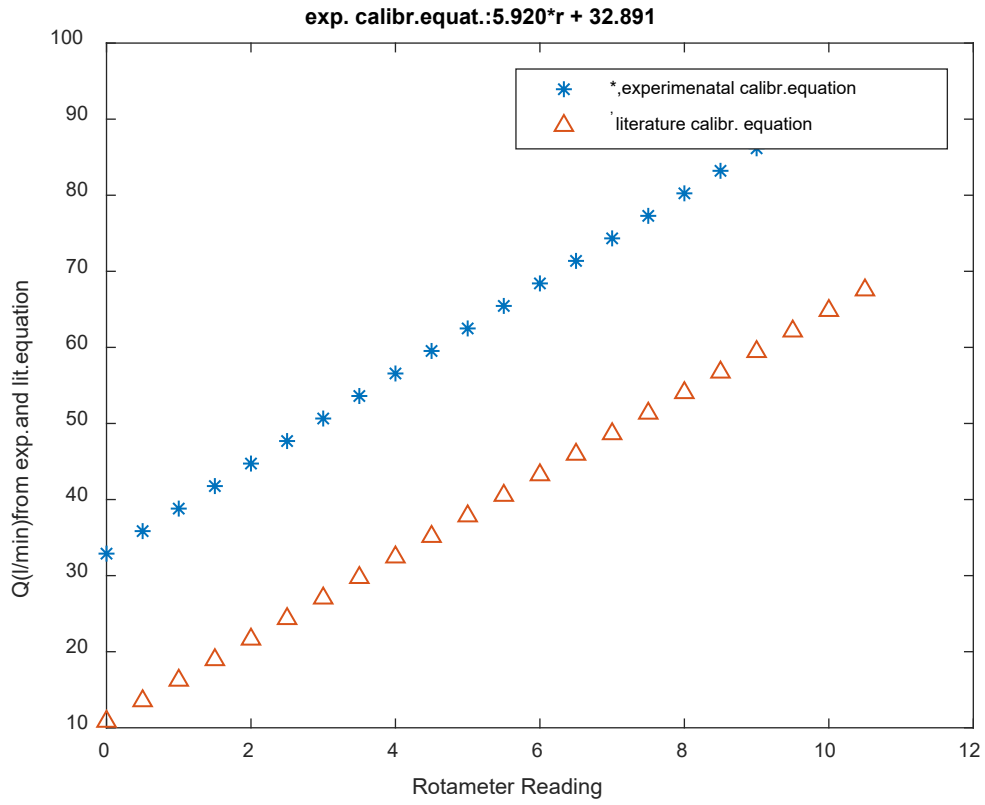

Figure 8. 33**: Calibration curve from the experimental and literature equations of Rotameter 1**

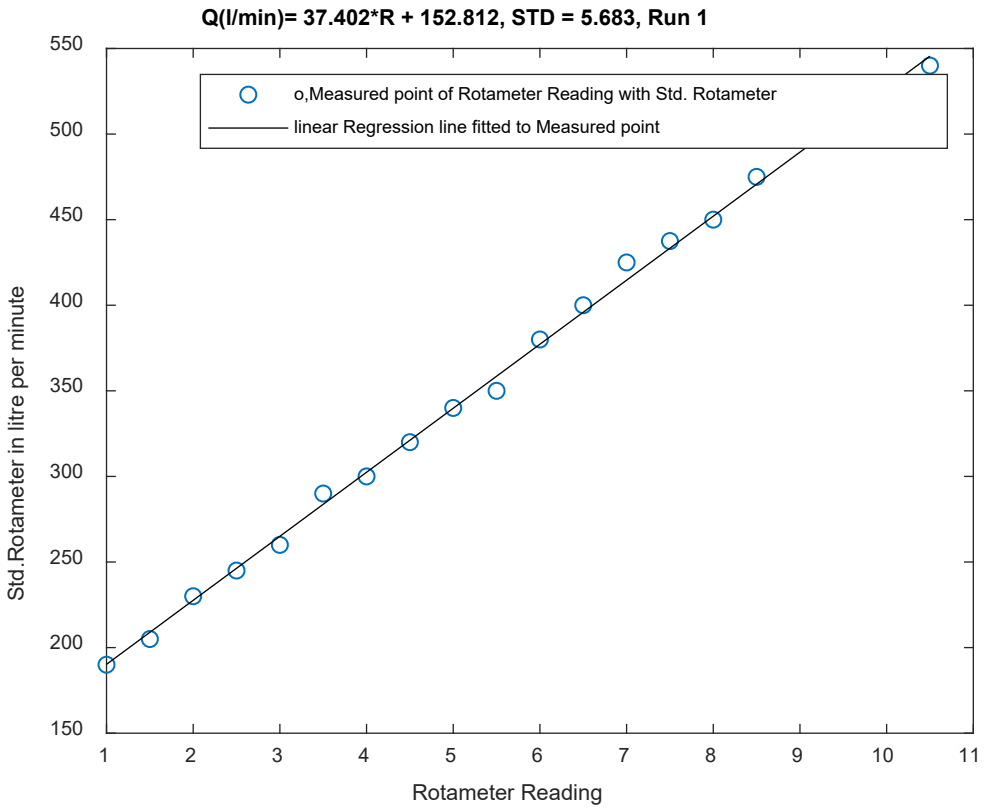

Figure 8. 34**: Calibration curve for the reading of the Rotameter 2 of the first run**

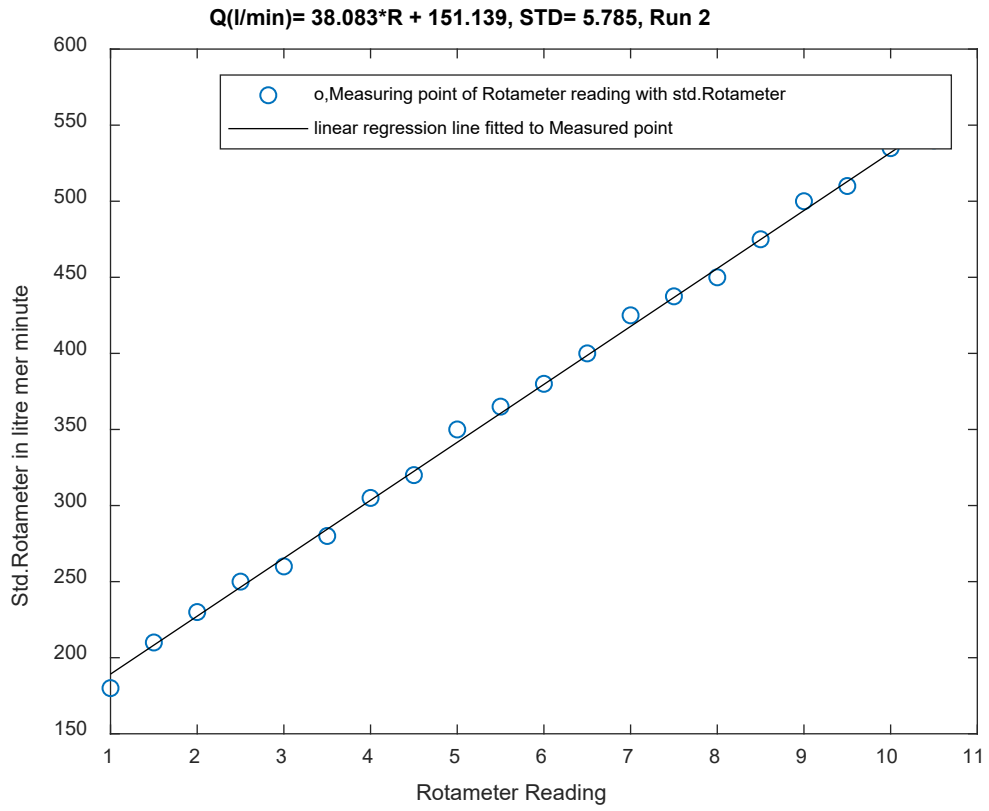

Figure 8. 35**: Calibration curve for the reading of the Rotameter 2 of the second run**

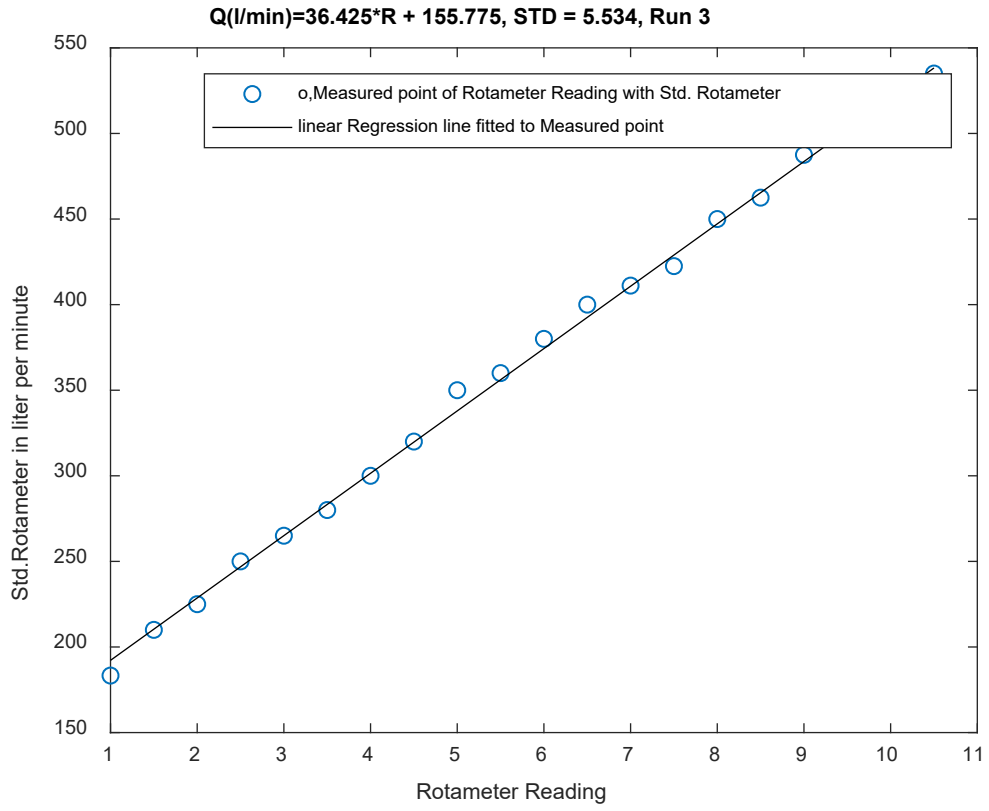

Figure 8. 36**: Calibration curve for the reading of the Rotameter 2 of the third run**

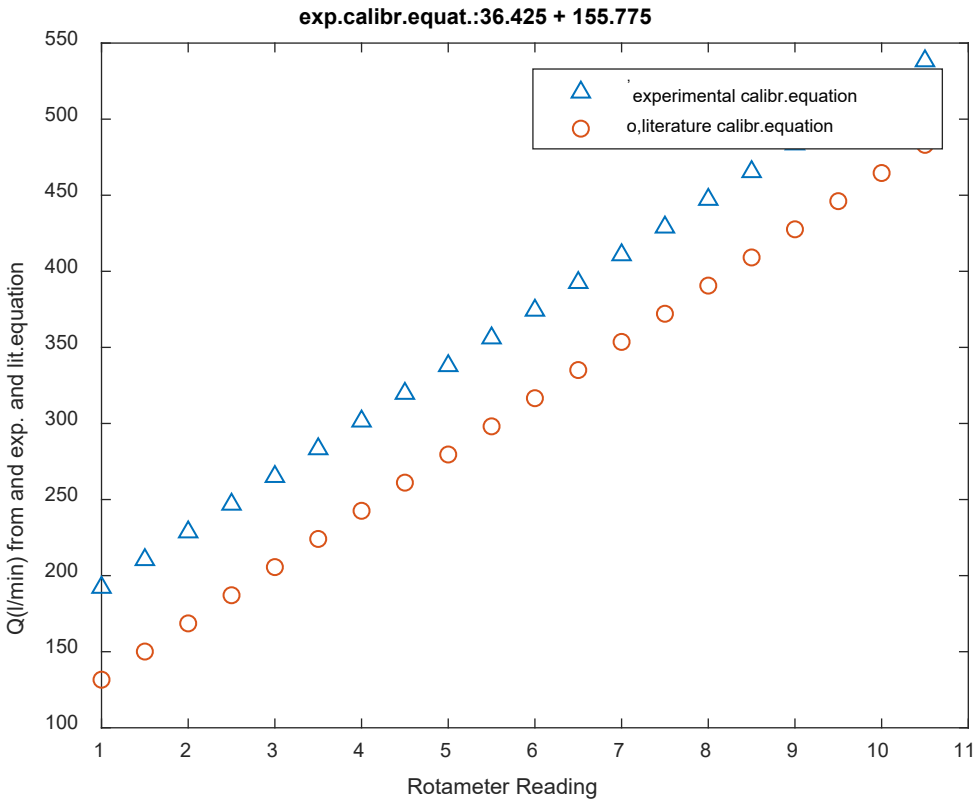

Figure 8. 37**: Calibration curve from the experimental and literature equations of Rotameter 2**

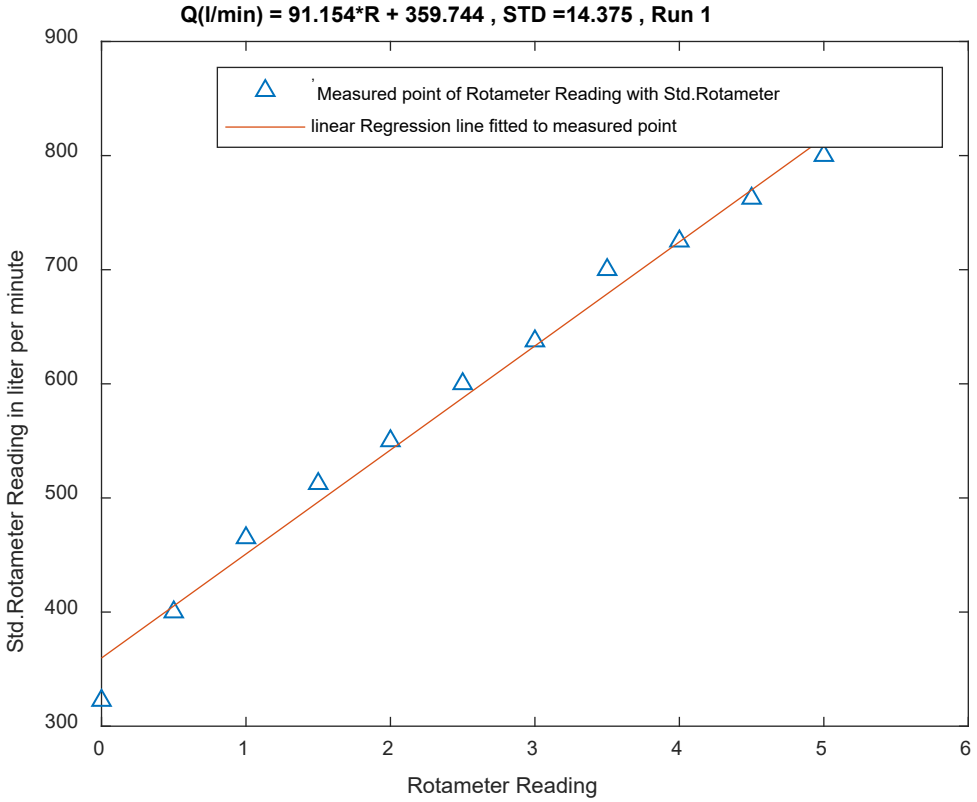

Figure 8. 38**: Calibration curve for the reading of the Rotameter 3 of the first run**

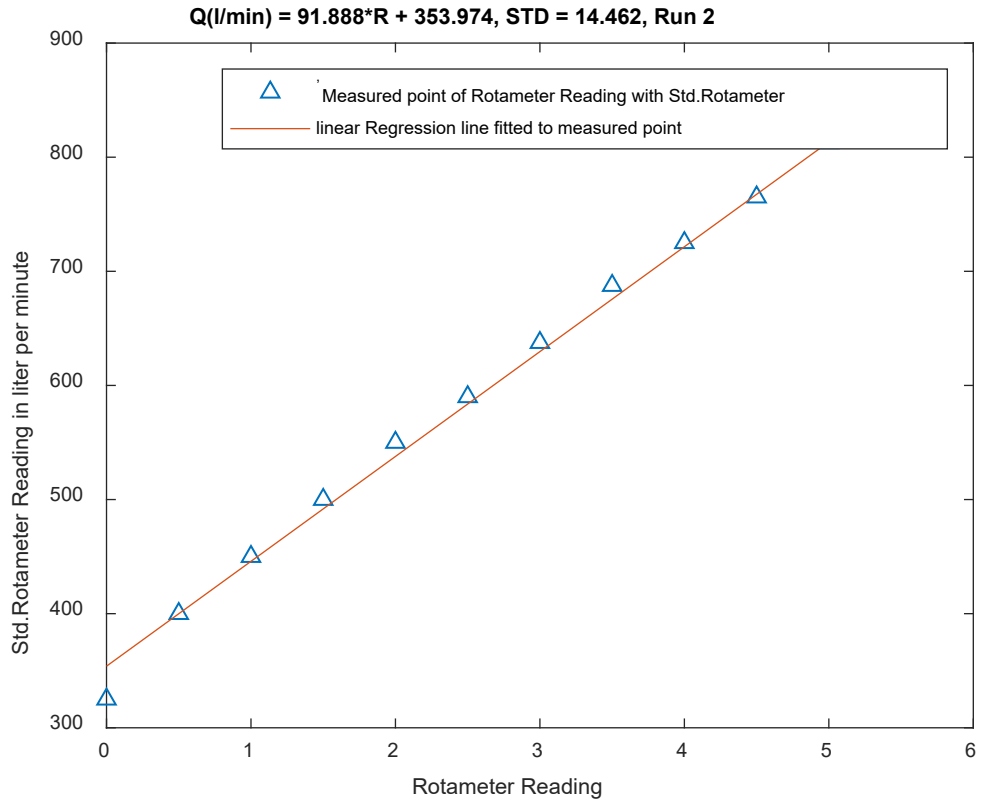

Figure 8. 39**: Calibration curve for the reading of the Rotameter 3 of the second run**

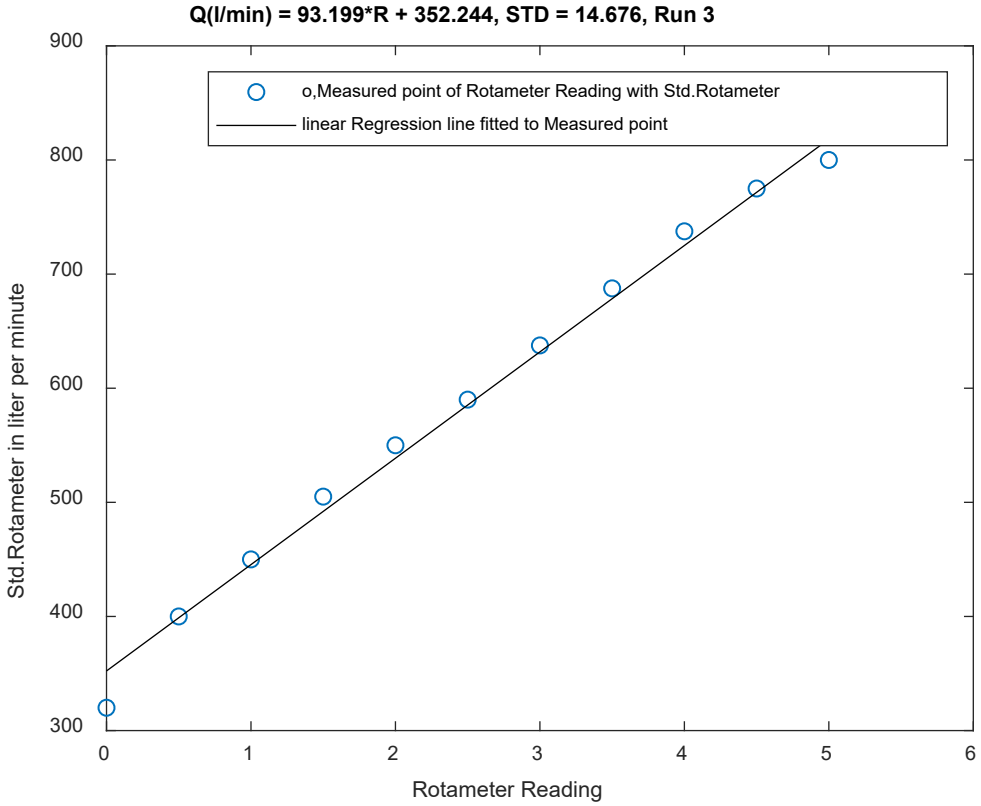

Figure 8. 40**: Calibration curve for the reading of the Rotameter 3 of the third run**

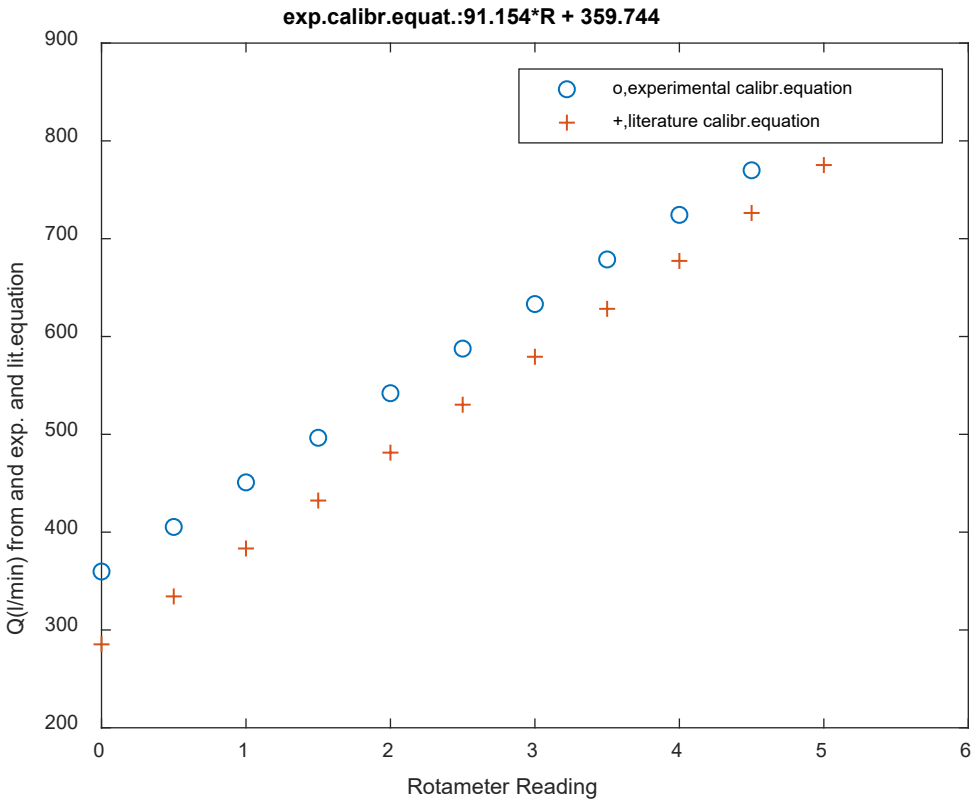

Figure 8. 41**: Calibration curve from the experimental and literature equations of Rotameter 3**

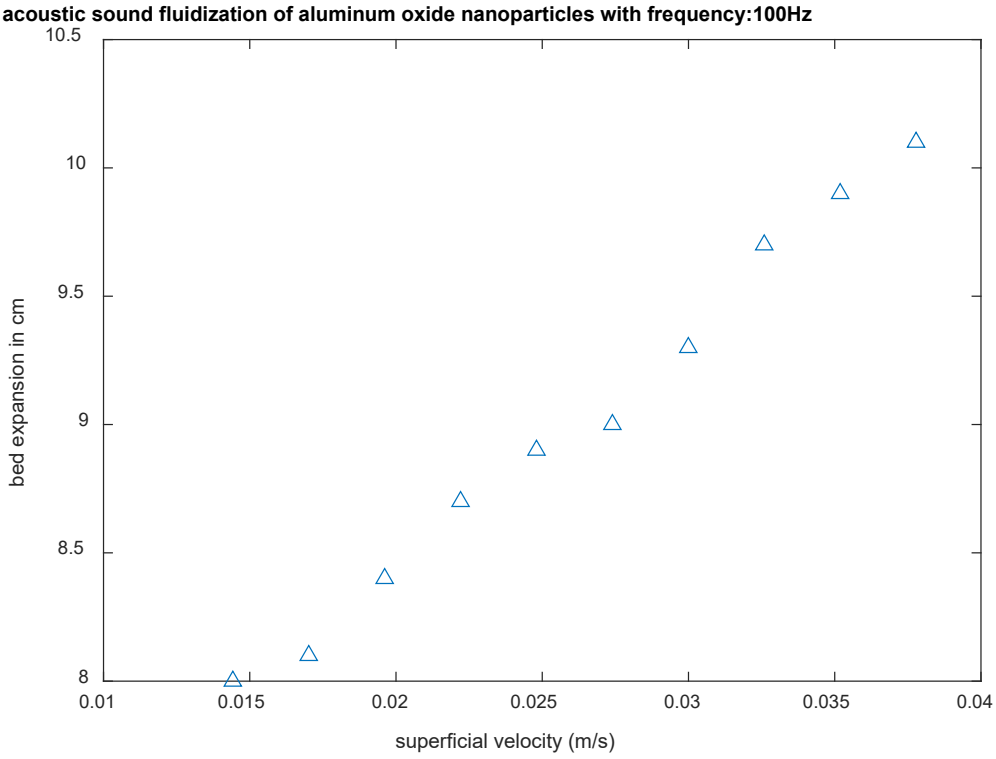

Figure 8. 42**: the expansion of the bed in an acoustic sound fluidized bed**

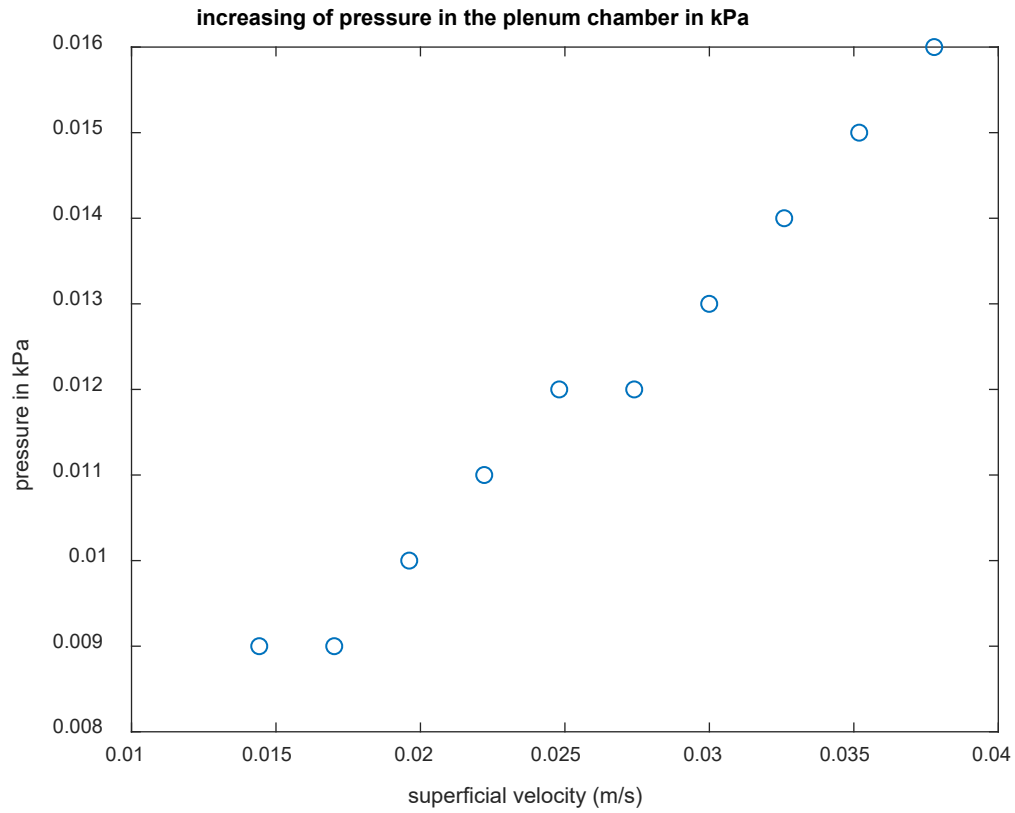

Figure 8. 43**: pressure profile in the plenum chamber of 0.12 diameter of acoustic sound FB**

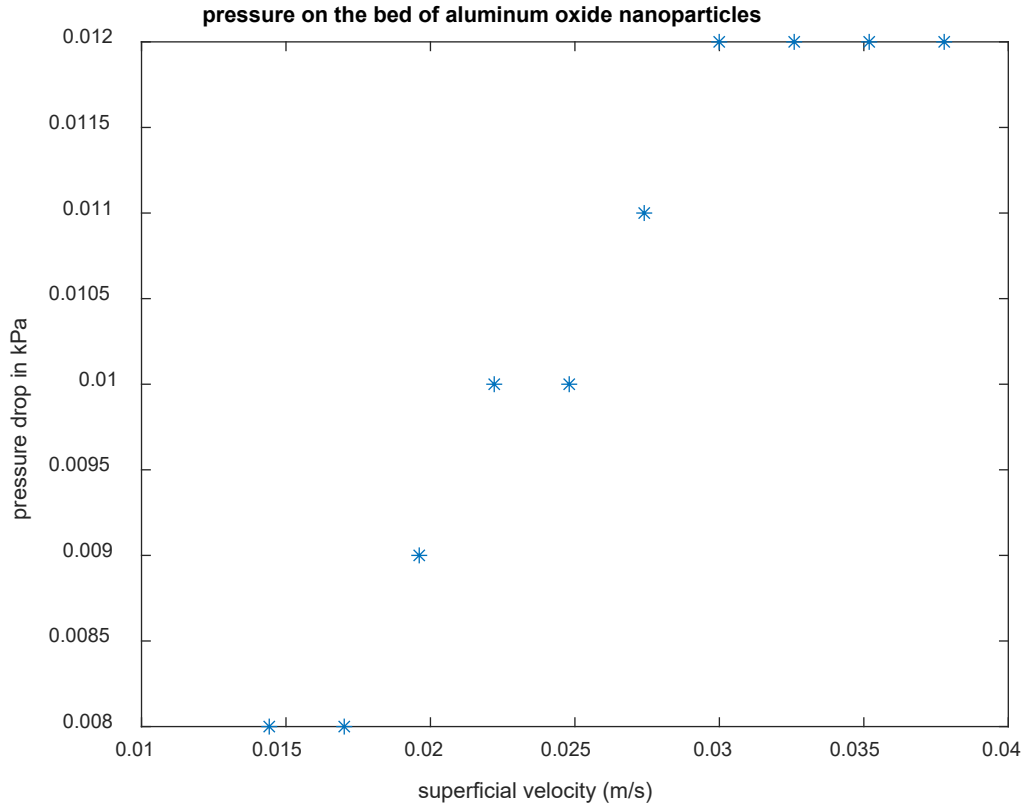

Figure 8. 44**: Pressure drop on the bed in acoustic sound fluidization at 100 Hz**

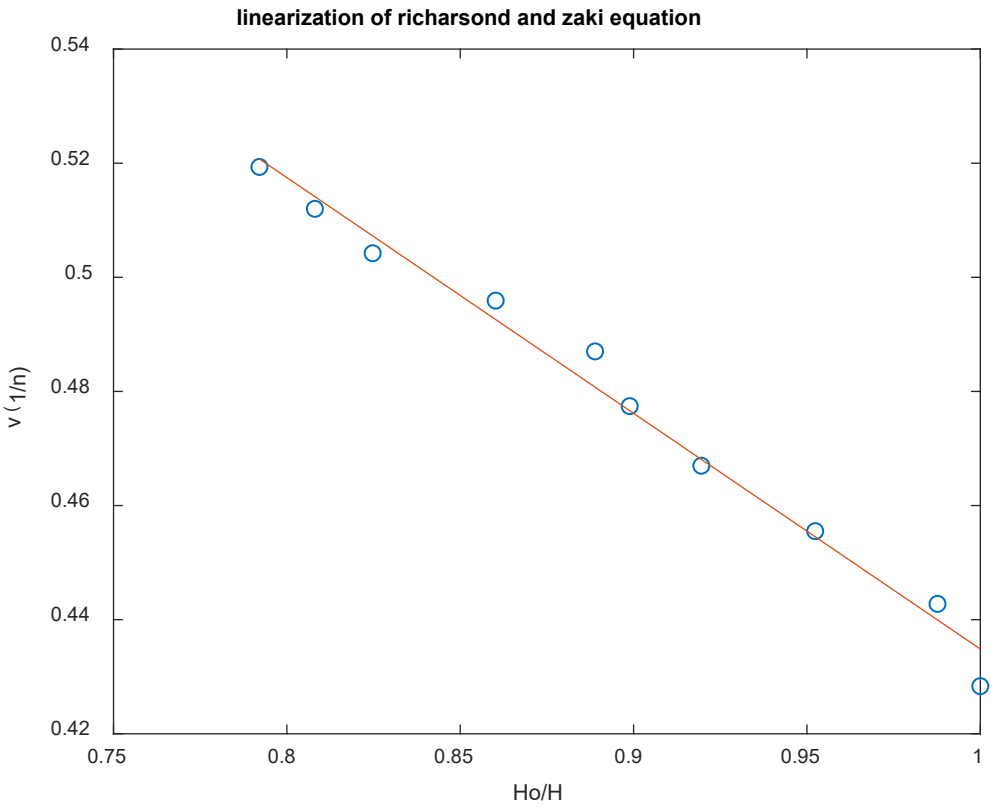

Figure 8. 45**: Plot of a linearized Richardson and Zaki equation after an acoustic sound FB**

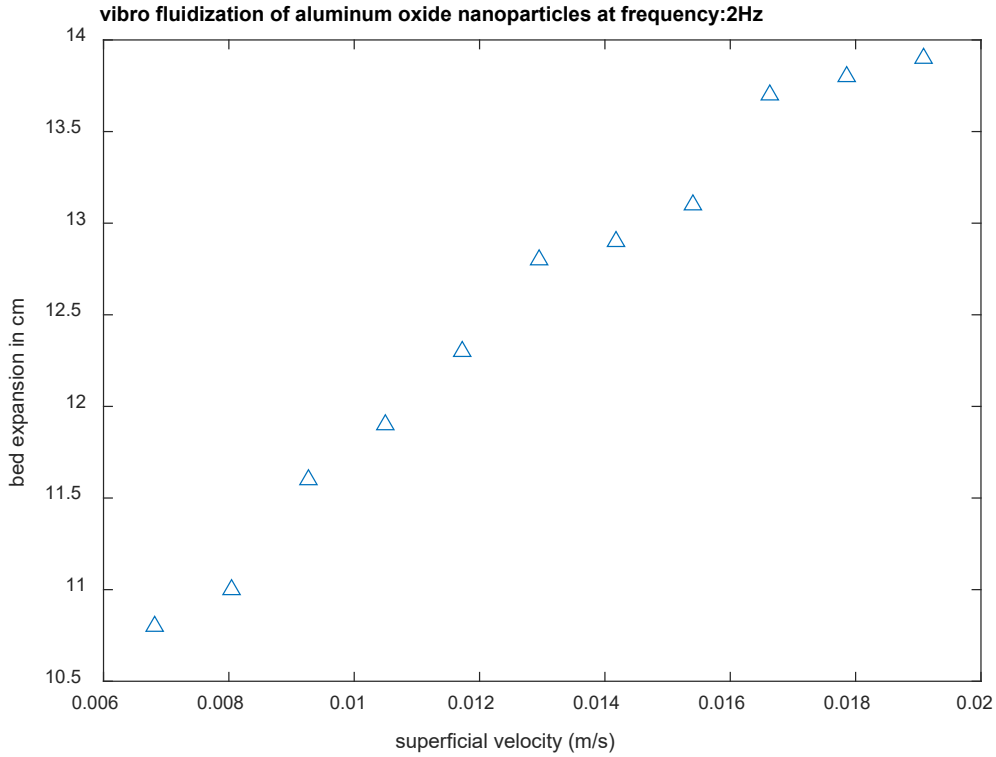

Figure 8. 46**: Bed expansion in a Vibro-fluidized bed**

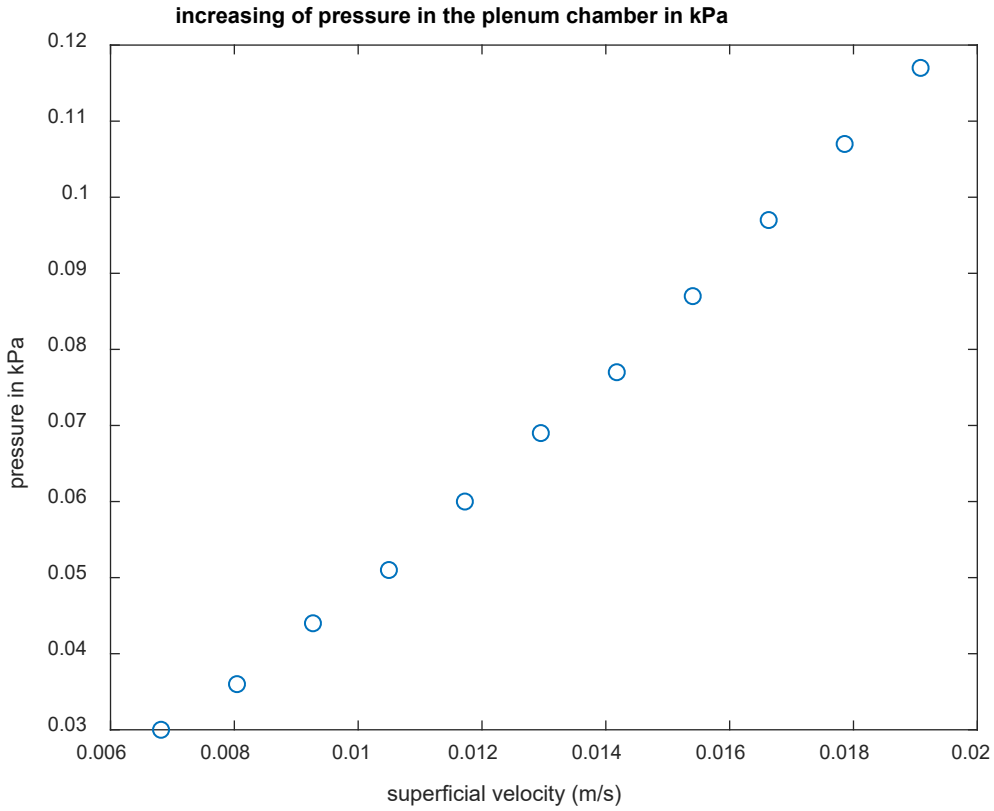

Figure 8. 47**: Pressure profile in the plenum chamber of a vibro-fluidization with a frequency of 2Hz**

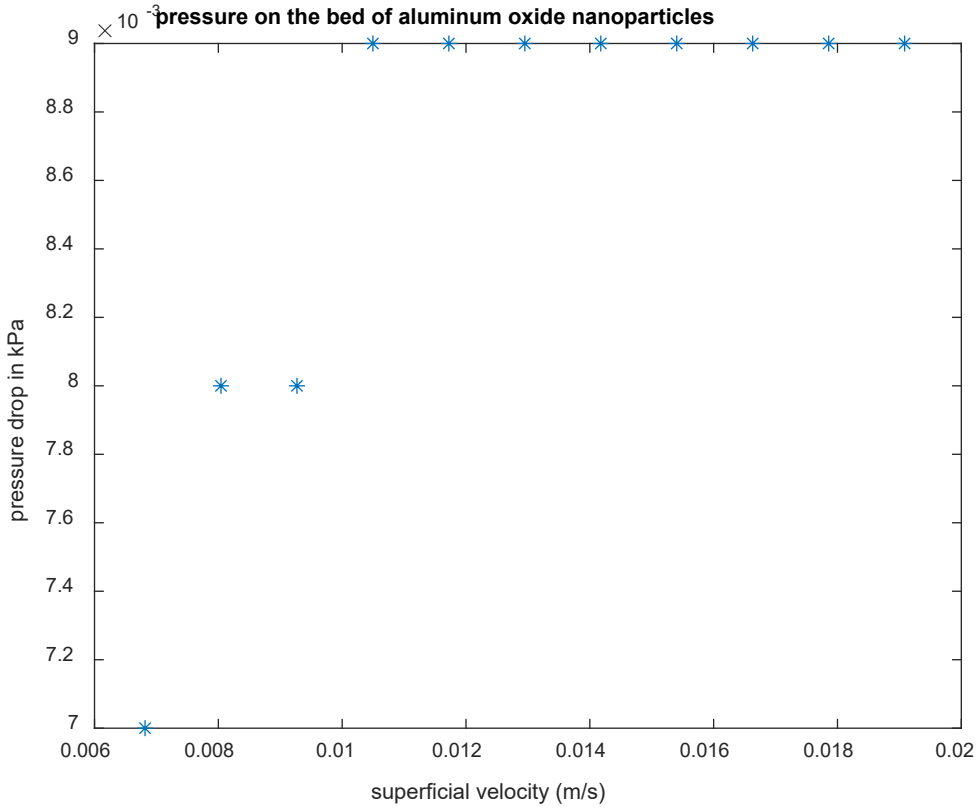

Figure 8. 48**: Pressure drop on the bed of Al_2O_3 nanoparticle at a frequency of 2Hz**

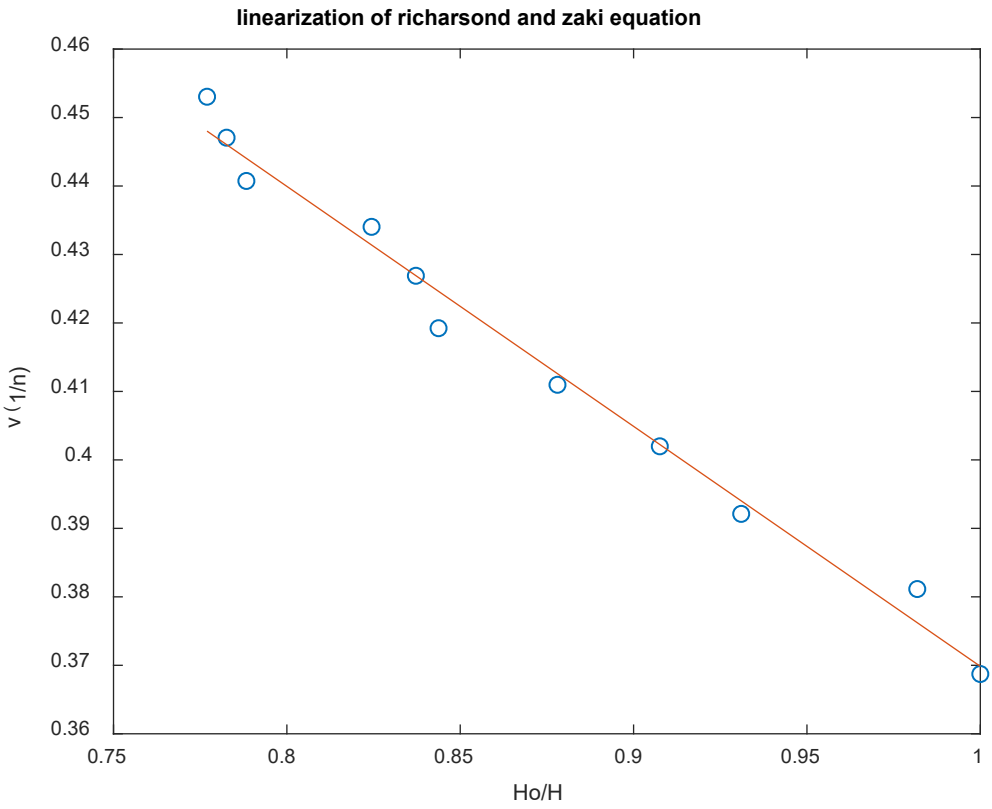

Figure 8. 49**: A plot of linearized Richardson and Zaki correlation after vibro-fluidization at a frequency of 2Hz**

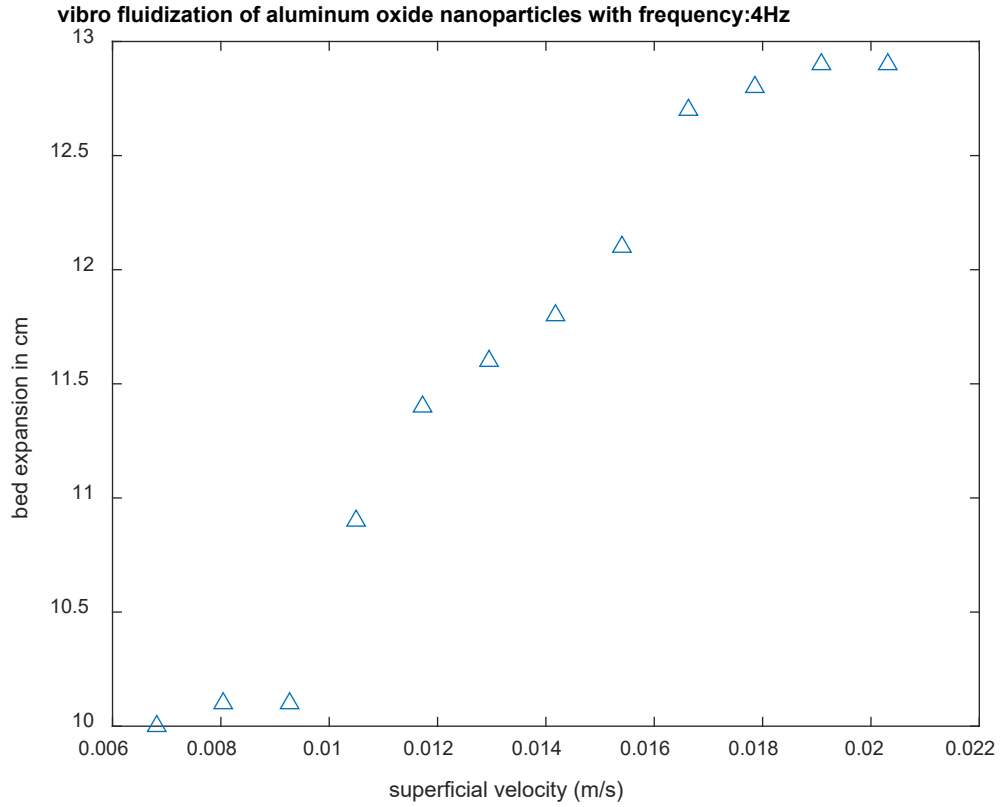

Figure 8. 50**: Bed expansion in a vibro-fluidized bed**

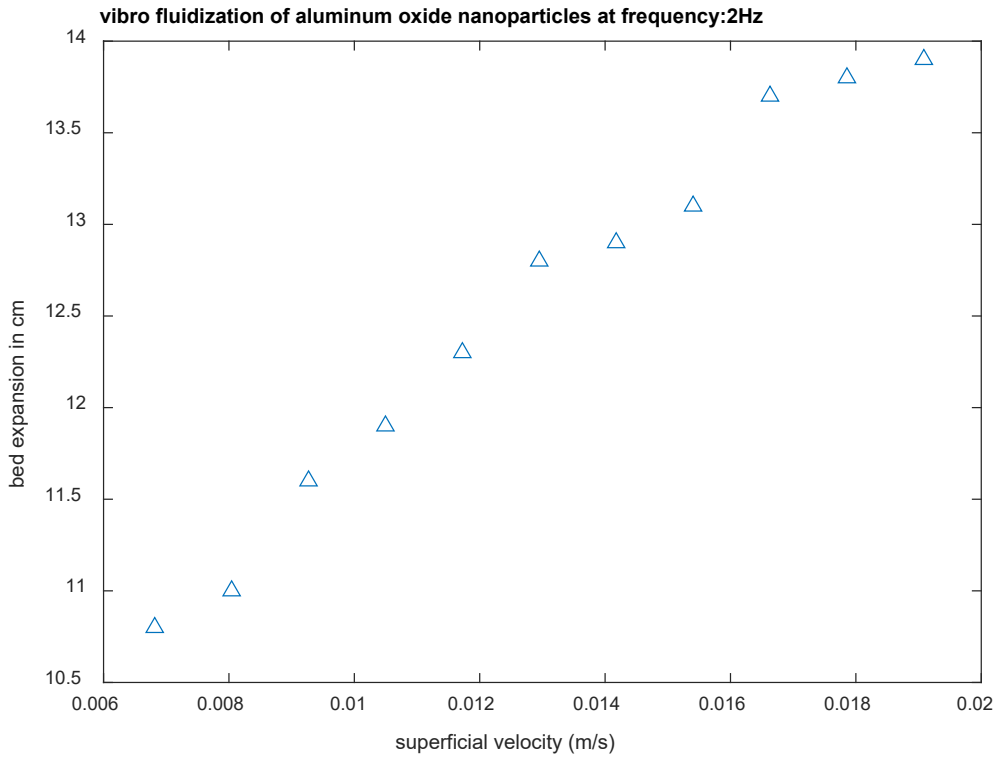

Figure 8. 51**: Bed expansion in a vibro-fluidized bed at a frequency of 2Hz**

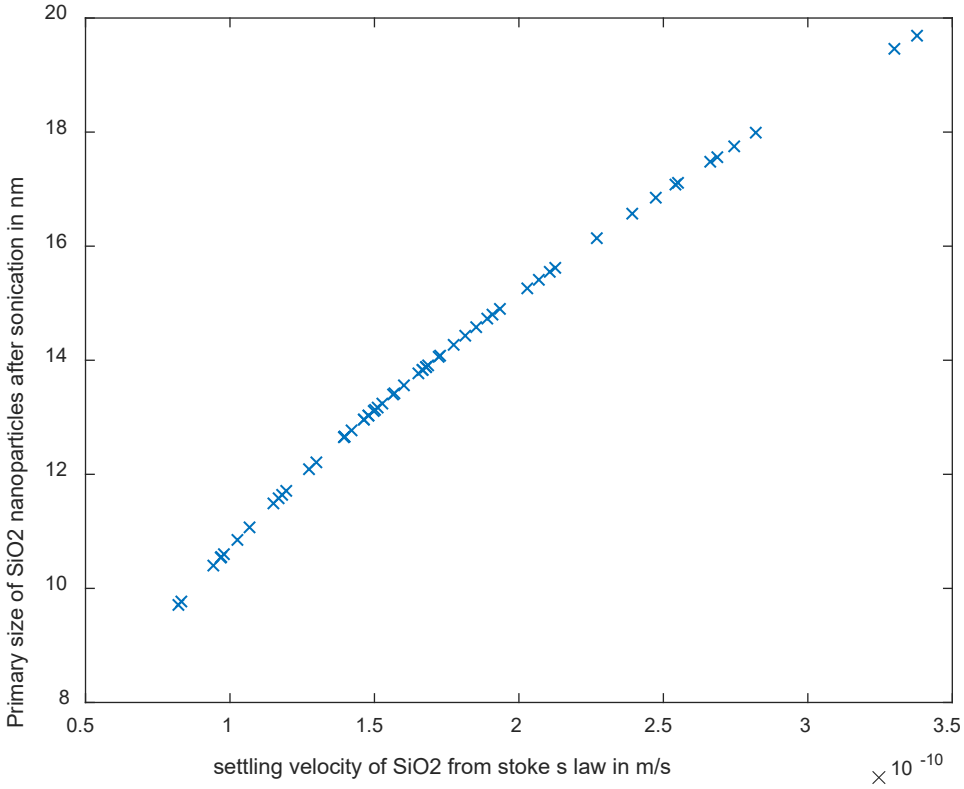

Figure 8. 52**: the settling velocity of the primary size of SiO_2 nanopowders**

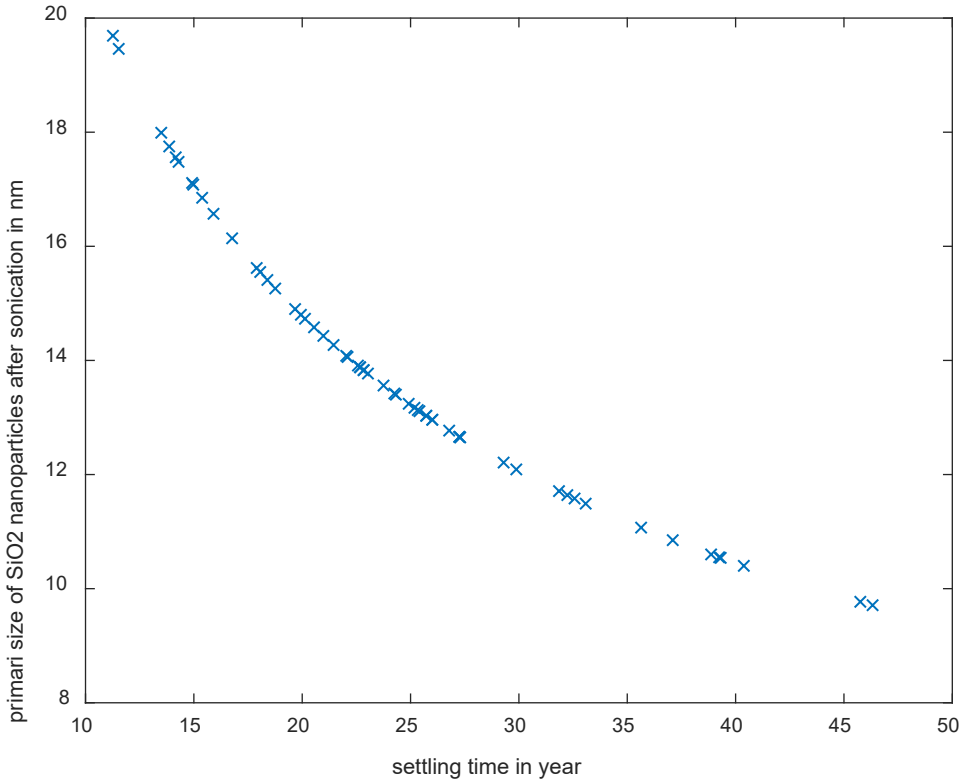

Figure 8. 53**: the settling time for the primary size of SiO_2 nanopowders**

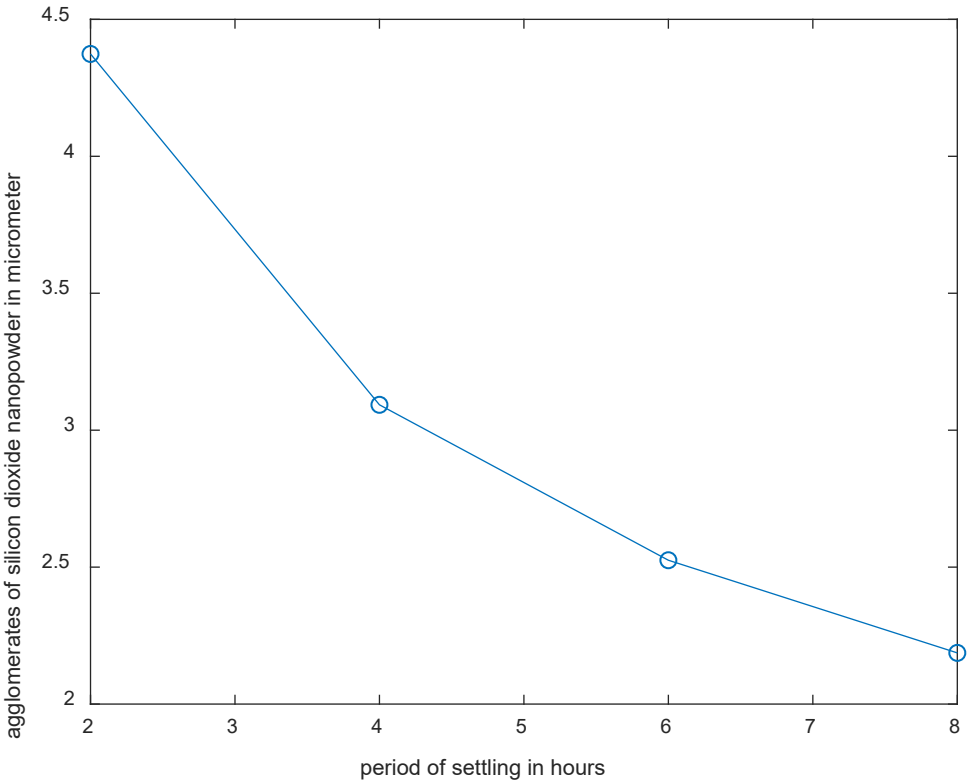

Figure 8. 54**: the batch settling test for SiO_2 agglomerates**

8.3. Appendix D: Sample calculations

Derivation of the variation of voidage from the minimum fluidization state.

Mass of the solid particles in a bed can be described as:

$$m_p = \rho_p \times v_p \quad (1)$$

The voidage Ɛ is defined as the fraction of the difference of the volume of the bed - the volume of solid particles to the volume of a bed of solid particles:

$$\varepsilon = \frac{v_B - v_p}{v_B} \quad (2)$$

Making the volume of solid particles as the subject of the formula in equation (1) and (2), result in:

$$v_p = \frac{m_p}{\rho_p} \quad (3)$$

$$v_p = v_B(1-\varepsilon) \quad (4)$$

By equating equation (3) and equation (4):

$$\frac{m_p}{\rho_p} = v_B(1-\varepsilon) \quad (5)$$

By definition, the volume of the bed of solid particles can be expressed as the height of the bed multiply by the cross-section area of the column of the fluidized bed as:

$$v_B = A \times H \quad (6)$$

Replacing the volume of the bed of solid particle in equation (5) result in:

$$\frac{m_p}{\rho_p} = AH(1-\varepsilon) \quad (7)$$

The mass of the solid particle m_p can be expressed as:

$$m_p = AH\rho_p(1-\varepsilon) \quad (8)$$

Mass balance across tree state of fluidization in a column.

Because mass is conserved in a fluidized bed column with a bed of solid particles in tree state of fluidization, the equation in a fluidized bed column can be expressed as:

At Initial.

$$m_p = AH_0\rho_p\left(1-\varepsilon_o\right) \quad (9)$$

At minimum fluidization state

$$m_p = AH_{mf}\rho_{bulk}\left(1-\varepsilon_{mf}\right) \quad (10)$$

The mass of solid particles at an initial state is the same as when the fluidization start, so equation (9) can be equated to equation (10)

$$AH_o\rho_p\left(1-\varepsilon_o\right) = AH_{mf}\rho_{bulk}\left(1-\varepsilon_{mf}\right) \quad (11)$$

The fluidizing medium, in this case, is air, thus the bulk density can be approximated to be equal to the density of the particles as the density of the solid particle is far higher than the density of air, equation (11) can be writing as:

$$AH_o\rho_p\left(1-\varepsilon_o\right) = AH_{mf}\left(1-\varepsilon_{mf}\right) \quad (12)$$

Looking equation (12) the cross-sectional area$A$, and the density of particle can be canceled out from the equation

$$H_o\left(1-\varepsilon_o\right) = H_{mf}\left(1-\varepsilon mf\right) \quad (13)$$

Increasing the air velocity above the minimum fluidization velocity, increased the voidage in the column of the fluidized bed, for each increase in the height from the minimum fluidization state, the voidage should be expressed when using the equation (13) as:

$$\varepsilon = 1-\left[\left(1-\varepsilon_o\right)\frac{H_o}{H}\right] \quad (14)$$

Calculations for sample 4.

Mass of sample =1.633 kg

Initial height of the bed of the sample = 10 cm

Density of particle = 1616 kg/m^3

Diameter of the fluidized bed = 0.11 m

Acceleration due to gravity = 9.81 m/s^2

Density of air = 1.225 kg/m^3

Viscosity of air = 1.862×10^{-5} Pa.s

The Sauter mean diameter of the sample = 337.960 μm.

Using equation (3) to calculate the volume of the solid particles result in:

$$V_p = \frac{1.633}{1616} = 0.001m^3$$

The volume of the bed of solid particles is evaluated using equation (6):

$$V_B = \pi \times 0.11^2 \times 0.1 = 0.0038m^3$$

The method of calculation of the initial voidage is derived using the equation (2):

$$\varepsilon_o = \frac{0.0038 - 0.001}{0.0038} = 0.734$$

The experimental minimum fluidization voidage is computed by using the equation (14), from this equation, experimentally the bed of solid particles attended it minimum fluidization state when the height of the bed reached 10.75 cm, it minimum fluidization voidage is as:

$$\varepsilon_{mf} = 1 - \left((1 - 0.734) \times \frac{0.10}{0.1075} \right) = 0.83$$

The use of Kunii and Levenspiel correlation to predict the minimum fluidization velocity.

The minimum fluidization velocity was predicted using the equation of very small particles where the Reynold number at minimum fluidization state is less 20. The equation for the prediction is described as, where the sphericity is measured from the experimental pressure drop, for sample 4, its value was measured to a value of 0.169 pressure measured using pressure transducers.

$$u_{mf} = \frac{d_p^2 (\rho_p - \rho_g) g}{150\mu} \frac{\varepsilon_{mf}^3 \phi_s^2}{1 - \varepsilon_{mf}} \quad (15)$$

From the above the equation the minimum fluidization is:

$$u_{mf} = \frac{\left(337.960\times10^{-6}\right)^2 \times (1616 - 1.225) \times 9.81 \times}{150 \times 1.862 \times 10^{-5}} \frac{0.83^3 \times 0.169^2}{1 - 0.83} = 0.062 \frac{m}{s}$$

To check if the minimum fluidization velocity is valid for the case of small particles, the Reynold was computed using the equation:

$$\mathrm{Re}_{mf} = \frac{d_p \times u_{mf} \times \rho_g}{\mu} \quad (16)$$

By using the equation (160 at minimum fluidization state result in:

$$\mathrm{Re}_{mf} = \frac{337.960 \times 10^{-6} \times 0.062 \times 1.225}{1.862 \times 10^{-5}} = 1.835 < 20 \implies \text{laminar flow}$$

Calculation of the parameters such as voidage, voidage after minimum fluidization, and terminal velocity using the Richardson and Zaki index.

The Richardson and Zaki equation is accommodated in the experiment for the fluidization enhanced by external forces for the nanoparticles due to their behavior. It was observed that the agglomerates particulate fluidization was formed during the fluidization enhanced by external forces for nanoparticles.

$$\frac{u_s}{u_t} = \varepsilon^n \quad (17)$$

Equation (17) described the Richardson and Zaki equation used to calculate the terminal velocity and the voidage of nanoparticle in the fluidized bed where the ratio of the superficial velocity to the terminal velocity is expressed as the voidage powered to the Richardson and Zaki index. In the experiment, the Richardson and Zaki index used was at a value of 5.

By combining equation (14) into equation (17), the result equation is shown as:

$$u_s = u_t \times \left[1 - (1 - \varepsilon_o) \times \frac{Ho}{H}\right]^n \quad (18)$$

By linearizing equation (18), the equation (17) reduces to the form of:

$$u_t^{\frac{1}{n}} - u_t^{\frac{1}{n}} \times (1 - \varepsilon_o) \times \frac{Ho}{H} = u_s^{\frac{1}{n}} \quad (19)$$

Which reduces to a linear equation

$$y = B - Ax$$

Where

$$y = u_s^{\frac{1}{n}}, \quad (20) \qquad x = \frac{Ho}{H}, \quad (21) \qquad A = u_t^{\frac{1}{n}} \times (1 - \varepsilon_o), \quad (22) \qquad B = u_t^{\frac{1}{n}} \quad (23)$$

The initial voidage of the nanoparticle in the fluidized bed was calculated from the slope of the plot of y vs x and the terminal velocity in the fluidization enhanced by the external forces was calculated as the y-intercept of the graph.

$$u_t = B^n \quad (24)$$

$$\varepsilon_o = 1 - \frac{A}{B} \quad (25)$$

Estimation of the size of the agglomerates of nanoparticles during fluidization enhanced by external forces.

The stoke law relation was used to estimate the size of the agglomerates of nanoparticles; the equation is described as:

$$d_a = \sqrt{\frac{18 \times \mu \times u_t}{(\rho - \rho_f) \times g}} \quad (26)$$

Sample calculation for the calculation of the average diameter of the agglomerates for aluminum oxide nanoparticles in the acoustic sound fluidization.

From the plot from **figure 4.6.2.** the slop find was as – 0.413 with the y-intercept as 0.845; from the result above the terminal velocity of the agglomerates particulates fluidization of the aluminum oxide nanoparticle for the acoustic sound fluidization was find as:

$$u_t = 0.447^5 = 0.192 \frac{m}{s}$$

The initial voidage was calculated using equation (25) and resulted as:

$$\varepsilon_o = 1 - \frac{0.413}{0.845} = 0.513$$

The mean diameter of the agglomerates from equation (26) was estimated as:

The viscosity and the density of air were taken at the operating condition of the fluidization enhanced by external forces which were at room temperature.

$$d_a = \sqrt{\frac{18 \times 1.862 \times 10^{-5} \times 0.192}{(400 - 1.225) \times 9.81}} = 128 \mu m$$

8.4. Appendix E: Results and discussions for the calibration

8.4.1. Recalibration of rotameters

The recalibration of the rotameters was necessary to ensure the applicability of the calibration curves from the reference to the present condition. The three calibration curves from the references coming from the three different rotameters are equations from calibration on the rotameters at a certain particular condition. To improve the accuracy and precision of the future experimental data from the equipment and decrease the uncertainty, the recalibration was important before any collection of the experimental data from the equipment.

8.4.2. Calibration of rotameter 1

The recalibration of rotameter 1 was produced following up on the methodology described in chapter 3. Section 3.3.1 the process of the recalibration of rotameter 1 was performed by three different runs. In the first run, the calibration points resulted from rotameter reading to the standard rotameter were fitted by mathematical linear regression analysis. The recalibration curve produced from the linear regression line was found with a slope of 5.920 and a y-intercept of 32.891 with standard deviation performed on the standard rotameter reading at 0.897. To increase the rate of accuracy and precision, the second run produced after a linear regression analysis a slop of the line fitted to the calibration point of the rotameter 1 at 5.916, and a y-intercept of 32.606 with a standard deviation of 0.902. Followed by the third run where the slop was 6.160 with a y-intercept of 31.532 with a standard deviation of 0.932. These equations are produced from the plot from the standard rotameter reading expressed in cubic meter per minute with the reading from the rotameter 1.

To reduce the uncertainty and improve the accuracy in the choice of the calibration equation necessary to apply to the present condition, the run with the lowest standard deviation was considered and compared to the calibration curve from the literature. The first run in the calibration process produced a standard deviation of 0.897. This run was compared to the calibration curve from the literature which has a slop of 5.4 and y-intercept of 10.83. We have observed the deviation of the calibration curve of rotameter 1 from the calibration curve from literature was due to the difference in the slop and the y-intercept.

8.4.3. Calibration of rotameter 2

After calibration of rotameter 2, a slop of 37.402 and a y-intercept of 152.812 of a regressed line fitted to the calibration reading was found in the run first of the calibration process. On this run, a standard deviation of 5.683 was calculated. In the second run, after a linear regression analysis on the calibration reading of rotameter 2, a line produced where the slope of the line was 38.083 and y-intercept of 151.139, a standard deviation of 5.785 was calculated from the standard rotameter reading.

For the viability of the calibration reading of rotameter 2, a third run was conducted and from this run, after a linear regression analysis on the experimental data, a slop from the regressed line was 36.425 and y-intercept from the regressed line of 155.775. A standard deviation from the experimental data was calculated to 5.534. After choosing the run with the lowest standard deviation, run 3 was considered as a run to be used to compared to the calibration curve from the literature. Noting that the calibration equation from the literature for this rotameter 2 was having a slope of 37 and a y-intercept of 94.6. The deviation of the calibration equation of the rotameter 2 at the present condition to the calibration equation from the literature differs since the slopes and y-intercepts are different.

8.4.4. Calibration of rotameter 3

If all three rotameters have to work simultaneously, calibration of rotameters is necessary. And rotameters were different in size. The calibration of rotameter 3 has the object of investigating the applicability and how its calibration equation deviates from the literature.

Three calibrations equations were produced from three different runs; each run was covering the calibration reading of the standard rotameter expressed in cubic meter per minute to the reading of the rotameter 3. The calibration reading was fitted to a line from linear regression analysis to evaluate the calibration equation of the reading of the rotameter 3.

In the first run, the calibration process produced a slop of 91.154 and a y-intercept of 359.744. with a standard deviation of 14.375.

In the second run, the calibration process produced a slop of 91.888 and a y-intercept of 353.974. with a standard deviation of 14.462.

In the third run, the calibration process produced a slop of 93.199 and a y-intercept of 352.244 with a standard deviation of 14.676. The run with the lowest standard deviation was considered as run 1 and was compared to the calibration equation of literature. The deviation from the slop from the present condition was from 93.199 to 98 of the slop from the literature, the y-intercept of the calibration of the present condition deviates from the literature at 359.744 to 285.3.

The application of the calibration equation when using this rotameter comes from the judgment from the equation produced from calibration equations. The emphasis in the calibration process was pointed out on the precision and availability of its application to the present condition. Because the calibration instrument chosen was taken into consideration, and reducing uncertainty and calibration time considered as an important factor, the usage of the calibrations produced from the rotameters in this process of calibration will be considered for the continuous measurement of parameters such as airflow.

8.4.5. Calibration of the conventional fluidized bed column

It was necessary to calibrate the fluidized bed for the use in the fluidization of solid particles of samples. To ensure that the pressure is well distributed in the air chamber below the perforated plate before the use of the fluidized bed, a pressure profile was produced after calibration on this section of the fluidized bed column.

8.4.5.1. Calibration with pressure transducers

This section of the fluidized bed was found very important in a way that it was the source of the distribution of the flowing superficial velocity necessary to fluidize the bed of solid particles of samples. It was found that the pressure profile in this region of the fluidized bed was linear. A sensitivity analysis on the use of the electronic digital display with controllers was investigated to verify the reading of the pressures in the air distributor chamber when using the lowest superficial velocity. It was found that with the use of the rotameter 1, the lowest reading, was captured only by the digital display, and an increased further of the rotameter 1 reading, the controller 1 and controller 2 could read the pressure. Similarity on the pressure profile on the air distributor chamber occurred when the digital display and controllers were used when rotameter 2 was utilized. Above the air distributor chamber, the pressure profile in this section was calibrated by verifying the pressure located at 3.5 cm above the perforated plate and the pressure located at 20.5 cm above the perforated plate. The pressure profile in these two locations in this second section of the fluidized bed with the use of rotameter at different reading intercepted in the pressure profile, proofing the well-functioning of the fluidized bed. Because the upper part of the fluidized bed was calibrated without any solid materials on it, the resulted pressure profile has proven that fluidized bed could be used for fluidization. The minimum pressure measured during calibration at lowest rotameter reading was found to be 0.23 kPa and the highest pressure measured at selected maximum rotameter reading was 0.46 kPa in the air distributor chamber and,

0.17 kPa and 0.27 kPa as a minimum and maximum pressure measured during calibration in the region above the perforated plate.

8.4.6. Calibration of the vibro-fluidized bed column

The importance of calibrating the column before the fluidization of solid particles was a better interpretation of the results to be collected during fluidization, the accuracy, and precision of the results, the reduction of the uncertainty. These factors were the majors' reasons for calibrating the vibro-fluidized bed before usage.

8.4.6.1. Calibration with inverted U-tube manometers

The inverted U-tube manometers were used as measuring pressure equipment in the calibration of vibro-fluidized bed. One inverted U-tube manometer amount the set of the inverted U-tube manometers was inserted into two different regions in the vibro-fluidized bed. The inverted U-tube manometers possessed two legs where one leg was attached to measuring location in the air distributor chamber and the second leg was located at region above the perforated plate. By opening different readings of the rotameter 1, we have observed an increase in pressure head in the region. The pressure profile in the air distributor chamber was showing linearity. The plotting of the rotameter 1 reading with the pressure in the region was evidence that there was no difference in pressure produced from the inverted U-tube manometer and pressure transducers, this can be referred to the figure 8.5. On the other hand, the pressure profile above the perforated plate was increased as the rotameter 1 reading increased, showing a minimum pressure at lower rotameter 1 reading of 0.04 kPa and maximum pressure at selected maximum rotameter 1 reading of 0.17 kPa. The plotting of rotameter 1 reading to the pressure in the upper part of the vibro-fluidized bed when referred to figure 8.6 using an inverted U-tube manometer and pressure transducers, showed that the measured pressure was high using pressure transducers than inverted U-tube manometers.

8.4.6.2. Calibration with pressure transducers

Two pressures transducers were installed in the vibro-fluidized column, one pressure transducer was located at the air distributor chamber for measuring the pressure in the air distributor chamber while the air was flowing into the column. This pressure transducer transmitted a signal to a digital

display located in control hut 2 where pressure was displayed. The second pressure transducer was located a few centimeters above the perforated plate. This pressure transducer was sending the signal to a controller 1 connected to connection cable CMD-001, this connection cable was further connected to a LapTop via USB cable, the pressure was displayed from the LapTop using a SHINKO software. The pressure profile in the air distributor chamber after measurement of pressure at different rotameter 1 reading demonstrated a linear profile between the rotameter 1 reading and the pressure in the air distributor chamber. The minimum measured pressure in the air distributor chamber during calibration was 0.33 kPa; at selected maximum rotameter 1 reading, the pressure was measured at 1.8 kPa. The measure of the pressure in the region above the perforated plated show an increase of pressure as the rotameter 1 reading is increased, thus still we are observing linearity on the region above the perforated plate. The minimum pressure reading at the lowest rotameter 1 reading was found to be 0.06 kPa and the highest pressure at selected maximum rotameter 1 reading was 0.20 kPa, this can be referred to figure 8.6 in the appendices.